

Determining the Accuracy and Repeatability of Citizen-Derived Imagery as a Source for Structure-from-Motion Photogrammetry



Michael Lusty

This dissertation is submitted for the degree of

Master's by Research

August 2019

Lancaster Environment Centre

Dedication

I would like to dedicate this thesis to my Grandfather, David Grenville Lusty, whose support, wisdom, energy and encouragement helped me achieve everything that I have to this day and will continue doing so.

Acknowledgements

I would like to thank everyone who has supported me through my last year. I could not have done it without the funding nor the huge support that The Rabbit Patch Ltd. has provided me with over the last year: Jane Littlewood and Kevin Littlewood both have provided the most caring support every step of the way. I would also like to thank Wyre Borough Council for helping shape my project and providing data I have used to develop my understanding of the Fylde coastline: Carl Green has had tremendous input towards this project.

This thesis most certainly would not have been accomplished had it not been for the care and attention provided to me by my supervisors, Suzana Ilic, Mike James and Ally Gormally. Their support has not gone unnoticed and has helped me unlock a career path I never thought I would be able to achieve. Vassil Karloukovski has been especially helpful throughout this last year in survey training and help in the field.

Special thanks go to my close family whose words of advice and constant support have helped me along the highs and lows this last year has brought. They have also provided academic support in the writing and proof reading of this thesis. Lastly, but certainly not least, I would like to thank Alexandra Geraghty for helping me through any issues I came across and the encouragement I have received all the way through my higher education.

Declaration

This thesis has not been submitted in support of an application for another degree at this or any other university. It is the result of my own work and includes nothing that is the outcome of work done in collaboration except where specifically indicated. Many of the ideas in this thesis were the product of discussion with my supervisors Dr Suzana Ilic, Dr Michael James and Dr Alexandra Gormally.

Abstract

Globally, sea levels are rising and continue to rise at an accelerating rate. Developments built near the coast are vulnerable from coastal flooding due to a direct rise in sea level and an increase in storm severity, persistence and frequency. As storm events become more prevalent and powerful they will consequently exacerbate the effects from rising sea levels and increase coastal flooding. It is therefore relevant for coastal managers to build and maintain a comprehensive understanding of the coast to predict what a future heightened sea level might bring. Building understanding at a time when resources are limited due to budget cuts is often difficult requiring cost-effective monitoring approaches. Citizen Science is a rapidly developing research method whereby scientific projects utilise public input at one or more stages of the research process. CS projects can tackle scientific research which often cannot be done by scientists alone due to human, financial, time and spatial constraints. Alongside the benefits afforded to scientific research, CS projects help in building scientific understanding within the public domain. By increasing public understanding of the coastal environment, citizens become more empowered to contribute towards coastal decisions.

This project takes on the framework defined by CS by engaging a community group with data collection methods for coastal monitoring. Focus is placed on the Structure-from-Motion (SfM) photogrammetric workflow to build 3D models of the coastal environment using citizens and their personal standalone cameras or inbuilt smartphone cameras. This project aims to assess the accuracy of point clouds derived from citizen-derived imagery of a coastal environment and thus determine its potential as a source of data for coastal practitioners. It also aims to recognise the

response from participating members of the public towards the SfM imaging procedure.

Contents

| | |
|---|----|
| Dedication | ii |
| Acknowledgements | ii |
| List of Figures | ix |
| List of Tables | xi |
| 1. Introduction | 1 |
| 2. Literature Review | 6 |
| 2.1. Monitoring Coastal Morphologies | 6 |
| 2.2. Existing Topographic Coastal Data | 7 |
| 2.2.1. Satellite Imagery | 8 |
| 2.2.2. Airborne LiDAR | 10 |
| 2.2.3. Beach Profiles | 12 |
| 2.3 Coastal Monitoring using Structure-from-Motion | 14 |
| 2.4. The Coast in Context | 21 |
| 2.4.1. Citizen Science | 21 |
| 2.4.2. Contributory Citizen Science | 22 |
| 2.4.3. The Contextual Model | 24 |
| 2.4.4. Lay Expertise Model | 26 |
| 2.5. Validation of Citizen-Derived Data | 28 |
| 2.5.1. The Purpose of Coastal Photogrammetry | 28 |
| 2.5.2. Measuring Accuracy of Reconstructed Topography | 29 |
| 3. Methodology | 34 |
| 3.1. The Volunteer Group and Study Site | 34 |
| 3.1.1. The Study Site | 34 |
| 3.1.2. The Volunteer Group | 36 |
| 3.2. The General SfM Workflow | 37 |
| 3.2.1. Image Collection | 37 |
| 3.2.2. Reconstructing 3D Geometry | 39 |
| 3.2.3. Georeferencing | 40 |
| 3.3. Pilot Study: Hest Bank | 41 |
| 3.4. Volunteer SfM Sessions | 44 |
| 3.4.1. Building an Understanding of the Project | 44 |
| 3.4.2. Georeferencing: GCP Network Configuration | 47 |
| 3.4.3. Image Collection on the Beach | 52 |

| | | |
|----------|--|-----|
| 3.4.4. | Data Transfer..... | 56 |
| 3.5. | Assessing the Volunteer Session..... | 56 |
| 3.5.1. | Image and Ground Control Quality..... | 56 |
| 3.5.2. | Assessing the Accuracy of Image Alignment..... | 58 |
| 3.5.3. | Assessing the Accuracy of Dense Reconstructions | 60 |
| 3.5.3.1. | Cloud Preparations..... | 61 |
| 3.5.3.2. | Measuring the Effect of GCP Configurations | 62 |
| 3.5.3.3. | Measuring the Effect of Different Imaging Devices | 63 |
| 4. | Results..... | 65 |
| 4.1. | Evaluation of Session 1 | 65 |
| 4.1.1. | Summary of the Obtained Models..... | 65 |
| 4.2. | The Evaluation of Session 2: 3D Models | 68 |
| 4.2.1. | Image and Tie Point Analysis | 68 |
| 4.2.2. | Optimisation and Tie Point Error | 73 |
| 4.2.3. | The Effect of GCP Configuration on Model Accuracy | 74 |
| 4.2.3.1. | Evaluation of Dense Reconstructions | 78 |
| 4.2.4. | The Effect of Different Devices on Model Accuracy | 84 |
| 4.2.4.1. | Evaluating Tie Point Geometry | 84 |
| 4.2.4.2. | Comparison of Dense Reconstructions..... | 91 |
| 4.3. | Implementing Citizen-led Coastal Photogrammetry | 94 |
| 4.3.1. | Session 1..... | 94 |
| 4.3.2. | Session 2..... | 97 |
| 5. | Discussion..... | 99 |
| 5.1. | Comparison of Session Frameworks | 99 |
| 5.2. | The Optimum GCP Configuration..... | 100 |
| 5.3. | Configuration Application Along the Fylde | 101 |
| 5.4. | Device Performance..... | 103 |
| 5.5. | Citizen Motivations | 105 |
| 5.6. | A Comparison to Other Topographical Methods..... | 106 |
| 5.7. | The Potential Framework for a Citizen Science Coastal Data Collection Programme | 107 |
| 6. | Conclusions | 109 |
| 6.1. | Assessing the Accuracy of Citizen-derived Coastal Point Cloud Products | 109 |
| 6.1.1. | Suitability of Citizen-Derived Imagery..... | 109 |
| 6.1.2. | Point Clouds Prior to Georeferencing | 110 |
| 6.1.3. | Georeferenced Clouds | 111 |

| | | |
|------|--|-----|
| 6.2. | The Response from Participants | 113 |
| 6.3. | Contributions to Research and Coastal Management | 114 |
| 6.4. | Contributions to Public Engagement within Coastal Science | 115 |
| 6.5. | Future Work | 115 |
| 7. | References | 117 |
| | Appendix 1A – GCP Configuration Linear Regressions (Sparse) – PL50..... | 120 |
| | Appendix 1B – GCP Configuration Linear Regressions (Sparse) – iPhone 6s..... | 120 |
| | Appendix 1C – GCP Configuration Linear Regressions (Sparse) – iPhone X | 122 |
| | Appendix 1D – GCP Configuration Linear Regressions (Sparse) – Galaxy S5..... | 123 |
| | Appendix 1E – GCP Configuration Linear Regressions (Sparse) – EOS 450D | 124 |
| | Appendix 2A – DoDs for PL50 | 125 |
| | Appendix 2B – DoDs for iPhone 6s | 126 |
| | Appendix 2C – DoDs for iPhone X..... | 128 |
| | Appendix 3 – DoDs Between Devices | 131 |
| | Appendix 4A – GCP Configuration - Linear Regressions (Dense) – PL50 | 134 |
| | Appendix 4B – GCP Configuration Linear Regressions (Dense) – iPhone 6s..... | 135 |
| | Appendix 4C – GCP Configurations Linear Regressions (Dense) – iPhone X..... | 136 |
| | Appendix 5 – Feedback Questionnaire 1 | 137 |
| | Appendix 6 – Feedback Questionnaire 2 | 141 |
| | Appendix 7 – SfM Instructions | 144 |
| | Appendix 8 – Session 1 Feedback | 145 |
| | Appendix 9 – Session 2 Feedback | 146 |

List of Figures

| | |
|---|----|
| Figure 1 Imaging diagram for SfM data capture. (Agisoft, 2018) | 15 |
| Figure 2 A progressively zoomed map of the location of the groyne cell used for study (outlined in red). It is bounded by a seawall and two groynes (a-d). (f) A satellite image of the Fylde coast displaying the sea defence types (red-seawall and groyne, orange-seawall only, purple- dunes). (a-d) - Ordnance Survey maps retrieved from digimap.edina.ac.uk (e-f) – Google Maps | 35 |
| Figure 3 (a) An aerial image of the two artificial headlands. (b) An image taken from the northerly headland facing south..... | 36 |
| Figure 4 Drainage outlet pipe, Hest Bank. Used as the scene for SfM image collection..... | 42 |
| Figure 5 The dense reconstruction of the drainage outlet. The blue rectangles show each camera position. | 43 |
| Figure 6 The SfM process displaying (a) the real-time image alignment procedure with the associated sparse cloud and (b) the dense reconstruction. | 46 |
| Figure 7 (a) dGNSS base mounted on a tripod set to a calibrated height. (b) dGNSS rover mounted on a pole set to a calibrated height. | 48 |
| Figure 8 (a) A GCP target measuring 0.09 m/0.09 m used within the survey. (b) GCP Locations superimposed onto a DEM produced. Some GCPs are within the area of interest however appear in areas showing no data..... | 49 |
| Figure 9 (a) An A4 coded target for use as a GCP. (b) Groyne post with a yellow paint spot for use as a GCP. (c) GCP Locations from session 2 superimposed onto a DEM produced from an iPhone 6s..... | 50 |
| Figure 10 The groyne cell of interest. This figure shows the chosen configurations of GCP setup. The 'Full' configuration is a mixture of all types, starting from 'Point 1' and then every other point. 'All Defence' is constituted of all solid red and yellow circles. 'All Seawall' is all solid red circles. 'High Seawall' is shown in solid red circles with a yellow perimeter. 'Mid Seawall' is shown in solid red circles with a blue perimeter. 'Low Seawall' is shown in solid red circles with a green perimeter. 'All Groyne' is constituted of all solid yellow circles. 'Low Groyne' is shown in solid yellow circles..... | 51 |
| Figure 11 Segmented beach. Each colour represents a different segment of beach imaged. Green, purple and red segments were all successfully processed. Data for the blue section was not retrieved and thus no data was processed. | 53 |
| Figure 12 Area of coverage provided by each participant. Red and blue circles represent the starting point for each group. The red and blue lines display the route taken by each group. | 55 |
| Figure 13 The rover pole measuring 0.03 m in diameter. | 58 |
| Figure 14 Camera positions superimposed onto a DEM of the merged point clouds. Not all data was retrieved from each volunteer – hence a discontinuity in camera positions. The purple region outlined in red shows the area obstructed by the berm. | 67 |
| Figure 15 Image residual vectors from each participant's device. These are representations of how each point on the image correlates to a real-world point (each axis is an arbitrary spatial axis with the scale shown in pixels). Different camera models can be applied and are usually radial. A well calibrated camera model should produce small and image residuals in a random distribution (caused by noisy photos). (a) PL50 (b) iPhone 6s (c) iPhone X (d) CUBOT X15 (e) Galaxy S5 (f) EOS 450D. (a) Reprojection errors are random and concentrated around | |

image regions with smooth/waterlogged features. (b), (c), (d), (e) and (f) show systematic reprojection errors suggesting an incorrect camera model. (a), (b), (c), (d) and (e) are all taken by participants. (f) was taken by the researcher. (a) and (f) are standalone cameras. . 71

Figure 16 (a) An oblique image taken on an iPhone 6s showing the positions of 2 GCP targets. (b) and (c) GCP targets showing oblique pixelated centroids..... 72

Figure 17 Sparse linear regressions of GCP configurations using the PL50 as an example. RMSE values are displayed for each respective plot. Red lines display a perfect positive 1:1 correlation between the configurations. Minor deviations are evident towards lower elevations..... 77

Figure 18 (a) iPhone X DoD between the benchmark Full Distribution Model and the Seawall Mid model. (b) Shows the distance from the camera (red) to the GCP (yellow) (c) Shows an example of the oblique viewing angles for marker placement. 79

Figure 19 iPhone X DoD between the Full Distribution model and the Groyne Low model. .. 80

Figure 20 Dense linear regressions of GCP configurations using the PL50 as an example. RMSE values are displayed for each respective plot. Red lines display a perfect positive 1:1 correlation between the configurations. Minor deviations are evident towards lower elevations..... 82

Figure 21 ‘Full Distribution’ histograms displaying the spread of error in the x horizontal dimension for each device. The PL50 shows the highest concentration of error around 0m, whereas the iPhone 6s, iPhone X, Galaxy S5 and EOS 450D all show outliers greater than ± 0.4 m. 85

Figure 22 ‘Full Distribution’ histograms displaying the spread of error in the y horizontal dimension for each device. The PL50 shows the highest concentration of error around 0m, whereas the iPhone 6s, iPhone X, Galaxy S5 and EOS 450D all show a wider spread of error. Error in this dimension is lower than that in the x dimension..... 86

Figure 23 Histograms displaying the spread of error in the z vertical dimension for each device. All devices show a high concentration of error around 0 m with the EOS 450D showing the most spread error..... 87

Figure 24 GCP locations with a colour grading representing z error for the ‘Full Distribution’ for each device with respect to the GCP position..... 89

Figure 25 Linear Regressions of elevations between device DEMs generated from sparse clouds. The red lines represent a perfect positive correlation..... 90

Figure 26 Linear Regressions showing relationships between dense reconstructions generated from each device. Red lines represent a perfect positive correlation. 91

Figure 27 DoD between PL50 and EOS 450D. The DoD displays deviations in elevation of the EOS 450D DEM with reference to the PL50 DEM. 93

Figure 28 DoD between PL50 and iPhone 6s. The DoD displays deviations in elevation of the iPhone 6s DEM with reference to the PL50 DEM. 93

Figure 29 Pie charts displaying views expressed by The Rossall Beach Residents and Community Group. (a) Shows the proportion of participants who understand the benefits coastal monitoring has on developments. (b) The level of difficulty encountered for 3D model generation by participants..... 95

Figure 30 Pie charts displaying views expressed by The Rossall Beach Residents and Community Group. (a) How participants performed the imaging technique. (b) Participants’ willingness to have coastal photogrammetry incorporated into their set of activities. (c) Participant views on how often they might conduct this type of data collection in the future. 97

List of Tables

| | |
|---|----|
| Table 1 The primary factors of each monitoring method..... | 14 |
| Table 2 The number of participants for each session (indoor and outdoor) and the dates they were conducted. | 37 |
| Table 3 Specifications for the Canon EOS 450D used for the pilot survey at Hest Bank. | 42 |
| Table 4 Laptop specifications for 3D point cloud generation with the Rossall Beach Residents and Community Group..... | 45 |
| Table 5 Computer processing specifications | 59 |
| Table 6 Device Processing Parameters | 60 |
| Table 7 Device Processing Parameters | 60 |
| Table 8 Successful dense reconstructions for each device and their respective GCP configurations. Successful reconstructions are indicated by an 'x'..... | 62 |
| Table 9 GCP configurations and their respective control and check point counts..... | 63 |
| Table 10 Camera details displaying the various internal setups for session 1 | 64 |
| Table 11 Camera details displaying the various internal setups for session 2 | 64 |
| Table 12 Device specifications from session 1, images aligned, and dense point clouds generated from aligned images. Clouds reconstructed in PhotoScan..... | 65 |
| Table 13 Devices from session 2, the number of images aligned, and the dense point clouds generated from the aligned images. Clouds were reconstructed in PhotoScan. | 68 |
| Table 14 GCPs removed from geometry calculations due to RMSE values beyond the threshold..... | 73 |
| Table 15 All device configurations and their respective average RMSE for control and check points | 74 |
| Table 16 A table showing details on the dense reconstruction..... | 78 |
| Table 17 A table displaying the difference in volumes between each GCP configuration. | 81 |
| Table 18 A summary table of RMSE derived from the dense linear regression analysis. Data here was based on the 0.5m grids for the PL50, iPhone 6s and iPhone X exported from CloudCompare. | 83 |

1. Introduction

In an age where climate change is having major influences on rates of sea level rise, the need for comprehensive understanding and preventative action is paramount. It is estimated that around 600 million people live in coastal areas that are less than 10 m above sea level globally (United Nations, 2017). This equates to approximately 8% of the world's population whom are most vulnerable to coastal flooding events. The events are likely to become more frequent, persistent and severe as global temperatures rise and the climate changes. As the climate changes and sea levels rise, there is a necessity to understand the coastal processes that shape our coastline, as these processes have direct and indirect impacts on developments near the sea. Erosional effects are often unwanted where there is land which holds economic value, and thus methods to mitigate them are usually sought after. Beaches act as energy sinks for incoming waves and thus greatly reduce the erosional effects caused by them, however, they themselves are subject to sediment loss through these hydro-mechanical forces. It is therefore crucial to maintain and monitor beaches as they evolve. Government organisations aim to develop an understanding of not only the driving forces responsible, but the effects they have on coastal morphology. However, resources are often limited due to budget constraints and the implementation of research methods can be restricted by a lack of human resources. A newly re-emerged scientific research method – Citizen Science (CS) – can greatly enhance the scope and effectiveness of research where these restrictions are found.

Citizen Science is the practice of involving citizens within the scientific research process to achieve goals set out by project leaders. CS projects are typically a collaboration

between experts and non-experts to gather information about the natural world. The degree of participation from citizens varies dramatically depending on the nature of the objectives set out by the project. Passive engagement methods can utilise resources owned by the public but not require the cognitive ability possessed by them, where more active approaches can lead to project objectives being constructed or shaped by the citizens themselves. A CS project can provide the ability to expand sensing coverage over much larger areas when compared traditional methods involving a few scientists -this is owed to the plentiful supply of human resources the public offers. Additionally, sensing frequency can be increased for same reason and data collection turnaround times greatly enhanced. CS projects do not just benefit the scientific community; they also increase the public understanding of science by engaging citizens directly with research and are crucial in developing confidence in scientific practices.

In recent years, Citizen Science has experienced rapid growth; owed largely to advancements in technology providing internet-capable portable sensing devices to the public - smartphones. This thesis is purposed to provide insight into a potential new monitoring method that will engage citizens in data collection. Not only will an integrative method for public participation help support and fill knowledge gaps in existing coastal data, but it can also serve as a tool for empowering the public within coastal decision-making. It will identify the framework required to initialise a citizen-led coastal monitoring solution using Structure-from-Motion (SfM) photogrammetry – a method that generates 3D point clouds from image datasets without requiring precise image locations and orientations - as a key tool in forming an enhanced understanding of the coast. The pilot study concentrates on the morphological setting

of the Fylde coast, northwest England whereby a segment of beach was selected as an illustrative setting of the Fylde coastline. A groyne cell situated along a section of beach in Cleveleys, Lancashire is used to analyse the feasibility of citizen-derived imagery as a source of data for coastal photogrammetry. To justify and prove the potential for citizen integration into coastal data collection, measures must first be taken to test the accuracy and repeatability of such an observation method.

SfM has developed rapidly over recent years, with an accelerated uptake of the surveying method across scientific domains. A particularly relevant discipline is that of the geosciences, where SfM has become a well-established tool for the geomorphological analysis of varied environments operating at multiple scales. This makes it an especially useful tool, as coastal processes tend to operate across the small-, medium- and large-scales. SfM has been well-tested at a range of scales (James and Robson, 2012) however, there is not much insight into how the method performs as a data collection method when carried out by citizens in a coastal setting. 3D models produced from imagery collected by citizens require measures to be taken that ensure their validity and usefulness as a scientific resource.

There have been numerous investigations into the accuracy and precision of SfM in the sciences when performed by experts, however, there has not been much application of the technique from non-experts. Traditionally, photogrammetry has usually been conducted by expert photogrammetrists, but with the development of new, robust algorithms that provide non-experts with a means to reconstruct 3D geometry, photogrammetry has experienced a rapid proliferation in users. Although it is recommended to have foundation knowledge of the mechanisms involved with the

SfM process, this thesis addresses the potential for community involvement where limited knowledge of the SfM pipeline is possessed. The community group involved with this study are The Rossall Beach Residents and Community Group, whose members proactively engage themselves with coastal-related issues. They were contacted through a small to medium enterprise (SME) – The Rabbit Patch Ltd. - who have strong links with coastal practitioners in both governmental and public bodies. The Rabbit Patch were a project partner and aided with the programme design and recruitment. This study will identify the motivations, if any, that the coastal community group have towards the continued monitoring of the coast and their perceptions towards the incorporation of SfM in coastal monitoring.

In this thesis 3D models produced from citizen-derived imagery were assessed for 'noise' in point cloud products, geometry trueness and erroneous model alignment with real-world GPS coordinates. Data was collected during 2 field sessions taking place in the same groyne cell location, in consecutive months. The field sessions took place in September and October, when energetic sea conditions are known to accelerate erosional processes. Analysis was performed using two key programmes: Agisoft PhotoScan, (2018) for image matching, alignment, and dense reconstruction, and CloudCompare (Girardeau-Montaut, 2003) for cloud manipulation and digital elevation model (DEM) production. Measurements to test the accuracy of citizen-data utilised a prior visual assessment of imagery, self-calibrating bundle adjustments for intrinsic and extrinsic camera model solving, and ground control point (GCP) networks to provide RSME values for 3D geometry reconstructions. 2D analysis is conducted on imagery, prior to, and after image matching and alignments are made, and 3D analysis is conducted on sparse clouds – a result from the bundle adjustment procedure – and

dense clouds – a result from an algorithm built in a similar way to Multiview Stereo (MVS). Data products derived from initial cloud generation and RMSEs derived from GCPs not used in geometry reconstructions, are further analysed in CloudCompare and the statistical computing environment, RStudio (2015).

The research objectives for this project are: (1) To assess the accuracy of point cloud products of a coastal environment derived from imagery collected by citizens, and (2) analyse the response from participating public members towards the SfM imaging procedure.

2. Literature Review

2.1. Monitoring Coastal Morphologies

Coastal environments are areas highly dynamic if left without human intervention. This is often not the case however, where human interests conflict with natural ocean processes. Developments built near the sea and accompanying infrastructure are usually immovable structures of economic value and thus are usually protected if economic value stored within assets outweighs the cost of defending them. An example of this is the £63 million Rossall Coastal Defence scheme along the Fylde coast in the northwest of England, which has been designed to protect 7500 properties and infrastructure (Visit Fylde Coast, 2018). Here, not only economic value was considered but social as well. Protection from the sea can come in a variety of forms both man-made and natural: hard defences, such as concrete structures such as seawalls, and soft methods such as the managed retreat of land. These engineering projects are often costly and subject to critical review from scheme developers (Nazia, 2018). For hard-engineered projects this results in additional pressures being placed on ensuring the successful performance of sea structures. A poorly performing seawall can have negative effects on the safety of residences, commercial property and infrastructural developments whilst also damaging social perceptions of government spending (Garcia-Soto and van der Meeren, 2017). With current trends displaying an accelerating increase in global sea levels, concerns over coastal protection will only become worse if measures are not taken to dampen the unfavourable effects of heightened water levels (Williams, 2013). For these reasons, it is paramount that the coastal interface is diligently monitored.

In this section, these processes and the conflicts between the natural order of coastal reshaping and human development are reviewed, and a variety of monitoring methods are investigated. Consideration of existing coastal data such as large-scale periodic imaging from satellites, medium-scale airborne LiDAR, photogrammetric techniques and the labour-intensive beach profiling surveys are reviewed.

2.2. Existing Topographic Coastal Data

Topographic coastal data is sought after by governing authorities to provide evidence and justify the development of new shoreline management plans (SMP). Collected data needs to address a variety of issues across a range of temporal and spatial scales (Miles, 2014). A multitude of methods are used to attempt to understand and tackle problems posed by changing coastal environments; however, the data collected by each method is often used to serve different purposes. In this section, existing monitoring solutions are reviewed for their strengths and weaknesses as a topographical surveying method. Since the first remote sensing technologies were implemented, systems have been advanced and developed to produce high-accuracy, topographical data. Satellite imagery, LiDAR and the more traditional methods such as ground-based beach profiling are all technologically progressing with increasingly accurate sensing abilities and either directly or indirectly provide a means to calculate surface elevations. In recent years, this data has become increasingly available within the public domain.

2.2.1. Satellite Imagery

The periodicity of satellite orbits allows for the consistent and regular monitoring of the Earth's surface which is beneficial to the consistent monitoring of areas. Satellites can host a huge variety of sensors to collect information about the Earth's atmosphere, surface and subsurface. For topographic data collection satellites are widely used to gather images in full-colour and false-colour to provide a perspective usually unachievable. Due to the lack of atmospheric disturbance and little energy required for the maintenance of orbit paths, satellites provide a predictable source of Earth observation (EO) data – although weather effects such as clouds can often interfere, limiting useful data acquisition. Satellites provide the ability for large spatial coverages due to the speed of the spacecraft and the large distance to nadir and offer observations of areas inaccessible on foot. Although these factors provide unequalled coverage capabilities, they also limit the achievable spatial resolution which is much lower than that offered by many ground-based or close-range aerial sensing systems – ranging from 0.41m (commercially available) to 100s or 1000s of meters. Despite this, satellite data is often freely accessible within the public domain resulting in the increase of scientific research across fields and playing a fundamental role in a host of new scientific discoveries (Wulder et al., 2012).

Coastal research has benefited from satellite imagery; however, local processes cannot be monitored through satellite imagery alone as usually these processes operate at scales below 10m—a resolution below that achievable by many of the freely available imaging satellites such as the Sentinel 2 constellation and the Landsat missions (ESA, 2013; USGS, 2018). Commercial imagery has yielded imagery

with pixel sizes down to 0.41 m using the panchromatic sensor (Satellite Imaging Corporation, 2007). Resolutions of this precision can be used for fine-scaled changes in coastal environments, but still limit spatial observations and usually lack the frequency necessary for coastal research. A report produced by the Defence and Space sector of Airbus showed the ability to reveal morphological changes along La Salie beach on the French Atlantic coastline to an order of magnitude of 1m using the 0.5m panchromatic/pansharpened imagery provided by the Pléiades 1 satellites (Airbus Defence and Space, 2015). This demonstrates the capabilities of commercial imagery, though is not representative of medium-scale, freely available satellite data.

As suggested by Cracknell (1999), it is fair to say that since the start of remote sensing (satellite data) there has been more success in other areas - meteorology, deep sea and land measurements—than there has been in the coastal zone. It has long been an area that often requires resolutions that are currently unachievable for space-borne data. Where satellite spatial ground sampling distances are sufficient for coastal change detection, as exhibited in the La Salie Beach case study, the temporal scales and volume of data required is often insufficient. Revisit times of satellites are dependent on a few factors such as orbital radius, orbital inclination, the latitude of the study area, and the size/direction of the spacecraft's sensor. To fully understand the coastal environment and the processes that shape them, systematic studies are often required, posing challenges for satellite imagery to be used as a successful monitoring solution for high frequency processes (Cracknell, 1999). This technology is rapidly developing, with lower orbital launch costs and thus higher frequency launches (Jones, 2018).

Stereo photogrammetry can be applied to space-borne imagery; however, digital surface models (DSMs) are limited by the imaging capabilities of the satellite and thus resolutions in the x, y and z dimensions are usually too low if derived from freely available sources. Another method to generate height information of is the 'waterline' or 'shoreline' method. Surface topography can be calculated in the intertidal zone by utilising a combination of satellite imagery and nearby tidal data. This technique is used to build a series of contours by observing the shoreline position at differing tidal elevations (Liu et al., 2013; Lipakis et al., 2018). However, this method requires the assumption that the surface topography did not change between observations and that the demarcation line of land and water is well-defined.

2.2.2. Airborne LiDAR

An advantage that airborne LiDAR possesses is the ability to directly gain 3D information at a higher resolution than currently available by satellite systems without the need for cumbersome techniques such as the waterline method (Liu et al., 2013). Airborne LiDAR is a useful tool for monitoring volumetric changes along coastlines and provides medium-large coverage of the environment (Miles, 2014). This method does not share the same periodicity as satellite-derived data, and thus requires dedicated flights which are costly and result in restricted data availability due to fewer airborne surveys being flown. Nevertheless, in recent years costs have been declining (Miles, 2014), allowing for more frequent survey flights in some parts of the coast; airborne LiDAR conducted by the Environment Agency (EA) is currently performed on an annual basis in the northwest of England. Airborne LiDAR surveys tend to be less affected by

weather than satellite data as they operate at lower altitudes and thus can avoid cloud layers, however, surveys can be cancelled if weather conditions do not permit safe or useful flight. Typically, airborne LiDAR data offered by the EA achieves resolutions of 2 m, 1 m, 0.5 m and 0.25 m ground sampling distance, although they do not state the achieved vertical accuracy. Due to the inaccessibility of detailed reports on the quality control, root-mean-square error values (RMSE) suggested by Miles (2013) are identified to be 0.12 m when compared to permanent features such as a road, and 0.35 m when compared to spot heights afforded by Ordnance Survey (OS). These accuracy values provide useful information for medium-large-scale processes; however, they fail to identify finer spatial details.

To fulfil finer-scaled monitoring, ground-based approaches are required, usually conducted by specialist surveyors. DEMs produced by Airborne LiDAR flown by the EA is freely available, and typically higher in resolution than that of the freely available satellite imagery. This therefore allows for finer coastal processes to be analysed, but would still have difficulty identifying localised erosional features such as toe scour. Earlie et al. (2015) utilise airborne LiDAR to assess rates of recession along rocky coastlines, with focus on the Cornwall coast. In this investigation, LiDAR data collection was carried out by the EA, who are responsible for the continuous airborne LiDAR-monitoring and provided yearly data over a 3-year period for 10 study sites within Cornwall. Although the EA conduct airborne LiDAR surveys annually, changes in the Cornish coastline occur annually, or multi-annually and thus a complete evolution is not understood. Here, it was possible to measure rates of coastal retreat to a precision of $<0.1\text{m year}^{-1}$ and provide greater detail than historic measurements in specific areas, many of which are inaccessible on-foot therefore preventing ground-

based monitoring. Surveys such as Terrestrial Laser Scanning (TLS) would have provided greater detail in 3D structure, however, methods like these are restricted by requiring access by foot. Despite this unrestricted access, airborne LiDAR does not cover the shorter temporal intervals and is difficult to link the observed changes with the driving conditions such as wave action.

2.2.3. Beach Profiles

Beach profile surveys have been performed since at least 1990 along the Fylde coast (Miles, 2014), and therefore provide long-term information on coastal dynamics. The surveys are typically conducted at approximately 500m intervals alongshore and occur twice a year (Wyre Borough Council, 2004). Current manual beach profiling measurements from Wyre Borough Council achieve an accuracy of $\sim\pm 0.02$ m in x/y/z using differential GNSS (dGNSS) equipment and can be assumed to have lower accuracies when grid surveys are carried out by mobile dGNSS or RTK GNSS surveys. Along the Fylde coast, beach profiling provides insight into the large-scale, long-term changes that shape the coastline. This data plays an important role in developing our understanding of the coastline, and hence is a fundamental data source in coastal strategy development needed for the continued protection of the coast. Although the cross-shore accuracies provide high-detail resolutions of beach topography, longshore resolutions are severely limited by human resources required to survey the many kilometres of coastline along the Fylde. The surveys provide useful information; however, they fail to monitor large portions of inter-profile beach. Additionally,

profiling requires the beach to be accessed by foot which may not always be possible and therefore requires monitoring by other means.

To provide topographical coverage in areas currently not monitored, a combination of other monitoring methods is currently the common practice—such as previously mentioned satellite and LiDAR data. Beach profiles are useful for observing topographic cross-sections measuring hundreds of metres in length and can thus be used in the monitoring of large portions of the intertidal zone. An example where they are particularly useful is when analysing sand bar migrations (Miles, 2014). Along the Fylde coastline, sand bars (or runnels and ridges) operate over hundreds of metres with shallow inclines which shift over time as a result of tidal and wave-driven processes (Wyre Borough Council, 2004). They effect on-shore wave action and have long-term impacts on the morphology of the coastline. Although beach profiles work well in the detection and monitoring of these crests and troughs, they often miss nearshore local erosional features that occur around coastal structures due to their 2D linear nature. This is especially prevalent when erosional features are perpendicular to the shoreline—for example, rip currents caused by groyne-induced water divergence (Bradbury et al., 2012). An approach to increase the longshore resolution issue is required.

To summarise the strengths and weaknesses for each method in coastal monitoring, Table 1 displays their primary characteristics.

Table 1 The primary factors of each monitoring method.

| Monitoring Method | Spatial Resolution (m) | Temporal Resolution | Cost | Weather Dependence |
|--------------------------|-------------------------------|----------------------------|-------------|---------------------------|
| Satellite (Optical) | 0.4 - 1000s | Days | Free | High |
| Airborne LiDAR | 0.1 - 10s | Year/s | High | Medium |
| Beach Profiles | | | | |
| a) Cross-shore | b) 0.1 - 10s | | | |
| c) Long-shore | d) 10s - 100s | Months | Medium | Low |

2.3 Coastal Monitoring using Structure-from-Motion

Structure-from-Motion (SfM) is a technique used to extract measurements from images – it is a form of photogrammetry whereby 3D models are generated from multiple images taken from different viewpoints. The 3D models are generated in the form of point clouds – large collections of individual points, each of which represent a specific point in space – and are easily manipulated in data processing software. This ability to produce 3D models from images has become prevalent in the sciences due to its practicality. Studies with focus on the geomorphology of environments have experienced a new growth in photogrammetric surveys being incorporated into method design in recent years. This is due to comparatively recent developments in the workflow pipeline of SfM, opening low-cost, user-friendly photogrammetry to a host of new disciplines (Micheletti et al., 2015b). SfM algorithms have been designed to be robust enough to handle data from most non-metric cameras, and process imagery that traditionally might not have been ideal. These new abilities allow for the application of SfM in environments which would have once been expensive to survey and would have required unwieldy equipment.

Although SfM algorithms are robust, there is an optimum data capture method that should be followed in order to produce the best results. The surveyor should

collect as many images as possible of the scene, but 3 is the minimum number for the processing software to run. Ideally images should be taken in a converging manner and each image should be captured within a few meters of the last and contain at least 60% overlap with previous images (Figure 1). The scene should be featureful, non-reflective and be lit by diffuse lighting. The camera being operated should not use distorted lenses such as fish eye lenses as these require complex correction algorithms and can lead to error. The operator should also avoid using the zoom function which changes the focal length, use a fast shutter speed to minimise image blur, and set the sensitivity to a low ISO value to reduce image noise. Images that are collected in these conditions and in this fashion are more likely to undergo successful model generation.

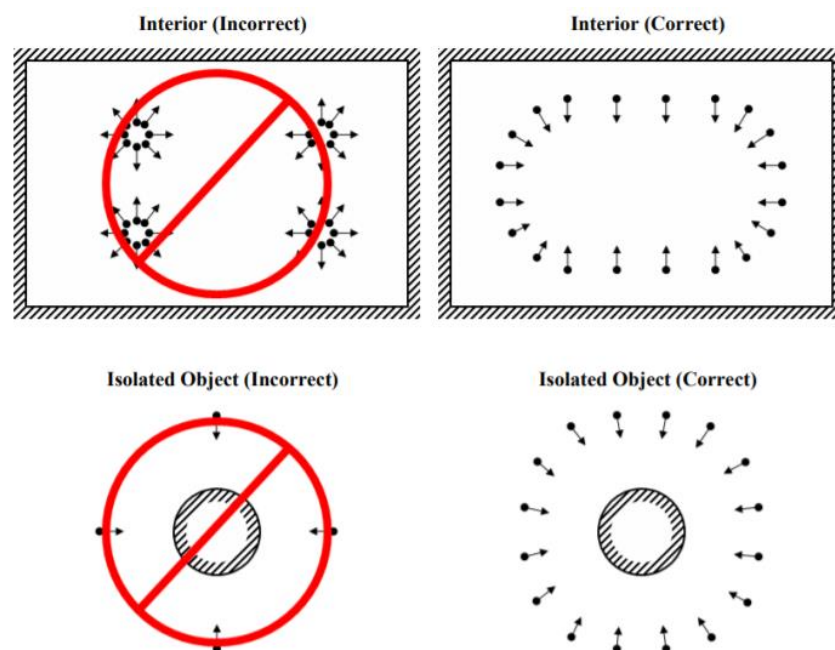


Figure 1 Imaging diagram for SfM data capture. (Agisoft, 2018)

Essentially, SfM is a scale invariant monitoring method which can be applied to many surveying scenarios to generate high-resolution topographical data, as demonstrated on the small-, medium- and large-scale (James and Robson, 2012). SfM

builds geometry from multiple images taken of a scene/object using numerous software designed to perform the SfM procedure. The reconstruction process utilises algorithms often using, or based around, the Scale Invariant Feature Transform (SIFT) algorithm that detects features stable under light variation and changes in viewing angle. Descriptors are generated based on their local neighbourhoods (Hassaballah et al., 2016), and used to detect feature correspondences between images in order to align imagery accordingly. Algorithms determine the intrinsic and extrinsic parameters for the camera model per image and locates the camera's position and orientation (James and Robson, 2012). Further refinement can be carried out by bundle adjustments using external points of known reference on which linear and non-linear geometry adjustments are made.

The applicability of SfM to multiple scales renders it a useful tool generating data that can support lower resolution satellite imagery, lower horizontal and vertical resolution of many airborne LiDAR surveys and the large longshore distances between beach profiles. It also provides a platform that facilitates a potential for high temporal resolution due to the low-cost, low-bulk equipment required.

Cameras, like LiDAR systems, can operate from a variety of platforms; satellite, plane, unmanned aerial vehicle (UAV) (Westoby et al., 2015; Clapuyt et al., 2015; Brunier et al., 2016; James et al., 2017a) and ground-based systems (James and Robson, 2012; Micheletti et al., 2015b; Prosdocimi et al., 2015). A prominent, newly developing platform to enable photogrammetry is the drone. There are some significant differences between UAV photogrammetry and LiDAR. UAV-based photogrammetry does not require the large, expensive UAVs currently necessitated

by LiDAR systems, but instead can collect imagery from lightweight, consumer-grade cameras mounted onboard UAVs. UAV photogrammetry has been demonstrated as a low-cost monitoring technique for measuring canopy heights and found that results showed a strong correlation to airborne LiDAR where tree density was low, however, where a closed tree canopy was present UAV measurements differed to height measurements collected in the field (Mlambo et al., 2017). The ability to perform these surveys at low altitude means that resolutions are greatly increased when compared to airborne or spaceborne imaging data. The resolutions obtained from SfM conducted onboard UAVs is similar if not slightly lower than ground-based SfM. Although UAVs are becoming increasingly public-owned, they have still not experienced the market saturation that smartphones have and are often limited in capability by restricted airspaces. They can also be affected by weather conditions such as high winds, and rain which could result in defective data or termination of the survey all together.

Where wind speeds are strong enough to ground UAVs, research has been conducted in Kite-mounted SfM techniques. One study attempted to utilise katabatic wind flows in the Andes, which proved difficult for powered UAVs to maintain flight in, as a mechanism to perform kite SfM (Wigmore and Mark, 2018). It found that the accuracy of DEMs that were generated using this technique were similar to 1 m DEM produced by aerial LiDAR in the area. However, the point cloud density was much higher allowing for finer-scale features to be measured. The study shows the success of unpowered kite systems in bad weather; however, the systems still face the same limitations from restricted airspaces implemented by the International Civil Aviation Organisation (ICAO).

Images are processed to produce 3D point clouds, however, to enable a real-world context georeferencing is needed which also serves as coordinate criteria for image alignment (James et al., 2017b). This usually requires the use of ground control points (GCPs) – identifiable features or targets that have a known position - to be used within scenery. If ground control is not established, then inertial measurement units (IMUs) attached to the camera can be used to measure camera orientation and relative positioning of the sensing device. Information collected from the IMU is run in parallel and combined with GNSS coordinate data for global positioning and correction. For ground-based photogrammetry, GNSS connectivity is often a problem if surveys are conducted in areas where obstructions to satellite connection are present (vegetation, buildings etc.). In a coastal environment this is usually not an issue due to the inherent nature of beach topography being free of restrictions from foliage and large man-made structures. If models do not need to be geographically referenced, then model scales can be determined by one or more known distance measurements within the scene, whereby distances that stretch across a large portion of the scene/object are best.

SfM has now been incorporated into many geoscience applications and tested extensively in a variety of scenarios. A few studies to mention are those covering a medium-scale environment, a scale that this study addresses. James and Robson (2012), assessed a 3 m-high cliff face that spanned 50 m in length, located at Sunderland Point, Morecambe Bay, U.K. The cliff face was poorly sorted glacial till that was undergoing slumping and collapse causing it to retreat. Here 3D reconstructions produced RMSE of 0.037 m on the control points when a GCP distribution that encompass the whole scene was used as control. This captures higher detail than

typical LiDAR surveys conducted by the EA along this section of coastline. In this study, an investigation was undertaken to determine the effects of GCP distribution on RMSE throughout the scene. The study highlights the sensitivity of geo-referencing when control is focused in one region – it displays the effect of extrapolated geometry away from the region encompassed by the control.

Prosdocimi et al. (2015) utilise ground-based SfM in the post-event analysis of agricultural drainage networks. Here, they detail the benefits of a low-cost method for monitoring volumetric changes in the Veneto floodplain. The study involves imagery derived from standalone cameras and built-in smartphone cameras and compares 3D products against products derived from a benchmark TLS DEM in a medium-scale environment. The scene of interest measured 30 m in length, and TLS reconstructed geometry contained error values ~ 0.01 m in the x and y axes, and ~ 0.005 m in the z axis when compared to GCP targets. The distance-from-bank was only about 7 m which explains the low error values acquired in this study. Interestingly, in this study the device that generated the lowest deviation in DEM topography when compared to the TLS DEM was an iPhone 5, which produced an SDE value in the order of ~ 0.03 m in relation to the TLS DEM.

These studies have shown SfM capabilities to perform beyond many of those currently achieved by other remote sensing methods. However, the extent of coverage which these studies have been tested on, do not achieve the same coverage as airborne or satellite remote sensing techniques, nor do they span the same cross-shore extent as beach profiles do. The nearshore environment is an area most prone to sediment loss, primarily from longshore, wave-driven transport (Wyre Borough

Council, 2004), which causes large shifts in sediment volumes immediately in front of sea structures (30–50 m offshore). It is at this scale that ground-based SfM has been proven to work effectively.

SfM has proven itself as a capable and scientifically useful 3D modelling. Due to the nature of the technique, low-bulk devices such as smartphones can be used to collect imagery which in turn allows for greater access to areas that would be inaccessible if using larger TLS instrumentation. The high-resolution imagery produced by present-day smartphones is able to generate point clouds with point spacings of <math><0.01\text{ m}</math>. Additionally to this, data acquisition times are relatively quick when compared to the same high-resolution laser scanning times of TLS. Furthermore, because the SfM procedure enable the use of portable, consumer-grade devices such as smartphones with inbuilt cameras for coastal monitoring it is an accessible monitoring method to most people. It is here, that the domain of citizen science can greatly enhance coverage capabilities currently achieved by ground-based SfM

2.4. The Coast in Context

2.4.1. Citizen Science

The collaboration between citizens and professional scientists in the field of scientific research is termed Citizen Science (CS). The extent to which citizens engage with the research can vary depending on the project goals and the framework setup by organisers. Government organisations are often symbiotic with scientific research and thus rely on their insight for strategy development across a range of domains. However, science is often limited by lack of human resources, and the failure to meet the scope of research needed for optimum decision-making. Additionally, if scientific research yields unfavourable outcomes, it is often the scientific community who are blamed for negative effects. This is only exacerbated by the chasm between the public and governmental/scientific communities. Citizen science initiatives are beneficial to society as they promote public understanding of science. The level of scientific understanding has raised concerns from scholars and led to new incentives to revitalise positive perceptions towards science. Many citizen science projects not only benefit academic research and strategy developments, but also enhance society by increasing awareness of the importance of scientific research.

It is here, that CS provides the potential to bridge the communication gap and empower citizens to become an integral part of decision processes. CS projects have become a prominent part of many areas of study including ecology, astronomy, palaeontology, archaeology and zoology (Lin et al., 2014; Anderson et al., 2002; Silvertown, 2009). CS projects have increased significantly since the dawn of a new

emergent technology – computing. The recent propagation of internet-connected smartphone technology has enabled a whole new domain of citizen-sensors (Haklay, 2013). This utilises the inbuilt sensors on smartphone devices: cameras, GNSS, accelerometers as well as the ability to programme apps that enable a refined data collection procedure. For this study, the inbuilt cameras are primarily of use along with the internet-capability offered by them to transfer data wirelessly.

2.4.2. Contributory Citizen Science

There are numerous citizen science engagement models, each with a unique set of skills and purposes. For this study, the CS project follows a ‘contributory citizen science’ model. This model spans a myriad of levels of engagement within itself from passive to more active approaches for citizen engagement. These style projects are most often designed by scientists to achieve scientific goals, however, they require a contribution from citizens. The model spans in breadth from passive engagement, where the participants have little if any physical or cognitive involvement but instead utilises crowdsourced computing power, and more active approaches usually involving physical or cognitive activity. An active approach such as Volunteered Geographic Information (VGI) can utilise current GPS capabilities to allow citizens to become sensors to their local environment (Haklay, 2013). This approach by-passes any needs for cognitive ability, which from a scientific viewpoint, is easier to collect results from. Instead, only information about the instrument is needed (i.e. GPS accuracy etc.). Alternatively, participants can upload geographic information of an area via dedicated web-based platforms such as OpenStreetMap (OSM, Wikimapia, Google MyMaps,

Map Insight and Flickr (Goodchild, 2007; Senaratne et al., 2016). This is a relatively sparse method for data capture and usually encourages participation from anyone for any location, with no need for prior knowledge. To allow for this style of information, the users' uploads are assessed by peers and against predetermined criteria to ensure the validity of data (ref).

Another method utilising human cognitive ability is 'distributed intelligence' (Haklay, 2013) whereby the participants carry out relatively simple tasks which are often difficult to replicate using machine intelligence. This is the model for engagement that has provided the foundation of citizen-led coastal photogrammetry. These citizen science projects usually require some basic training, then the participant carries out simple data collection tasks. It is these tasks that require cognitive intellect to achieve goals. Image collection as a source of data for coastal photogrammetry requires the application of a predetermined technique, however, requires it to be applied to a dynamic setting.

When coastal surveys are to be conducted by members of the public, there are two key groups to which survey objectives should be designed towards; active practitioner groups such as coastal community groups who regularly participate on coast related matters, and the wider public, who are a more dispersed a mixed social group. These groups can effectively address two scales in space and time; high-resolution, medium coverage and semi-frequent monitoring, and the wider public low resolution, high coverage and continuous monitoring. The two groups respond to information very differently, and the method of communication with them needs to be adapted to account for this. The active community groups are likely to already

possess a strong affiliation with the coast and therefore communication can be more relatable to the coastal environment, however objective and outcomes must be observable and understandable to maintain interest (see section 24). The wider public requires a broader approach to research objectives with simpler tasks to fulfil, but results do not have to be visible to the public. For this project, engagement with a coastal community group is the focus, as it provides a more thorough understanding of individual abilities and methods can be laterally translated for integration with the wider public.

2.4.3. The Contextual Model

If CS techniques are to be used in coastal monitoring, then special consideration towards social perceptions is needed to create an engaging framework for citizens to participate in. This section evaluates the effects of a contextual meaning that information has when being absorbed by the public and how it affects their perceptions towards scientific research.

The contextual model refers to the understanding that individuals do not simply respond to information as empty containers, retaining the whole volume of data provided. Instead, it incorporates the idea that the efficiency at which information is absorbed can be largely affected by individual current social and psychological states (Lewenstein, 2003). These states are shaped by previous experiences in a cultural context and from personal circumstances. When relating this in a coastal context, research outcomes and objectives need to mean something within

peoples' lives; loss of infrastructure, property damage and, commercial impacts all have effects on the residents' lives. It is these experiences that have often shaped public perceptions of coastal risk and develops their ability to absorb information. The model also understands that the attitude towards science or information of any kind can be amplified or dampened depending on modern social systems and media.

In a more general scenario, the 2016 Presidential Election was highly broadcast and has since been found to have had a huge increase in fake news in the 3-month prior run-up. These fake news stories are believed to have manipulated the public's view on current affairs, thereby changing the way information is recognized (Alcott et al., 2018). This is argued to have enhanced/impaired contextual meaning of policies and future plans put forward by democratic parties in citizens' lives. Although the extent to which misinformation affected the 2016 election is unknown (Alcott et al., 2018), it highlights the importance of the psychology of individuals and how their reactions can be shaped as a result of experiences they have with their environment. The ability to influence society through contextual meaning can be used as a major tool for the distribution of scientific knowledge.

A number of studies have identified how risk perception is greatly influenced by the context it has in personal lives and society. Krinsky and Plough (1998) reviewed a number of case studies whereby communities had been subject to water contamination. Although levels of contamination were of similar proportions, the reaction from the public differed between locations. Amongst other factors affecting their perception of risk, it was found that if residents discovered the contamination first and had to alert officials, then the following risk information received was often

met with distrusting perceptions. If, at the discovery of risk, other concerning issues are at play, then the response to risk can either be underestimated or overestimated, varying in magnitude and direction between social states. This is can be related to concerns over sea level rise, and government spending towards flood risk and disaster management in coastal areas. From these examples, it is suggested that by incorporating citizens within research, they would feel more empowered and therefore become a more integral part of the decision-making process. This would likely result in more confidence in scientific research from a more trusting public.

2.4.4. Lay Expertise Model

Citizens often contain large volumes of information that perhaps might have been overlooked by researchers or require long-term experience to understand and perceive. In areas of coastal development, citizens could hold information of their coastal environment that may be more applicable to a local setting. In this section, the lay expertise model is shown to have importance in the development of scientific study.

The lay expertise model has often been a subset of the contextual understanding model due to its similar ideology. However, it has been, on occasion, reviewed as a separate model. The contextual model regards scientific knowledge as a valuable asset but understands the complexities involved in delivering it, whereas the lay expertise model assumes that local expertise can be as relevant as scientific knowledge.

In one scenario the U.S. AIDS treatment activists – a diverse group of ‘lay experts’ – were established, and carry on to this day, as a credible participant in knowledge construction. This brought with it changes in biomedical research, and the subsequent attributed practices. The lay knowledge was implemented by way of a bottom-up approach. The lay expertise had always been present, though not structured in a scientifically practical manner. To engage fully within the realms of biomedical research, treatment activists had to learn the language and culture possessed by medical science. By doing so, their credibility was constructed, and their lay expertise fused into decision-making. Although this example was reverse-engineered by the lay people themselves, it signifies the success of unifying scientific and lay expertise into knowledge development. The same can be applied in a coastal community – communities who are immersed within the region of study, often have knowledge that has just as much relevance as knowledge derived from the scientific community. Integration of this understanding of the coast can benefit researchers by enhancing project efficiency and providing unexpected insight into investigations.

The lay expertise model is far from perfect, with itself being subject to criticism. Lewenstein (2003) identifies how the model favours local knowledge over the more reliable knowledge derived from the interworking engrained in the modern scientific system. For this reason, it can be described as “anti-science” (Lewenstein, 2003), and has been subject to dispute. This ideology is driven by the commitment to empowering local communities in decision-making. It is from this that participation within the data collection process is fundamental in engaging communities and, this being so, their local knowledge of the coastal environment can help frame an insightful and efficient project.

2.5. Validation of Citizen-Derived Data

2.5.1. The Purpose of Coastal Photogrammetry

The aim of citizen-led coastal photogrammetry is to have an additional source of data to those collected by existing monitoring methods. It is therefore apparent that accuracies of the 3D models obtained must be comparable with those obtained via traditional techniques. Also, this citizen-led method must be capable of providing useful information in regard to coastal processes in the small-, medium- and large-scales. The method of ground-based photogrammetry offers capabilities in the small- to medium-scale coastal environment; however, when paired with the concept of citizen-led coastal photogrammetry, large-scale monitoring is possible, for example, combining multiple monitoring groups over different stretches of coastline.

Along the Fylde coast, the primary losses of sediment are forced by longshore, wave-driven and tidal currents. However, cross-shore processes are equally important. As this an intertidal environment, shoaling, surf zone processes (e.g. wave breaking and resulting currents) and swash processes can take place immediately in front of sea structures and can extend out to 30–50 m offshore during storm events (Wyre Borough Council, 2004). The scouring around coastal structures such as seawalls and groynes take place at spatial scales of metres, however, smaller developing features can exhibit characteristics below <1 m (Bradbury et al., 2012). Scouring around groynes will take place along groynes at distances up to 100m. The artificial headlands on some seawalls along the Fylde coast are exposed to higher sediment

removal rates, and therefore experience lower beach levels and toe scour in these regions, again at several tenths of metres. This is a scale that is achievable from SfM surveying and has been performed by numerous researchers (James and Robson, 2012; Westoby et al., 2012; Ružić et al., 2014; Prosdocimi et al., 2015; Pikelj et al., 2018).

2.5.2. Measuring Accuracy of Reconstructed Topography

Accuracy is always important for any research project. However, the methods by which data quality is assessed are scrutinised in CS projects. Usually the aims of the project are to enable non-scientists to participate in at least one stage of the research process. Typically, this involves utilising imprecise, inaccurate data necessitating strict procedures to remove poor-quality data or implementing methods to prevent the production, or inclusion, of such information. In all scientific domains, accuracy plays a fundamental role in the validation of outcomes from a piece of research.

In the geosciences, topographical surveys rely substantially on the accuracy of data and the precision yielded by the instrumentation used to acquire it. Image quality can vary substantially when performing SfM photogrammetry. Although SfM algorithms are robust to changes in light conditions, camera parameters and non-ideal scene conditions, it is still useful to remove any defective imagery before processing photosets within SfM-based software (AgiSoft, 2016). Software such as Agisoft PhotoScan (AgiSoft, 2018) enables self-calibrating bundle adjustment to define camera parameters and orientation. Lens adjustments are made to identify the best-fit camera

model for each photoset. James et al. (2017a) inspected imagery by first identifying any outliers from the resultant sparse point cloud generated after image alignment has been performed. Visual inspection was also performed on residual error post-lens calibration to identify any particularly large vector errors, or if there were systematic image residuals. The presence of systematic error would suggest a poorly matched camera model and could require further parameter adjustments. From here dense reconstructions and DEM generation can follow.

The robust SfM procedure, ensure that as many sources of inaccuracy are removed. However, post validation of the 3D model is helpful to determine the deviation of model topography from real-world topography. The multitude of LiDAR applications and its longevity as a measuring tool has led to numerous studies being conducted utilising data retrieved from it as a benchmark. In a geomorphological context, some studies that empirically assess the accuracy of SfM photogrammetry include James and Robson (2012); Westoby et al. (2012); Prosdocimi et al. (2015); Clapuyt et al. (2015); Brunier et al. (2016).

Prosdocimi et al. (2015) compares DEMs from imagery taken by a range of imaging devices: A Canon EOS 5D Mark III, Nikon D3000 and an iPhone 5 and compares them to a DEM derived from TLS. The TLS equipment location was georeferenced using dGNSS and from this, the point cloud data was automatically georeferenced. This style of comparison - once validation through cross-checking known check point data with targets on the TLS point cloud has been performed – allows for each point in the cloud data to substitute as a check point (Prosdocimi et al., 2015), and thus allows for a fuller comparison. The point clouds were subsampled to a minimum spacing of 0.02 m to

make the models computationally wieldy and comparable with the TLS cloud. From here, unwanted point cloud data was manually removed using the open-source cloud manipulation programme CloudCompare (Girardeau-Montaut, 2003). These clouds were later interpolated to a 0.1 m (in x and y) resolution grid DEM using the natural neighbours method (Sibson, 1981). Here, 0.1m x 0.1m columns contain one value only, therefore removing excess data and producing a single-layer comparable cloud (Prosdocimi et al., 2015).

DEM comparison should be carried out in caution, however. James and Robson (2012), highlight the complications induced by the point cloud interpolation process. Although the resulting clouds produce a computationally more efficient and more wholesome comparison, issues can arise when comparing areas of high obliquity or vegetation cover. A coastal cliff located at Sunderland Point, Morecambe Bay, U.K. provided focus of study for analysis in the reconstruction process of 3D surfaces using a camera (James and Robson, 2012). Here, analysis was applied over different scales. Raw point cloud data showed differences in density and distribution. TLS data yielded a lower density but significantly more even distribution of points compared to those derived from SfM. High densities were focused around the vertical faces for the SfM clouds but lacked information around the crests of slumped material – areas with vegetation and high surface obliquity. TLS data did, however, return a more consistent spread of values within these SfM low-data regions. During the gridding process, large estimations were made on steep and vegetated surfaces, giving differences of up to 0.6 m – an inaccurate representation of true error.

When assessing the accuracy of point cloud data without the aid of a benchmark cloud, it is useful to use targets or features with known geospatial coordinates or permanent in-situ features with known relative positions as check points. These check points serve as reference markers with 'true' coordinates, which in the case of Prosdocimi et al. (2015), can be assumed to be each individual point in the TLS cloud due to sensor georeferencing. Ground control points (GCPs) to be used in bundle adjustment optimisation should be ideally distributed throughout the scene with special focus to encompass the area of interest (Agisoft, 2016). James and Robson (2012) investigate the loss of accuracy in point cloud data when GCP distribution is biased towards certain regions of the scene. This is especially important when scene conditions and circumstances limit GCP distribution. When GCPs were limited to the 3 most dispersed points (out of 8), it was found that the overall scale of the scene changed by 0.01% with RMSE increasing from 37 mm (using all GCPs) to 50 mm. When restricting GCP to just one end of the cliff, the scale changed by 0.17% and resulted in RMSE values increasing to 181 mm. This emphasises the importance of having well distributed GCPs and introduces the need to identify key thresholds in model accuracy for useful coastal monitoring.

Another factor to consider is the quantity of GCPs within a survey. In geomorphology the process of GCP setup can be laborious and time consuming. James et al. (2017a) conducted research into the efficacy of increased GCPs in a study. In the Souss-Massa-Drâa region of Morocco, an investigation into the quality and quantity of GCPs was performed by UAV to understand the effects that GCP quantities has within a survey. A comparison between RMSE values derived from GCPs used as control and check points was performed. It was found that the two were inversely proportional to

each other; as you increase the points used for control, the respective RMSE increases as they become more difficult to match in the bundle adjustment, however, the global model is better confined to a 'real world' form. Matching positions of the control becomes easier during bundle adjustment; however, global accuracies are less constrained and thus RMSE on the check points increases. James et al. (2017a) found that over a sample size of 30 GCPs, as you increase the number of GCPs used as control points the error on the check points becomes lower. However, it is evident that when 50% of GCPs are used as control points, the magnitude of error plateaus and minimal further accuracy is achieved. This has important implications not only for the time required for survey preparation, but more specifically for the interests of this thesis, it can be used as guidance for determining the ideal number of GCPs in a given scenario – the researcher would have to account for additional non-uniform spatial distribution of GCPs caused by the unique properties of any given scene.

In summary, SfM has the potential to be applied by the general public, however a strict framework and validation procedure would need to be implemented to ensure data quality. The ground control network should be appropriately designed to achieve suitable GCP distribution and quantity. With surveys conducted using either a configuration of GCPs, or a TLS survey, points of known coordinates can be established and used as reference for aligning point cloud data and measuring their respective accuracies. Where possible, a good framing of network control and a strict procedure for data filtering and quality assessment is required. This study aims to identify the quality of data derived from different devices and what effect on 3D reconstructions a change in control network structure has.

3. Methodology

3.1. The Volunteer Group and Study Site

3.1.1. The Study Site

The Fylde coast is a heavily defended coastline in northwest England, Lancashire. Historical developments of sea-side towns like Cleveleys close to the sea, require coastal defences. Several structure types were implemented along the coast in last 100 years or so: seawalls, revetments and groynes. Along the 26km stretch of coast between the Model Yacht Pond, Fleetwood and Lowther Pavilion, Lytham, 17km is protected by a seawall with 6km being additionally reinforced with sediment trapped by groynes (Figure 2f). This stretch of coast is subject to a macrotidal regime whereby spring tidal ranges experienced here can be ~10m. The beach around Cleveleys is host to a mixture of sand shingle with Shingle being more present at lower chainages. This stretch of coastline has been monitored by the Wyre Borough Council, taking beach profiles along the whole stretch at least once and mostly twice per year since the early 1990s (Miles, 2014). In 2006, the new seawall was built to replace the deteriorated seawall, and new groynes were built along the Cleveleys frontage. A video-monitoring system was introduced to monitor interaction of new structures with the beach (de Alegria Arzaburu et al., 2007; Miles et al., 2013).

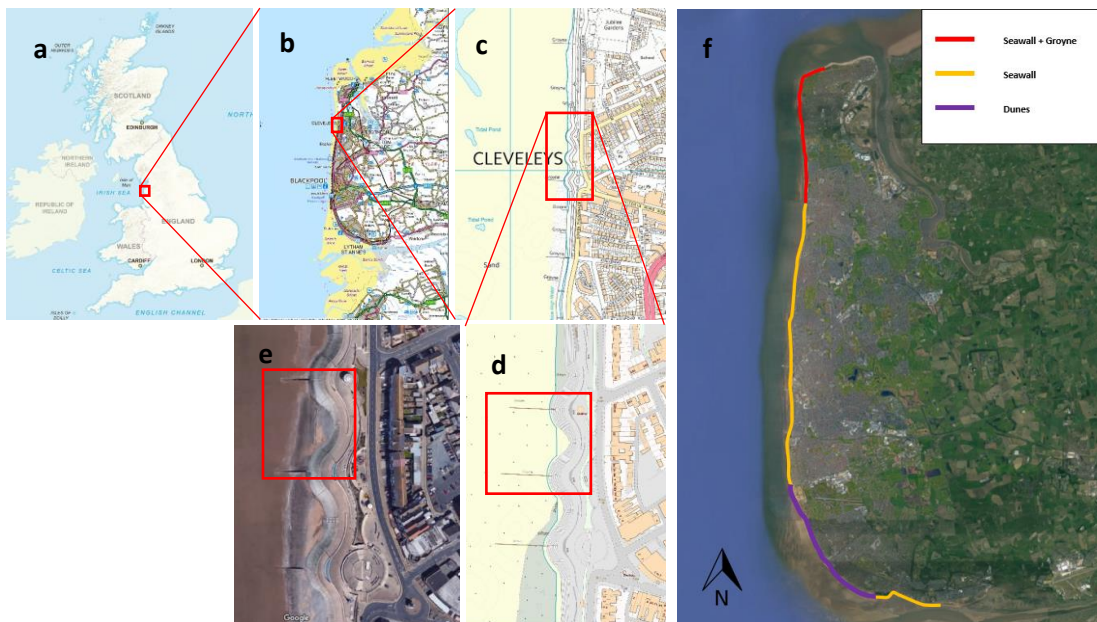


Figure 2 A progressively zoomed map of the location of the groyne cell used for study (outlined in red). It is bounded by a seawall and two groynes (a-d). (f) A satellite image of the Fylde coast displaying the sea defence types (red-seawall and groyne, orange-seawall only, purple- dunes). (a-d) - Ordnance Survey maps retrieved from diagmap.edina.ac.uk (e-f) – Goole Maps

The Cleveleys frontage provided an ideal test site. When choosing the site, three considerations were taken into account: i) beach changes that are of particular concern to the local authority, namely beach lowering near structures; ii) that the area of interest has dimensions that are appropriate to allow for imaging in a semi-convergent manner by foot and pose minimal risk to health; iii) that the area of interest has permanent features such as coastal structures, which are crucial to enabling the repeated georeferencing and comparison of derived models. A groyne cell measuring ~65m by ~80m (including a stepped revetment) was chosen as a suitable site for testing the feasibility of the method, repeatability and accuracy. The seawall is curved resulting in two artificial headlands (Figure 3) resembling pocket beaches studies by (Pikelj et al., 2018). It also allowed for the experimentation of different GCP

configurations. Most importantly, this combination of groyne and seawall includes features that occur in numerous locations along the Fylde coast and other parts of UK.

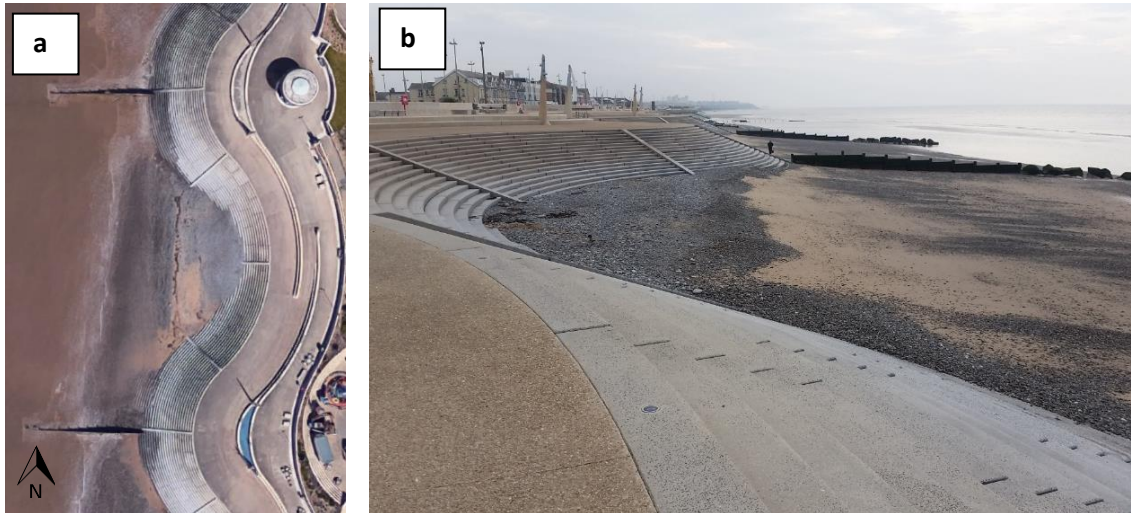


Figure 3 (a) An aerial image of the two artificial headlands. (b) An image taken from the northerly headland facing south.

3.1.2. The Volunteer Group

Members from the Rossall Beach Residents and Community Group were recruited for this study. The community group consists of 332 members on the social media platform Facebook, however, a group of 30-40 active members consistently take part in community events such as regular beach cleaning. The active members are ~30-70 years old with a large number of them being retired. The group is chaired by the SME project partner, which made establishing a point of contact with the group easier. There are approximately an equal number of female and male members.

It was decided to start with the active community group. This was preferred over the choice of the wider public as it is much easier to train a smaller group, assistance in the field could be provided more easily, and importantly, this group is more familiar with the beach. It is envisaged that once this group gains the necessary

skills for data collection, the data collection procedure can be taught to other members of the group.

For this study, there were two data collection sessions conducted, each with differing numbers of participants present. Table 2 shows the participation number for each session – the number of participants decreases due to prior commitments and inclement weather. The first session hosted an additional indoor session prior to data collection. This was designed to build understanding in the SfM procedure.

Table 2 The number of participants for each session (indoor and outdoor) and the dates they were conducted.

| Session | No. of Volunteers – Indoor Activity | No. of Volunteers – Outdoor Activity | Date (dd.mm.yy) |
|---------|--|---|-----------------|
| 1 | 18 | 12 | 10.09.18 |
| 2 | N/A | 5 | 25.10.18 |

3.2. The General SfM Workflow

3.2.1. Image Collection

The camera used to collect imagery should have a reasonably high resolution of 5 MP or more. To facilitate processing, the camera shouldn't have an ultrawide angle or fisheye lens and it is recommended that focal lengths should fall within 20 – 80 mm in 35mm equivalent (Agisoft, 2016). Lenses that have fixed zoom are preferred as they lead to more stable imagery taken.

Cameras with adjustable settings (some smartphones do not allow full control of internal settings) were setup as to allow for the maximum likelihood of successful model generation. Images were captured using the maximum resolution of the device where possible (e.g. tiff) to avoid the introduction of unwanted noise. The ISO value

determines the amplification of signal from the sensor in the imaging device – this was kept to a low value to minimise the amount of noise in the image (Brunier et al., 2016; Agisoft, 2016). The aperture value, or f-stop, was high (reducing the lens aperture size) to increase focal depth and help to ensure that the whole object/scene was in focus. Shutter speed was kept fast to remove unwanted motion blur where possible.

Once the camera settings had been correctly set, the next step was to ensure the object/scene conditions were as ideal as possible. The area of interest (AOI) was ensured to be relatively textured, helping for feature detection later in processing (James and Robson, 2012; Agisoft, 2016; Brunier et al., 2016; Hassaballah et al., 2016). Objects that are reflective or transparent do not process well and therefore should be avoided or kept to minimum – water and water-logged sand were kept to a minimum. Diffuse lighting conditions (e.g. cloudy skies) helped reduce reflection and shadows which helped feature detection as to provide optimal results. Objects that are near to the observer in the foreground can confuse software during geometry reconstruction so where possible these were avoided. Moving objects result in less accurate reconstructions or even result in a failed SfM workflow (Agisoft, 2016) – to address this, cameras were pointed away from pedestrians and other moving objects.

When capturing the imagery, as many photos as possible were taken of the scene. Is it better to have more photos than what might be required than too few. Effort was taken to minimise the number of blind zones in images as SfM software can only reconstruct geometry that is visible from at least two cameras. Images were ensured to contain the sufficient overlap between images as recommended by Agisoft – at least 60% - as feature detection algorithms require some extent of similarity

between images (Agisoft, 2016; James and Robson, 2012). The AOI took up most of the frame consistently between images within the photoset. In some cases, parts of the AOI were missing in some images, however, as they had been captured in at least two other images, they could still be reconstructed. When collecting the images, the images were parallel or converging towards the centre of the AOI to ensure the successful SfM workflow.

3.2.2. Reconstructing 3D Geometry

Once loaded into the SfM software the photoset needed to be aligned. Here, a Scale Invariant Feature Transform (SIFT) algorithm was run. These detect points in the source photos which are stable under lighting and viewpoint variations and generate descriptors for each point based on their local neighbourhood (Agisoft, 2016; Hassaballah et al., 2016). Using these descriptors, correspondences across the photoset were detected. Algorithms then solved the camera intrinsic (internal camera characteristics) and the extrinsic (location and orientation of the camera with relation to the real world) parameters. As part of this process, the object coordinates of the features were derived resulting in the sparse point cloud.

Using information derived during this sparse reconstruction step a denser point cloud was generated. SfM algorithms produced dense geometry by deconstructing 3D geometry into clusters using neighbourhood and camera parameter information from the SIFT process. This is called Cluster Multiview Stereo (CMVS) and was used as a precursor to the Patch-based Multiview Stereo (PMVS) algorithms (James and Robson, 2012; Agisoft, 2016; Brunier et al., 2016). Here, each points local neighbourhood was

mapped and small details preserved whilst outliers – points too far from a reasonable surface – were discarded (Yao et al., 2018). The resulting point cloud was much higher in density than the prior sparse cloud – this is called a dense point cloud.

Dense point clouds are inherently large in file size due to the high detail that has been preserved. To make the dense point clouds more computationally manageable, they were interpolated to DEMs. This interpolation procedure resulted in a systematic grid of x,y coordinates to be established and z (or elevation) values to be estimated for each corresponding x,y location. There were a few different interpolation methods available, however, this study used nearest neighbour (Sibson, 1981) interpolation. By subsampling the clouds to a lower density grid, the cloud size was dramatically reduced.

3.2.3. Georeferencing

To apply real world coordinates to a point cloud external measurements are required which were recorded through a GNSS survey conducted on non-moving features within the scene. These coordinates were used as an integral part of the geometry reconstruction process or used as check for model accuracy. Where there were permanent non-moving features present within the scene, a ground control point (GCP) network was setup as these were crucial for repeatability of SfM-derived results. GCPs were printed as targets with centroid positions that are visible across all, or most of, the photoset. The centroids were measured with high accuracy (± 0.02 m) by dGNSS or RTK GNSS equipment (Harley et al., 2011). For each centroid a true coordinate was assigned to it. Following the creation of the sparse point cloud the geometry can be

georeferenced using the recorded GNSS coordinates. The GCP locations were identified within the uploaded imagery and a best-fit position was then calculated from the photogrammetry – In Agisoft’s photogrammetry software, Photoscan, these virtual points are called markers. The markers were then assigned the real-world coordinates recorded by the GNSS equipment (Agisoft, 2016). To best fit the markers the model geometry underwent rotation, translation and scaling which maintains a linear transformation (James and Robson, 2012; Prosdocimi et al., 2015). At least 3 markers are required to align model geometry (to represent each x,y and z), however, in general more markers leads to a truer model position and orientation.

GCPs that were not used in this transformation procedure were used as check points as they represent points which have not influenced the georeferencing. At this point, error values were stated for the global model as well as for each individual check point. These error values represent the average closeness of all check points (global error) and of each individual check point to the true GNSS coordinate. For a better fit, a non-linear transformation was applied to the model using bundle-adjustment algorithms that optimize model geometry (James and Robson, 2012; Prosdocimi et al., 2015; Agisoft, 2016). This process still requires the use of markers in the reconstruction, and as error values were sought, check points were left out of the adjustments.

3.3. Pilot Study: Hest Bank

Before any sessions were conducted with any community members a pilot study was conducted to determine a suitable image capture technique for a shingle beach. The

survey was conducted in Hest Bank, northwest England. The location consisted of a shingle beach and a drainage outlet pipe surrounded by rock armour (Figure 4). The scene consisted of two major type of surface roughness: fine-scale shingle features and large-scale rock armour features.



Figure 4 Drainage outlet pipe, Hest Bank. Used as the scene for SfM image collection.

Both these surfaces did not provide any issue during the SIFT step in the SfM workflow. A Canon EOS 450 D was used for imaging the scene with settings that best matched those recommended (Table 3).

Table 3 Specifications for the Canon EOS 450D used for the pilot survey at Hest Bank.

| Device | ISO | Focal Length (mm) | F-Stop | Exposure |
|----------------|-----|-------------------|--------|----------|
| Canon EOS 450D | 200 | 28 | 10 | 1/320 |

Images were collected in a converging manner around the AOI with image locations at around 1m apart (Figure 5). An individual image would not cover the entire

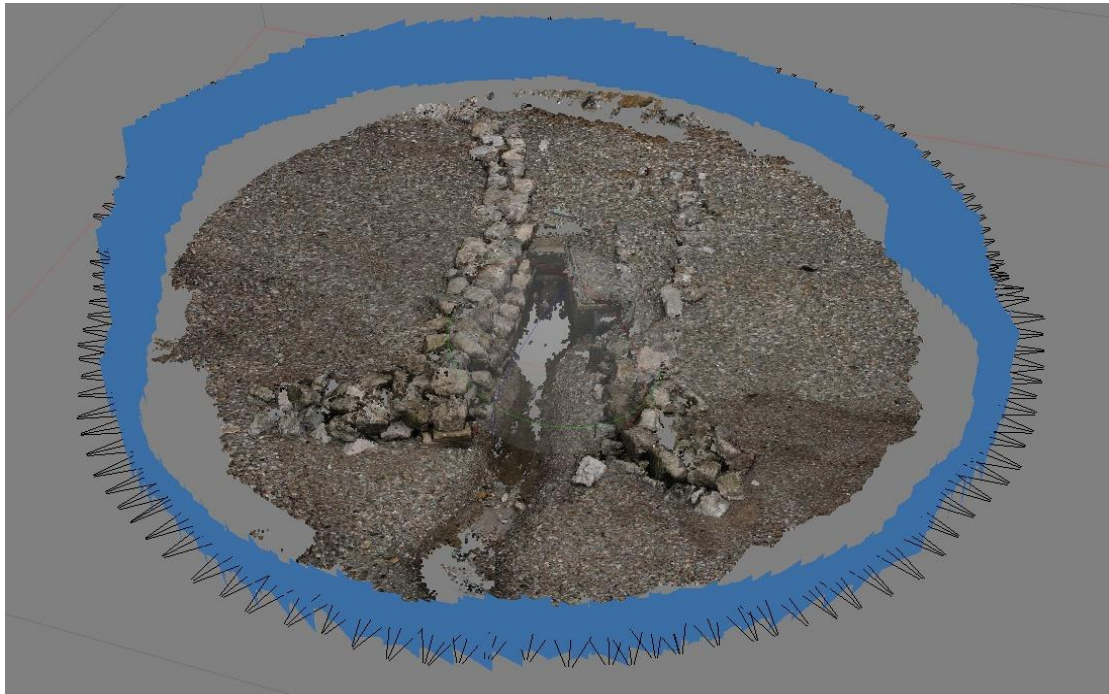


Figure 5 The dense reconstruction of the drainage outlet. The blue rectangles show each camera position.

scene, and thus 3-4 photos were taken at each spot. Weather conditions were cloudy, providing the optimal diffuse lighting required for SfM. The scene contained a small amount of running water beneath the opening of the drainage pipe which could have introduced some reflection, however, the diffuse lighting helped to reduce this.

There were ~400 photos taken during this session along one plane (a circular perimeter around the scene). Although at each photo point the imagery was divergent, to encapsulate to whole scene, the overall survey was convergent.

Processing of the imagery took in the order of hours as expected on a laptop with 16 Gb RAM and a Core-i7 processor. The dense point cloud was accurate and suggested the survey conducted with citizens should be spaced at 1m intervals, however, a convergent fully circular imaging procedure could prove difficult. This is

because the chosen groyne cell at Cleveleys would make it difficult to rotate through full 360 °.

3.4. Volunteer SfM Sessions

3.4.1. Building an Understanding of the Project

The engagement of the citizen group with the data collection started with informative introductory workshops on in Session 1 and 2.

Session 1:

The aim of this first session was to inform the citizen group of the aims of the project and current understanding of coastal processes, and to find out the motivation and lay expertise of the group. The 18 volunteers from the coastal group attended the workshop. Facts about climate change and the relevance a rising sea level has on coastal communities were disseminated, as well as an introduction into the methods of coastal monitoring posed by this study. The workshop enabled community members to interact with the researcher and the project partner. The aim was to form two-way interaction between the researcher and community by understanding the knowledge already attained by participants and their motivations, if any, towards coastal monitoring.

Next, a practical activity was conducted indoors to form familiarity with the image collection and processing. Information was provided on the technique for data capture, which, in theory, is transferable to large-scale scenery, although there are multiple hindrances that emerge as scale increases. The aim for volunteers was to generate 3D point clouds of small-scaled objects. Large rounded pebbles from the shingle beach were used -- Imagery was taken across a range of smartphone devices

and was ingested by the freely available SfM software VisualSfM (Wu, 2011) on laptops hosting dual Core i5 processors with 4 GB RAM (Table 4) to yield 3D products. The participants were advised to take 50-60 images of the object taking care of image overlap and different angles of view. Five laptops were used to process the images.

Table 4 Laptop specifications for 3D point cloud generation with the Rossall Beach Residents and Community Group.

| PC | CPU | GPU | CPU Clock Speed | No. of Cores | RAM | Processor Architecture |
|---------------------|---------------|-----|-----------------|--------------|-----|------------------------|
| Dell Latitude E5430 | Core i5-3210M | N/A | 2.5 GHz | 2 | 4GB | 64-Bit |

An additional benefit to VisualSfM is the real-time visual 3D reconstruction process. This helps public understanding of the mechanisms involved with the SfM pipeline and provides better understanding of the correct technique required for successful model generation. A concise set of instructions were designed and distributed among the participants prior to the outdoor session to facilitate useful image collection. They contained information on the ideal scene requirements, camera settings, imaging technique, data upload procedure and contact details for guidance. Objectives were set whilst on the beach for participants to follow and help and guidance were always available.

Questionnaires were distributed to the participants (see Appendix 5 – Feedback Questionnaire 1) during the outdoor activity (see 3.4.3) to get feedback on usefulness of the indoor session, their confidence in the procedure and view towards the continued monitoring method.

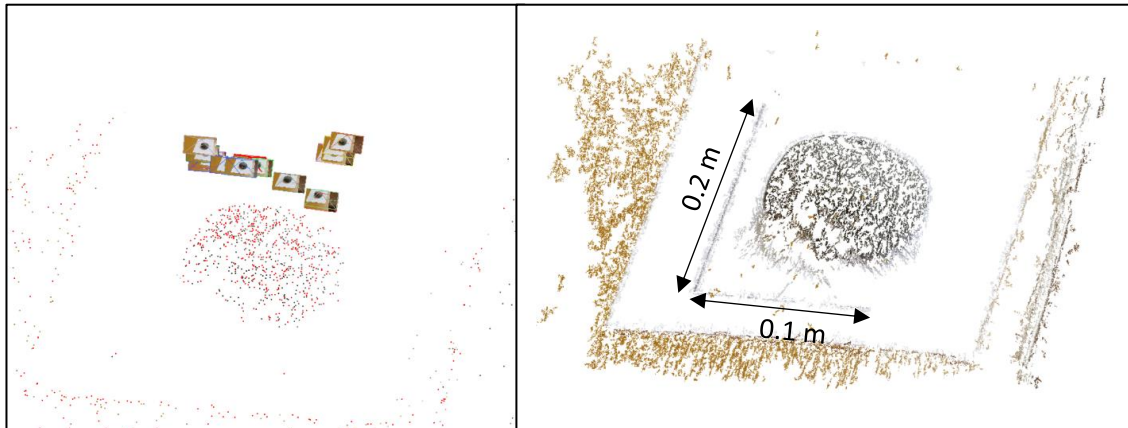


Figure 6 The SfM process displaying (a) the real-time image alignment procedure with the associated sparse cloud and (b) the dense reconstruction.

Session 2:

Feedback from the first session (see section 3.4.1) indicated that citizens did not find all parts of the indoor session interesting and relevant. For this reason, the indoor session was removed from activities conducted in the second session. Instead emphasis was focused on the technique for image capture rather than the method behind the processing of imagery. Visual and clear information packs had been created (Appendix 7 – SfM Instructions), informing the participants of a correct data collection procedure. Volunteers were handed information packs detailing the requirements for coastal photogrammetry.

The second session hosted fewer participants than before; only 5 volunteers were present for this session. A talk was given on the beach, however, a consistent cold wind reduced time on the beach and thus the briefing did not span the same amount of time as the first session. A description of features that are indicative of coastal erosion was communicated and a demonstration of the image capture technique was performed by the researcher. Guidelines on how to take the images,

what settings should be used, and the ideal scene conditions were all conveyed verbally and through the information packs provided.

3.4.2. Georeferencing: GCP Network Configuration

For easier comparison between the models produced by different participants and potential comparison with existing data, georeferencing was included. This required GCPs and thus positioning of targets or the marking of structures with visible yellow paint. The researcher placed GCPs prior to both sessions in a manner that best suits the recommendations from literature, although, an investigation into the effectiveness of non-conforming layouts is also performed. A conforming layout would suggest an enclosing distribution of GCPs around the scene/object of interest. GCPs were located throughout the scene, with efforts made to ensure coverage of the groyne cell in its entirety was accomplished. Usually measurements should not be made outside the area encompassed by the GCPs, as confidence in accuracies decrease substantially outside this zone (James and Robson, 2012). However, an investigation into the magnitude of error outside this area is implemented to determine rates of propagated error. Georeferencing can be achieved using a minimum of 3 targets, however confidence in cloud accuracies increases with GCP count (James and Robson, 2012). Hence here 67 GCPs were measured using an accurate dGNSS system. The dGNSS measurements were acquired using two Trimble R4 GNSS systems; one as a base receiver and the other as a rover (Figure 7).



Figure 7 (a) dGNSS base mounted on a tripod set to a calibrated height. (b) dGNSS rover mounted on a pole set to a calibrated height.

Session 1:

For the first session, ground control points were dispersed and relatively low in number. 17 GCPs were used for temporary placement on beach. Temporary cardboard targets measured 9cm/9cm for this session and were not laminated (Figure 8). Although a total of 17 GCPs were effectively within the scene, not all could be used due to visual obstructions when viewing from beach level thus limiting data retrieval and inclusion within the point cloud generation process. Figure 8 shows how GCPs located on the sediment traced the shape of the stepped revetment, whilst concrete dividers were used for identifiable features on the steps of the revetment – these were retrospectively assigned from measurements acquired in session 2.

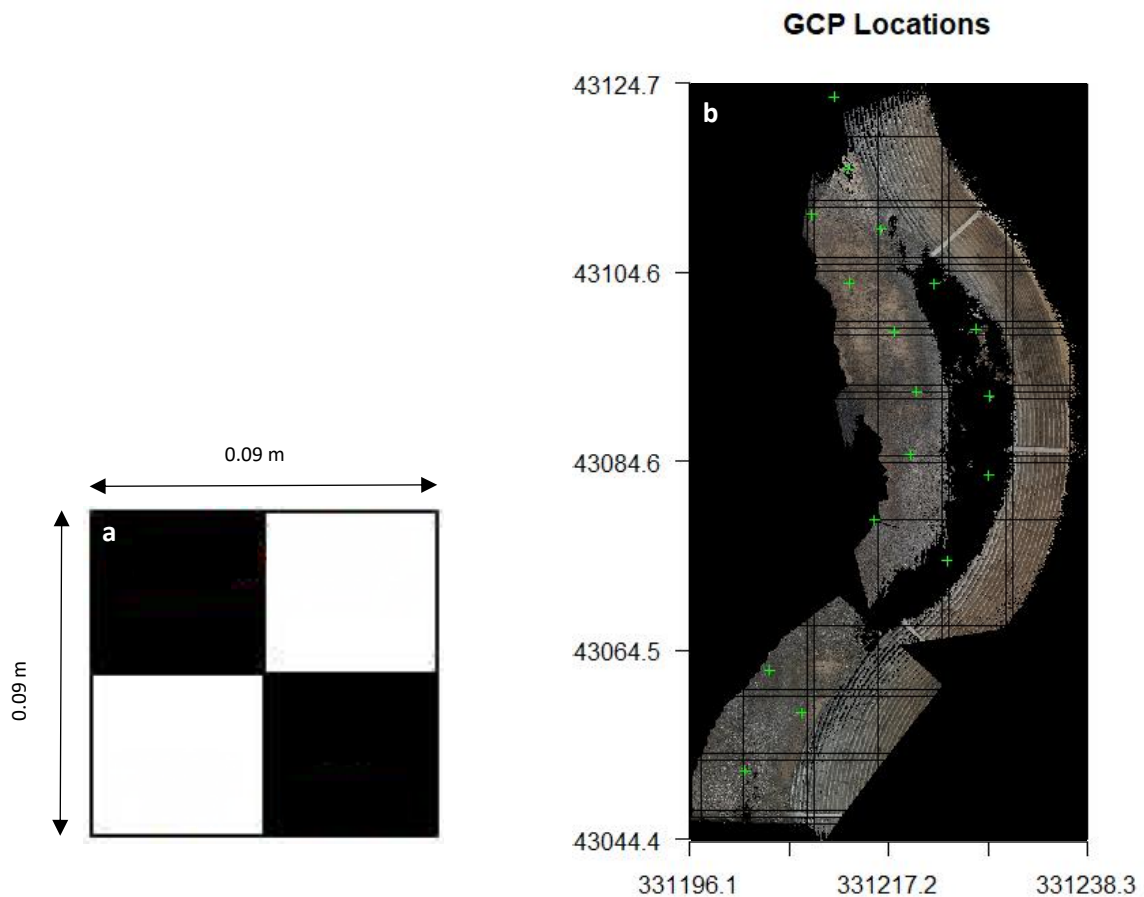


Figure 8 (a) A GCP target measuring 0.09 m/0.09 m used within the survey. (b) GCP Locations superimposed onto a DEM produced. Some GCPs are within the area of interest however appear in areas showing no data.

Session 2:

For the second session GCPs were laid out in a similar fashion, however, the extent of GCP coverage was greater both spatially and in quantity. In this session 67 markers were measured in total: 25 on the seawall, 27 on beach sediment, and 15 along the groynes. GCPs were distributed evenly throughout the scene to allow for variations in control point and check point configurations to be input into the processing software (PhotoScan) for georeferencing. Placement of GCPs followed the curvature of the stepped revetment with spacings of ~5m east-west and ~8m north-south. Targets used as GCPs were matt-laminated A4 coded targets downloadable from PhotoScan (Figure 9a). Due to the larger size used in this session, targets are more identifiable and were

easily marked in PhotoScan. Targets used on the groynes were spray painted yellow dots around ~ 0.07 m in diameter (Figure 9b). Spray paint was selected over A4 targets to improve setup time and better visibility. Figure 9c shows the spatial distribution GCP targets within the scene.

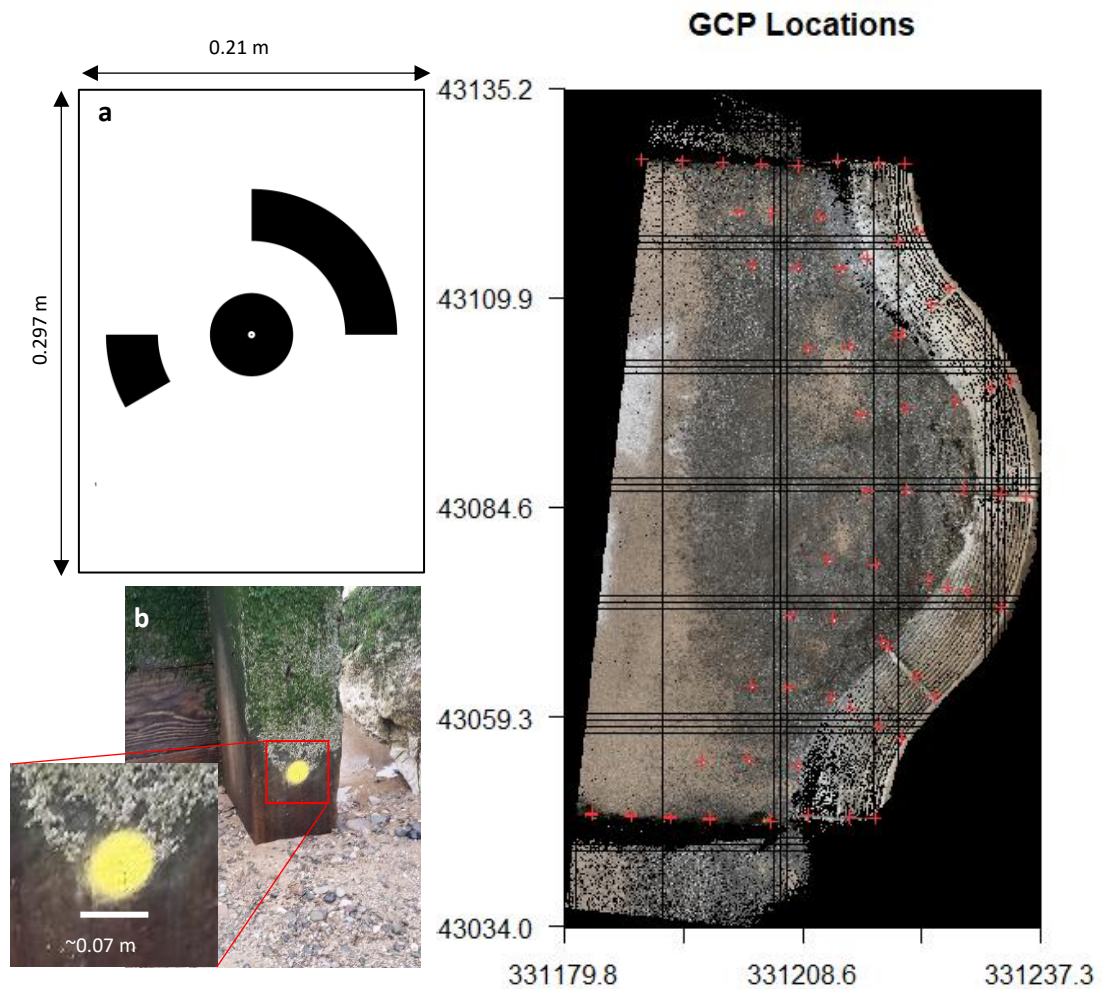


Figure 9 (a) An A4 coded target for use as a GCP. (b) Groyne post with a yellow paint spot for use as a GCP. (c) GCP Locations from session 2 superimposed onto a DEM produced from an iPhone 6s.

The 67 GCPs were assigned into 8 configurations to test a multitude of different GCP scenarios. Each scenario plays on the different characteristics of the groyne cell: a) the seawall wall, b) the wooden groyne, c) the beach sediment. Figure 10 displays the various configurations used in this study.



| Configuration | Points |
|---------------|---|
| Full | Starting from with Point 1, every other point |
| All Defence | ● + ● |
| All Seawall | ● Points only |
| High Seawall | ● Points only |
| Mid Seawall | ● Points only |
| Low Seawall | ● Points only |
| All Groyne | ● Points only |
| Low Groyne | ● Points only |

Figure 10 The groyne cell of interest. This figure shows the chosen configurations of GCP setup. The 'Full' configuration is a mixture of all types, starting from 'Point 1' and then every other point. 'All Defence' is constituted of all solid red and yellow circles. 'All Seawall' is all solid red circles. 'High Seawall' is shown in solid red circles with a yellow perimeter. 'Mid Seawall' is shown in solid red circles with a blue perimeter. 'Low Seawall' is shown in solid red circles with a green perimeter. 'All Groyne' is constituted of all solid yellow circles. 'Low Groyne' is shown in solid yellow circles.

3.4.3. Image Collection on the Beach

Session 1:

Participation numbers for the outdoor activity of session 1 declined from 18 to 12. This was due to various commitments that participants had and could not stay for whole day. Nevertheless, the 12 volunteers who did participate in the outdoor session, engaged with the data collection, followed the correct procedure and showed great enthusiasm.

They also coped well with a change in scale, from an indoor practice with a single object to a stretch of the beach. The data collection process here, refers to image capture on the beach.

Images were captured in a semi-linear fashion along the beachfront facing east towards the stepped revetment to help avoid surface reflections from waterlogged sand or sea. For this reason, the images did not encapsulate the full 360° of the scene (Figure 11). This design setup intended for maximum groyne cell coverage using relatively few images per participant. The group was split into 4 sub-groups, covering different segment of the beach. Each group's observation segment spanned ~20 m which covered the groyne cell (Figure 11). Images were collected at 1 m spacing facing the seawall, with 3 or more images taken at each location These had all different view angles.

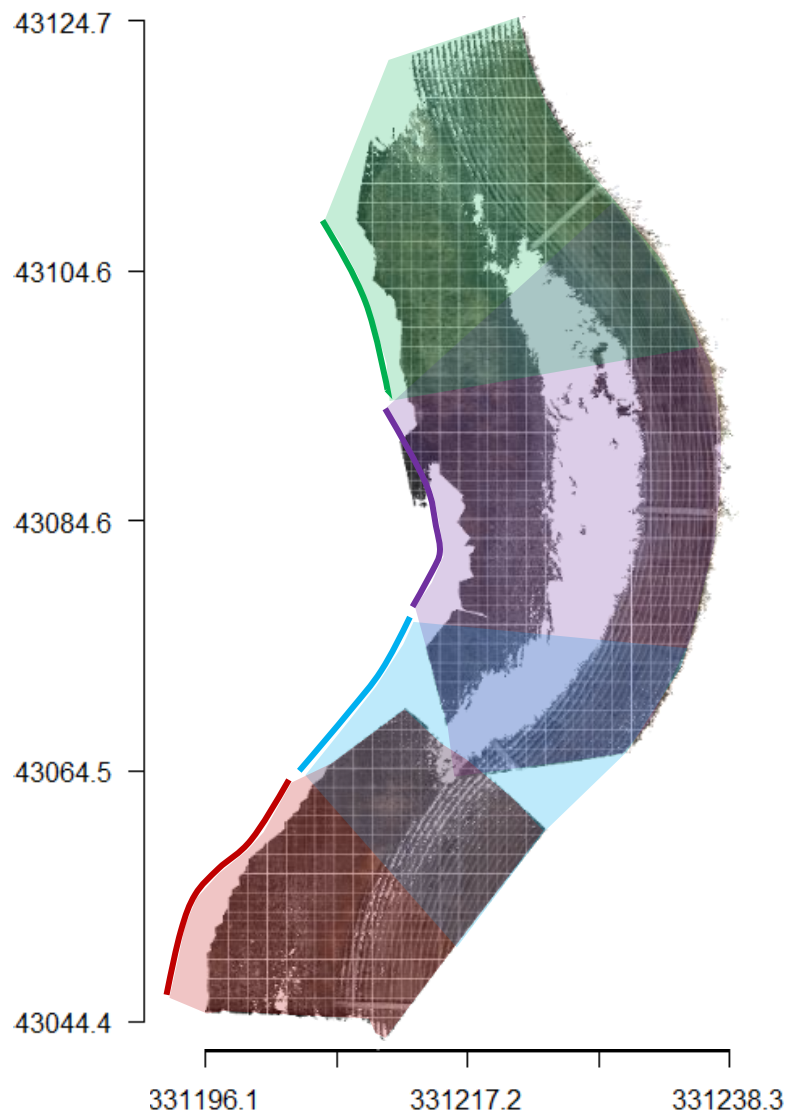


Figure 11 Segmented beach. Each colour represents a different segment of beach imaged. Green, purple and red segments were all successfully processed. Data for the blue section was not retrieved and thus no data was processed.

Session 2:

The second session hosted fewer participants than before, and thus a more in-depth engagement was able to be established. 5 volunteers were present for this session but due to better engagement there were more images collected by each participant. For

session 2, data collection was performed in a similar fashion to session 1, however, changes in imagery locations, orientation and quantity were made to improve on previous results. In this session the images were taken from the top of the stepped revetment facing west towards the sea (Figure 12). This was opted for to enable better view as images taken from the beach in session 1 were affected by presence of beach features e.g. berms/bars. Taking photos in this manner allowed for greater coverage of the scene from the respective viewpoints. Following the line of the seawall ensured that all participants follow the same track for capturing images.

The 5 volunteers were split into two groups of 3 and 2 participants. Each group started collection imagery from opposite end of the groyne cell (north and south). This was to reduce the chance of obstruction from volunteers within imagery. Citizens followed the same data collection procedure at 1m intervals, taking 3 or more images per location to cover the whole scene. Three of those participants had been present at the last session, so carried out the task with no issues. Two new participants did not require much assistance and performed the task efficiently after a few initial questions. Motivation from the volunteers was high, and the procedure was conducted as required despite a relatively strong persistent wind. The day was overcast and thus provided ideal light conditions for photogrammetry. Manual hard-wired data collection was instigated for this session due to the low volume of data retrieved from the last session.

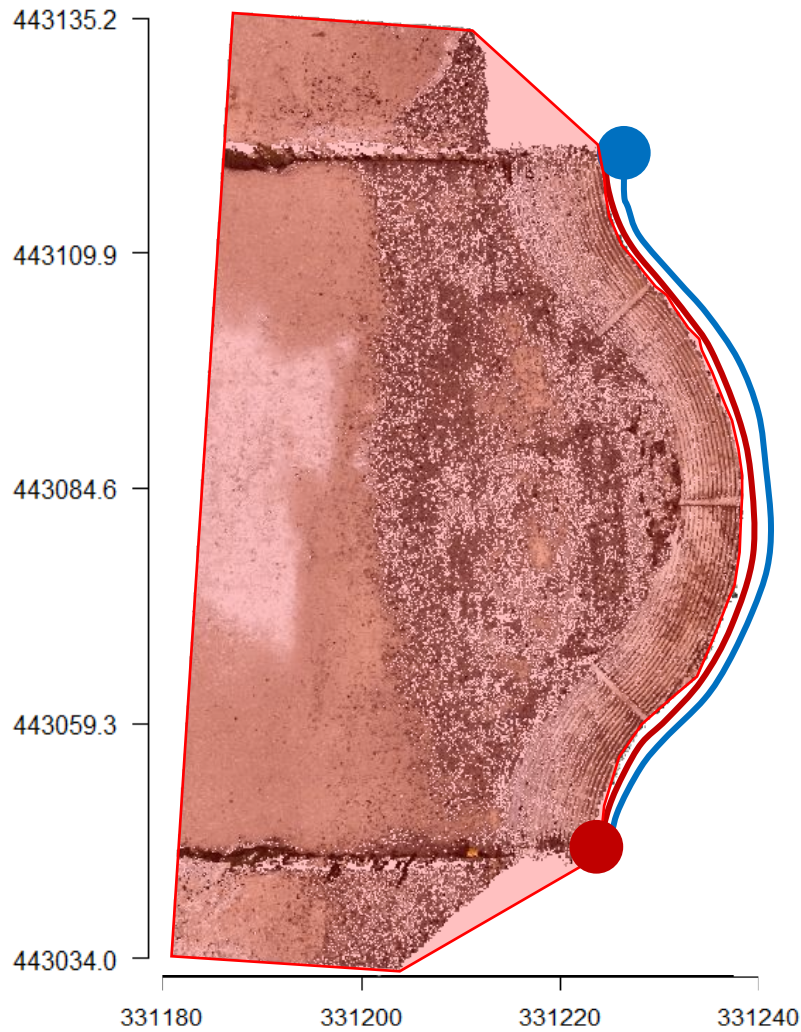


Figure 12 Area of coverage provided by each participant. Red and blue circles represent the starting point for each group. The red and blue lines display the route taken by each group.

Due to larger photosets the groyne cell was encompassed fully and a more wholesome volume of data was acquired. Due to substantial model overlap between participants in this session, cloud comparisons were now able to be performed. Alongside this, the higher number of GCPs present enabled variations in their configurations to be evaluated.

3.4.4. Data Transfer

Session 1:

Upon completion of the outdoor session, participants were asked to transfer their collected photosets. As part of the instructional package provided to those who attended the activities in session 1, details were provided on how to successfully transfer large image sets to members of the research team via the data transfer website wetransfer.com. This method required further participation of volunteers in their own time. It was necessary to send data via a data transfer website due to size constraints on files being sent from a typical email address. This added complexity to the transfer process which presented risks in further voluntary participation, and successful data transfer.

Session 2:

Data collected in session 2 was transferred immediately after the field session. This was to ensure the successful transfer of citizen data, rather than relying on the continued participation of volunteers. Data was transferred via micro usb data cables to a laptop near the study site.

3.5. Assessing the Volunteer Session

3.5.1. Image and Ground Control Quality

Visual inspection of imagery was undertaken to identify obvious low-quality data; large zoom, incorrect focus, motion blur etc. Images with these characteristics were

removed from the photosets to enable successful processing and reducing potential sources of errors in the models.

Due to the oblique nature of ground-based photogrammetry when observing gently sloping beaches, considerations into sources of human error when identifying centroids on GCP targets needs to be acknowledged. The software used in this study is Agisoft PhotoScan (Agisoft, 2018) and contains tools for the placement of markers at locations of GCPs (Figure 10) in the aligned images. This is used for removing markers with significantly large pixel error or spatial error. A value of 0.2 m was set as a threshold based on the resolution stated by the Environment Agency of a 0.25 m ground sampling distance (Environment Agency, 2018). 2D targets were preferred over the use of 3D targets for reasons of efficiency when measuring GNSS coordinates. This allowed for a greater number of total GCPs and therefore provided more flexibility when analysing the various GCP configurations.

A small but noticeable human error was produced when measuring GCPs on the lower section of groyne. Recordings for the low points were made on a vertical surface, and thus actual GCP locations were shifted by the radius of the rover pole – 0.015 m (Figure 13). Hence, GCP coordinates were corrected to account for an offset produced by the dGNSS rover pole diameter. Due to the north-south orientation of the Fylde coast, recorded GCP locations were easily corrected by changing the northing values only during post-processing. However, an incorrect measurement of the diameter of 0.01 m resulted in a 0.005 m semi-systematic error. The southern low groyne GCPs experienced a negative shift in northing by 0.005 m and the northern

groyne low GCPs experienced a positive shift by the same amount. These error values would cancel, and thus not affect the global model.



Figure 13 The rover pole measuring 0.03 m in diameter.

3.5.2. Assessing the Accuracy of Image Alignment

All images were processed using PhotoScan V.1.4.5 (Agisoft, 2018), which has robust algorithms that attempt to identify and construct camera models based on imagery ingested (Agisoft, 2018). Imagery was uploaded into the software and assigned the task of image matching and alignment. Here, PhotoScan identifies and tie points within imagery, estimates camera intrinsic and extrinsic parameters as well as projecting point coordinates and reconstructing surface geometry. It uses one camera model for each photoset, unless parameters are too discontinuous, for example large changes in focal length – in which case PhotoScan assigns a separate model. Focal length,

principal point coordinates, and the distortion parameters radial (K1, K2, K3) and tangential (P1, P2) are adjustment-enabled to minimise image residuals.

Once the 3D geometry has been reconstructed, a sparse point cloud was qualitatively assessed for any visual defects. Points located in 3D space are usually in the order of tens of thousands of points. The sparse point cloud was used to identify, GCPs and the model was georeferenced. Accurate GNSS data points collected in the field are manually located within the images, but automatically guided by PhotoScan by using the tool “Guided marker” approach. The software translates, rotates and scales the model to best match marker placements with the coordinates assigned, but does not account for non-linear misalignments. This is followed by optimisation of the model, in which the software utilises the GNSS data to perform non-linear corrections. Accuracy in model geometry is displayed as values of displacement between coordinates assigned to GCPs, which were not used for georeferencing and their GNSS coordinates. RMSE values are listed to describe the cloud’s overall accuracy; however, individual values are also important to assess how error differs spatially.

In session 1, 23-75 photos were used for processing (Table 12). In session 2, photosets ranged from 331 images to 679 (Table 13) and were processed on a Dell XPS 15 Laptop and a Dell Optiplex 790 with specifications listed in Table 5.

Table 5 Computer processing specifications

| PC | CPU | GPU | CPU Clock Speed | No. of Cores | RAM | Processor Architecture |
|-------------------|----------------|-----------------|-----------------|--------------|------|------------------------|
| Dell XPS 15 9560 | Core i7-7700HQ | NVIDIA GTX 1050 | 2.8 GHz | 4 | 16GB | 64-bit |
| Dell Optiplex 790 | Core i7 - 4790 | NVIDIA GTX 745 | 3.6 GHz | 4 | 16GB | 64-bit |

Sparse clouds were all done on the XPS 15 and dense cloud reconstructions were shared between the two computers. After image alignment was performed, the sparse clouds were assessed with respect to GCP coordinates. GCPs with excessive RMSE values were removed, as it was often due to inadequate marker placement due to oblique viewing angles and large distances in images meaning they were not representative of true GNSS coordinates.

3.5.3. Assessing the Accuracy of Dense Reconstructions

Once bundle adjustments were made to best-fit the model to GCPs, dense reconstruction could be performed in PhotoScan. Here, pre-set reconstruction parameters were selected to best suit the photoset and perform efficient and accurate dense point clouds without losing significant cloud quality (Table 6 and Table 7). These parameters govern the speed and quality at which 3D geometry is reconstructed.

Table 6 Device Processing Parameters

| Session 1 | | |
|------------------|----------------|------------------------|
| Device | Quality | Depth filtering |
| CUBOT MAX | High | Aggressive |
| CUBOT X15 | High | Aggressive |
| iPhone 6s | High | Aggressive |
| Galaxy S5 Neo | High | Aggressive |
| Galaxy A5 | High | Aggressive |
| Galaxy S5 | High | Aggressive |

Table 7 Device Processing Parameters

| Session 2 | | |
|------------------|----------------|------------------------|
| Device | Quality | Depth filtering |
| PL50 | Medium | Aggressive |
| iPhone 6s | Medium | Aggressive |
| CUBOT X15 | Medium | Moderate |
| iPhone X | Medium | Moderate |
| Galaxy S5 | Medium | Moderate |
| EOS 450D | Medium | Moderate |

For the purpose of this study, full-scaled imagery was not required for dense reconstructions and thus to maximise processing efficiency, a quality factor of medium was selected. This downscaled the images by a factor of 4 to enable efficient feature detection. The depth filtering was also applied to remove outliers in the cloud, reducing the chance of these being included in the analysis stage. For each data set, a different filter was used. An aggressive model was used first but if required long processing time (e.g. couple of days) it was replaced by a moderate depth filter.

3.5.3.1. Cloud Preparations

Upon successful completion of 3D geometry reconstruction, the models are inspected visually to identify any prominent defects. Excessive 'noise' generated during processing is visible in both the sparse and dense point clouds, however, it becomes more obvious after dense reconstruction. Where unwanted artefacts or objects are present, cropping can be performed in either PhotoScan or CloudCompare by using polygon selector tools to manually remove data. CloudCompare is useful if multiple clouds require cropping, and hence was chosen for cloud manipulations. Clouds were uploaded into the software and collectively selected, whereby data removal was efficiently performed and clouds with identical boundary limits were produced.

To compare clouds, DEMs were generated in the x,y plane and sampled to uniform grids to ensure the data was computationally manageable. This was done through CloudCompare, as it provided a few options on the interpolation process. Despite models showing defects below the scene of interest, the elevation value

chosen for each cell was based on values with the average height and tested – this was achieved using the nearest neighbours method.

3.5.3.2. *Measuring the Effect of GCP Configurations*

By optimising geometry using different control point combinations, the extent of spatial error was tested. Configurations were selected to utilise GCPs on the beach and structure at first, and then just those on structures. In total, 67 GCPs in an area of 80 m x 70 m were used. Although attempts were made to produce 8 GCP configuration models per device, not every model was successfully completed - Table 8 shows the successful GCP models generated. Those GCPs which were not used for georeferencing, were used as validation points. Table 9 shows the number of GCPs used as control and check points in each variation of GCP distribution.

Table 8 Successful dense reconstructions for each device and their respective GCP configurations. Successful reconstructions are indicated by an 'x'.

| Camera | Full set of GCPs | All Defence | All Seawall | High Seawall | Mid Seawall | Low Seawall | All Groyne | Groyne Low |
|---------------------|-------------------------|--------------------|--------------------|---------------------|--------------------|--------------------|-------------------|-------------------|
| Samsung PL50 | X | X | X | X | X | X | X | X |
| iPhone 6s | X | X | X | X | X | X | X | X |
| CUBOT X15 | | | | | | | | |
| iPhone X | X | X | X | X | X | X | X | X |
| Galaxy S5 | X | | | | | | | |
| EOS 450D | X | | | | | | | |

Table 9 GCP configurations and their respective control and check point counts.

| GCP Configuration | Max Number of Control Points | Check Points |
|--------------------------|-------------------------------------|---------------------|
| Full Distribution | 53 | 14 |
| All Defences | 40 | 27 |
| All Seawall | 25 | 42 |
| High Seawall | 9 | 58 |
| Mid Seawall | 9 | 58 |
| Low Seawall | 7 | 60 |
| All Groyne | 15 | 52 |
| Low Groyne | 10 | 57 |

Additionally, the difference in DEMs obtained by using reduced set of GCPs and the DEM obtained by using 'Full distribution' GCPs was calculated. As there were no other measurements taken at the same time, it was decided that the most accurate cloud obtained from check-point validation should be used as the 'benchmark' for other comparisons to be made. The RMSE values were exported from PhotoScan or CloudCompare into R Studio for statistical analysis. Histogram analysis, kernel density plots, linear regression analysis and associated GCP distribution data were collated in R Studio.

3.5.3.3. Measuring the Effect of Different Imaging Devices

Matching DEMs obtained from images obtained with different mobile device allows for differences in models to be visualised and quantified. Each device had a different set of internal settings for: ISO values, focal lengths, f-stops and exposures. For

smartphones this is unable to be adjusted manually, and therefore tend to be camera specific in this study. For all devices, the exposure times vary within the photosets themselves; due to a fixed f-stop and ISO value. Summary of the devices used and their parameters are given in Table 10 for Session 1 and Table 11 for Session 2.

CloudCompare was used for visual inspection of DEMs and to calculate DEMs' difference (DoDs). Statistical analysis of elevation differences and spread of errors are undertaken using R Studio such as histograms analysis, and linear regression analysis.

Table 10 Camera details displaying the various internal setups for session 1

| Device | Type | ISO | Focal Length (mm) | F-stop | Exposure |
|-----------------------|------------|-------|-------------------|--------|----------|
| CUBOT MAX | Smartphone | 57 | 3.5 | 2.4 | Varied |
| CUBOT X15 | Smartphone | 60-66 | 3.5 | 2.2 | Varied |
| Samsung Galaxy A5 | Smartphone | 40 | 3.6 | 1.9 | Varied |
| Samsung Galaxy S5 Neo | Smartphone | 40 | 3.7 | 1.9 | Varied |
| Samsung Galaxy S5 | Smartphone | 40 | 4.8 | 2.2 | Varied |
| iPhone 6S | Smartphone | 25 | 4.15 | 2.2 | Varied |

Table 11 Camera details displaying the various internal setups for session 2

| Device | Type | ISO | Focal Length (mm) | F-stop | Exposure |
|--------------|------------|-------|-------------------|--------|----------|
| Samsung PL50 | Camera | 100 | 10.5 | 3.7 | Varied |
| iPhone 6s | Smartphone | 25 | 4.15 | 2.2 | Varied |
| CUBOT X15 | Smartphone | 60-66 | 3.5 | 2.2 | Varied |
| iPhone X | Smartphone | 16-20 | 6 | 2.4 | Varied |
| Galaxy S5 | Smartphone | 40 | 4.8 | 2.2 | Varied |
| EOS 450D | DSLR | 200 | 27 | 6.3 | Varied |

4. Results

4.1. Evaluation of Session 1

4.1.1. Summary of the Obtained Models

From images obtained in the first session, 6 point clouds were successfully obtained. Five of these were based on images from the participants and one is from the researcher (Samsung Galaxy S5). This was lower than anticipated and was mainly due to data transfer problems as some participants did not send the data. However, all 6 models had successful camera parameters and geometry solved by Photoscan – parameters which allow for the projection of points in 3D space and therefore arising to a 3D model. About 23-75 images were used for reconstruction (Table 12). The models derived for each of the four beach sections (Figure 11) were successfully merged in CloudCompare. Table 12 gives a summary of devices used, number of images and derived dense point clouds.

Table 12 Device specifications from session 1, images aligned, and dense point clouds generated from aligned images. Clouds reconstructed in PhotoScan.

| Device | No. Images Aligned/Total Input | Dense Point Cloud |
|-----------|--------------------------------|---|
| CUBOT MAX | 23/25 |  |
| CUBOT X15 | 49/49 |  |

| | | |
|-----------------------|-------|--|
| iPhone 6s | 75/75 |  |
| Samsung Galaxy S5 Neo | 49/49 |  |
| Samsung Galaxy A5 | 43/43 |  |
| Samsung Galaxy S5 | 44/44 |  |

Optimisation of image tie points (sparse point cloud) was not performed as many of the GCPs points were obscured by beach features such as berms and could not be identified. The effect of taking images from the beach, is clearly illustrated in the dense cloud points (Table 12 and Figure 14) where white patches show areas with no data. This is due to a presence of a high berm and a channel feature behind it.

Due to missing data and GCPs being out of view, RMSE values between the reconstructed coordinates and true coordinates were not calculated. Instead qualitative

observations were made. There were few outliers in the dense clouds, but these were easily removed, and the segment clouds were successfully merged.

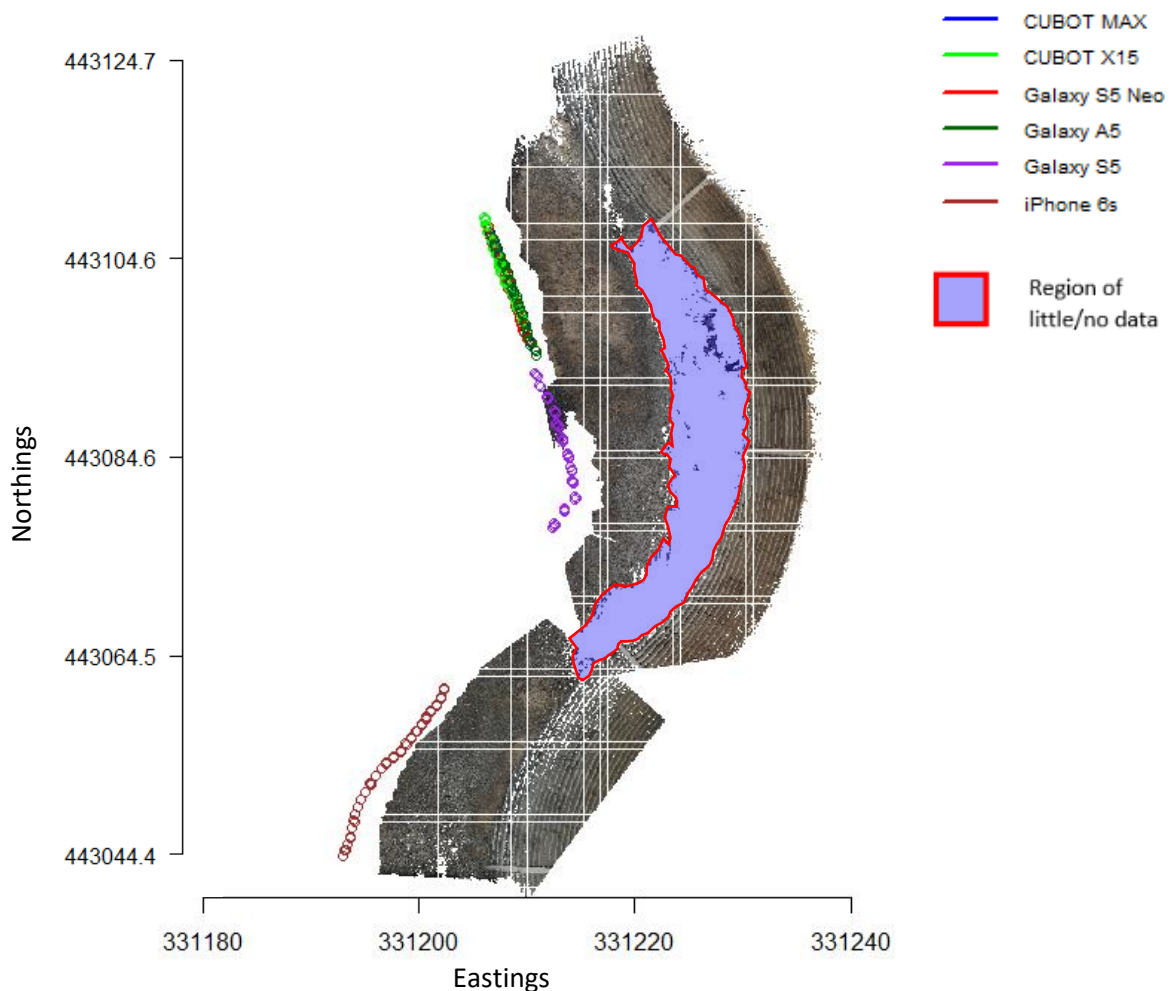


Figure 14 Camera positions superimposed onto a DEM of the merged point clouds. Not all data was retrieved from each volunteer – hence a discontinuity in camera positions. The purple region outlined in red shows the area obstructed by the berm.

Several important lessons were learnt in this pilot study. GCPs need to be placed on the beach or surrounding man-made structures or natural rocks taking care that they are visible from all locations from which the images are taken. Also, it is much better to take images from higher-up locations than from the lower beach as it reduces oblique viewing

angles. A pole can provide another solution to reduce the oblique viewing angles and might need to be used where accessible elevated areas are not present.

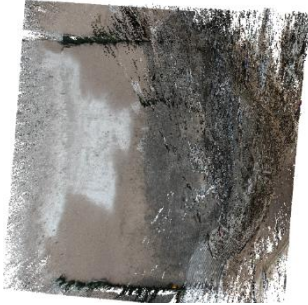
4.2. The Evaluation of Session 2: 3D Models

4.2.1. Image and Tie Point Analysis

Imagery from session 2 provided coverage of the whole scene. Photosets ranged from 331 to 679 images (Table 13). The volume of data per participant had grown by an order of magnitude from Session 1, yielding far more flexibility for analysis. However, the alignment process was not straightforward for each device.

Table 13 Devices from session 2, the number of images aligned, and the dense point clouds generated from the aligned images. Clouds were reconstructed in PhotoScan.

| Device | No. Images Aligned/Total Input | Dense Point Cloud |
|----------------------------------|--------------------------------|--|
| Samsung PL50 (Digital Camera) | 358/358 |  |
| iPhone 6s | 332/332 |  |

| | | |
|-----------------------|---------|--|
| iPhone X | 331/331 |  |
| CUBOT X15 | 679/679 | N/A |
| Samsung Galaxy S5 | 394/394 |  |
| Canon EOS 450D (DSLR) | 423/423 |  |

Upon visual inspection of the imagery provided by the participants, there were no obvious defects in each of the datasets. Pedestrians and other participants did appear in images, but only a relatively small portion of the photos, which due to robustness of the PhotoScan (AgiSoft, 2018), did not affect the models.

Images obtained by all listed cameras, except the CUBOT X15, underwent successful image alignment with minimal human input into the procedure. Time spent on feature-

detection-and-description generation and image alignment for these devices ranged from ~21 minutes (331 images from the iPhone X) to ~1 hour and 38 minutes (358 images from the PL50). The same processing for the CUBOT X15 took 2 hours and 15 minutes (679 images) but required manual intervention before full 3D geometry could be fully reconstructed. As the 3D reconstruction had not been fully successful, guided marker placement was not accessible through PhotoScan. This meant the visual input of markers in a sample selection of images from both the unsuccessful alignment and successful alignment to provide PhotoScan with a guide for feature detection. The alignment step was then re-run with these markers as guidance and the model geometry reconstruction was completed successfully.

Tie points produced from the alignment stage did not appear to show any immediately obvious defects. A disperse number of tie points had been incorrectly generated in areas without features, but these appeared mainly in regions of imagery containing sky, where outliers are expected due to instrument sensitivity.

Figure 15 shows average image residuals vectors derived by PhotoScan from each participant's device. When visually inspecting average image residuals, some devices showed systematic errors, which reflect complex radial distortion patterns that could not be completely modelled by the 4-parameter-lens model in PhotoScan. Despite this, the models did not have immediately obvious visual defects. Figure 15a shows that the PL50 is the only camera to contain randomly distributed and orientated image residuals which suggests it is the model that has been most accurately calibrated. Figure 15a, b and f all display minimal residual error and therefore the PL50, iPhone6 and EOS 450D are assumed to be well calibrated. The remaining models show systematic errors and larger residual

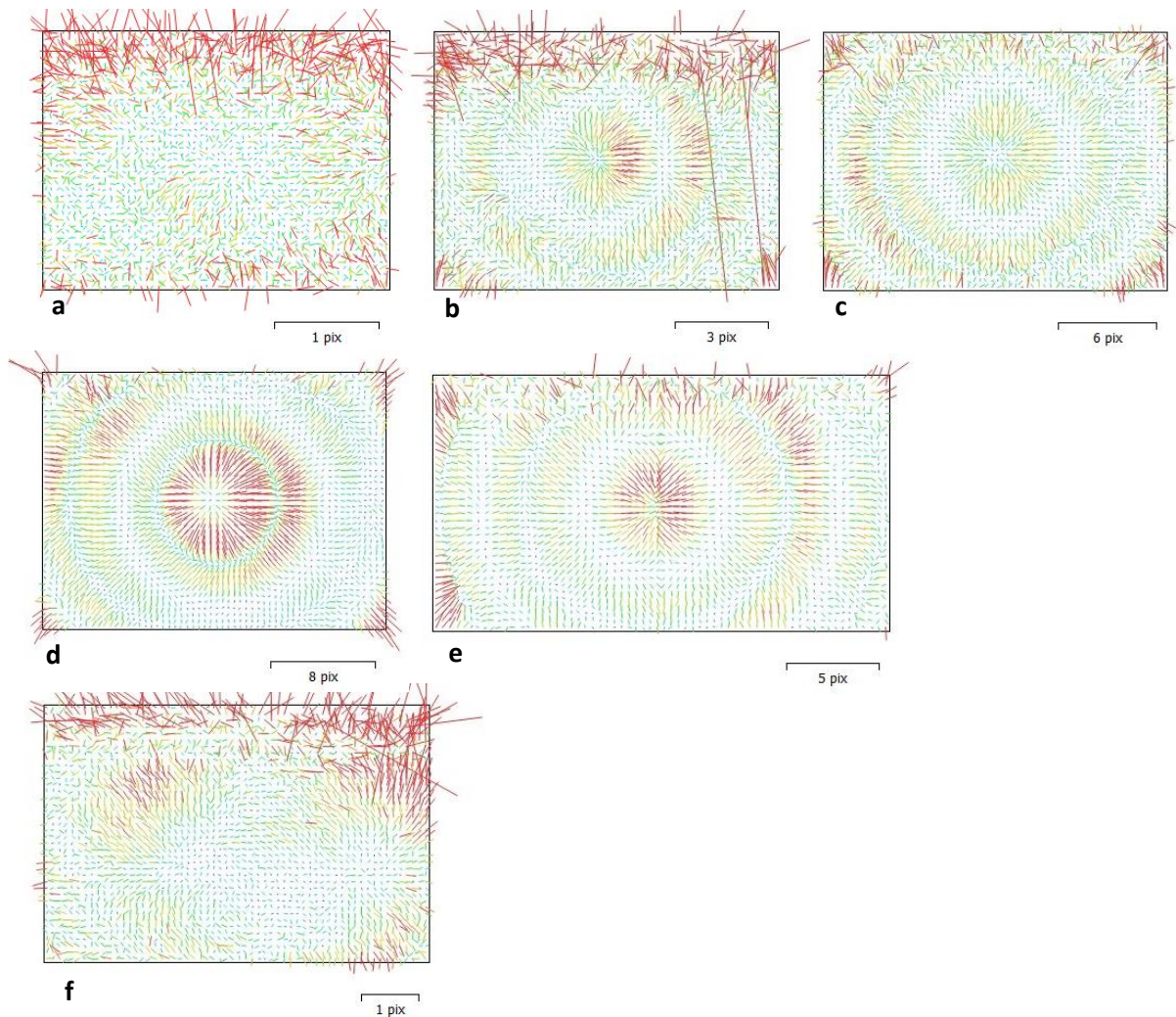


Figure 15 Image residual vectors from each participant's device. These are representations of how each point on the image correlates to a real-world point (each axis is an arbitrary spatial axis with the scale shown in pixels). Different camera models can be applied and are usually radial. A well calibrated camera model should produce small and image residuals in a random distribution (caused by noisy photos). (a) PL50 (b) iPhone 6s (c) iPhone X (d) CUBOT X15 (e) Galaxy S5 (f) EOS 450D. (a) Reprojection errors are random and concentrated around image regions with smooth/waterlogged features. (b), (c), (d), (e) and (f) show systematic reprojection errors suggesting an incorrect camera model. (a), (b), (c), (d) and (e) are all taken by participants. (f) was taken by the researcher. (a) and (f) are standalone cameras.

errors magnitudes. Figure 15d shows larger residual error for CUBOT X15 than other camera model estimations and would therefore be expected to generate the least accurate model. A camera model with a large residual error would suggest that the model produced would be lower than that with a lower residual error. This is a photogrammetric cause for inaccuracies, however, more can be introduced further in the SfM workflow.

For some of the image collections, photos had been collected using the variable camera parameters. For example, the Samsung PL50 and iPhone X, focal lengths had been changed in a small proportion of images. However, SfM algorithms are robust towards minor image scale changes and hence the images were not rejected for matching and alignment (Micheletti et al., 2015b). The effects to model accuracy were minimal.

The problems with GCPs locations and their visibility were not present in session 2. However, there were some small issues with GCPs, which were corrected throughout the processing of images. While deploying and surveying 2D GCP targets made surveying more efficient, the 2D targets suffered from oblique viewing angles at the extremities of the area of interest (Figure 16). Oblique viewing angles combined with increasing distance from the camera made centroid detection difficult (see Figure 16 and Figure 18).

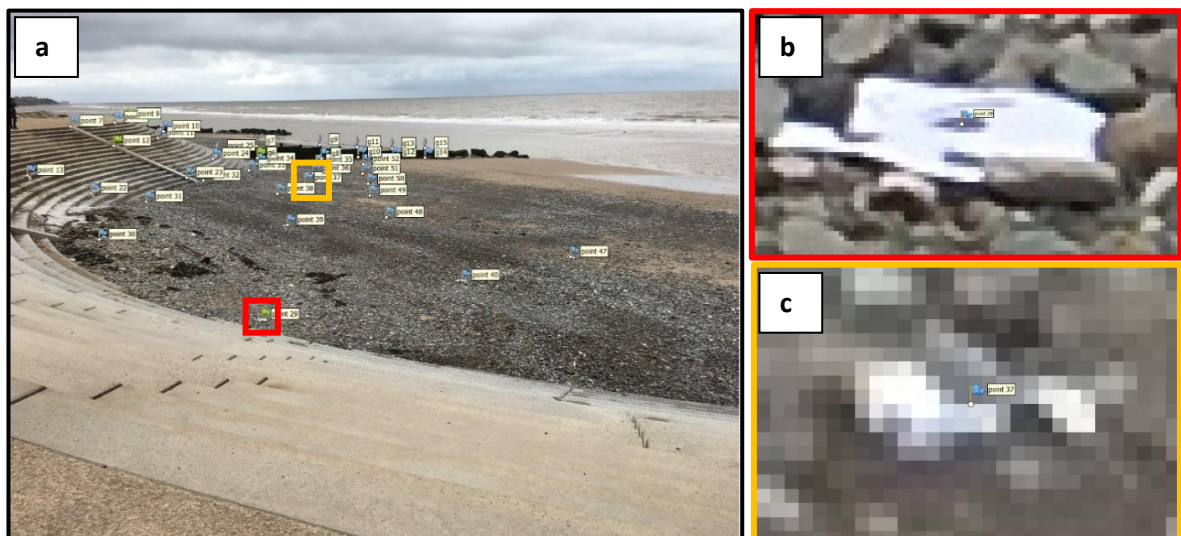


Figure 16 (a) An oblique image taken on an iPhone 6s showing the positions of 2 GCP targets. (b) and (c) GCP targets showing oblique pixelated centroids.

4.2.2. Optimisation and Tie Point Error

To further refine geometry, non-linear corrections were made through bundle adjustment to minimise x, y and z error values on the control points. When GCPs with associated GNSS coordinates are inserted into the software, bundle adjustment attempts to best fit the model to the coordinates provided for the control as well as refining the camera model. From this, it yields an error value based on how closely the model fits the coordinates, which is an average of the RMSE values on each GCP. To assess global accuracy, check points must be established as an external comparison source. GCPs, for which the match between the model and affiliated GNSS coordinates had an RMSE of >0.2 m, were removed from point clouds and re-optimised. However, lower values were also removed if they appeared anomalous to the rest of the GCP error for a particular model. The GCPs removed for each device are listed in Table 14 with associated locations displayed in Figure 10.

Table 14 GCPs removed from geometry calculations due to RMSE values beyond the threshold

| Device | Groyne point ID | Sediment/Seawall Point ID | Total No. Removed |
|-----------|-----------------|---------------------------|-------------------|
| PL50 | | 1,5,7,10 | 4 |
| iPhone 6s | | 1 | 1 |
| iPhone X | | | 0 |
| Galaxy S5 | | 1,9,10,17,24,25,34,35 | 8 |
| EOS 450D | 5 | 18 | 2 |

4.2.3. The Effect of GCP Configuration on Model Accuracy

In this section models were produced from each GCP configuration listed in Table 8. The same procedure as described in 4.1.1 was followed for each configuration. The RMSE values for each configuration in are shown in Table 15. Each RMSE value in the table is an average across the full control point (points included in geometry calculations) or check point (points excluded from geometry calculations but used as a test of model accuracy) range of GCPs. The RMSE is a measure of how well a model is fitted to the recorded GCP coordinates in the real world. The values are not attributed to a single dimension but instead are magnitudes of error in any direction from the GNSS position to the nearest point on the DEM surface.

Table 15 All device configurations and their respective average RMSE for control and check points

| Device | Cloud Name | Average Control RMSE (m) | Average Check RMSE (m) |
|-----------|-------------------|--------------------------|------------------------|
| PL50 | Full Distribution | 0.029 | 0.017 |
| | All Defences | 0.032 | 0.019 |
| | All Seawall | 0.039 | 0.026 |
| | High Seawall | 0.040 | 0.038 |
| | Mid Seawall | 0.033 | 0.034 |
| | Low Seawall | 0.028 | 0.037 |
| | All Groyne | 0.016 | 0.030 |
| | Low Groyne | 0.015 | 0.030 |
| | Average | 0.029 | 0.029 |
| iPhone 6s | Full Distribution | 0.035 | 0.036 |
| | All Defences | 0.035 | 0.038 |
| | All Seawall | 0.030 | 0.058 |
| | High Seawall | 0.025 | 0.051 |
| | Mid Seawall | 0.026 | 0.053 |
| | Low Seawall | 0.034 | 0.058 |
| | All Groyne | 0.021 | 0.073 |
| | Low Groyne | 0.023 | 0.070 |
| | Average | 0.029 | 0.055 |

| Device | Cloud Name | Average Control RMSE (m) | Average Check RMSE (m) |
|-----------|-------------------|--------------------------|------------------------|
| iPhone X | Full Distribution | 0.034 | 0.036 |
| | All Defences | 0.035 | 0.035 |
| | All Seawall | 0.031 | 0.047 |
| | High Seawall | 0.029 | 0.047 |
| | Mid Seawall | 0.025 | 0.055 |
| | Low Seawall | 0.031 | 0.039 |
| | All Groyne | 0.019 | 0.051 |
| | Low Groyne | 0.018 | 0.048 |
| | Average | 0.028 | 0.045 |
| CUBOT X15 | Full Distribution | n/a | n/a |
| | All Defences | n/a | n/a |
| | All Seawall | n/a | n/a |
| | High Seawall | n/a | n/a |
| | Mid Seawall | n/a | n/a |
| | Low Seawall | n/a | n/a |
| | All Groyne | n/a | n/a |
| | Low Groyne | n/a | n/a |
| | Average | n/a | n/a |
| Galaxy S5 | Full Distribution | 0.053 | 0.044 |
| | All Defences | 0.058 | 0.043 |
| | All Seawall | 0.063 | 0.080 |
| | High Seawall | 0.063 | 0.095 |
| | Mid Seawall | 0.064 | 0.107 |
| | Low Seawall | 0.038 | 0.097 |
| | All Groyne | 0.037 | 0.063 |
| | Low Groyne | 0.026 | 0.061 |
| | Average | 0.050 | 0.074 |
| EOS 450D | Full Distribution | 0.039 | 0.037 |
| | All Defences | 0.040 | 0.038 |
| | All Seawall | 0.027 | 0.060 |
| | High Seawall | 0.023 | 0.068 |
| | Mid Seawall | 0.023 | 0.048 |
| | Low Seawall | 0.022 | 0.054 |
| | All Groyne | 0.030 | 0.055 |
| | Low Groyne | 0.029 | 0.048 |
| | Average | 0.029 | 0.051 |
| Average | | 0.040 | 0.051 |

For each dataset except Galaxy S5 and across all GCP configurations, average RMS error values were below ~ 0.03 m on the control. Optimisation yielded less accurate results

for the Galaxy S5 with an average GCP control point RMS error of 0.05 m. Despite being significantly lower in accuracy than the models obtained using different cameras, the error values are still within the accuracy range required by many coastal monitoring programmes. Check point error for the PL50 matched the control error both displaying 0.029 m; errors were ~ 0.05 m for the iPhone 6s, iPhone X, EOS 450D and 0.074 m for the Galaxy S5.

As expected, accuracy increases with an increased number and a wider distribution of GCPs. In this case only 14 check points were used and 13 in case of the Galaxy S5. When only a few GCPs are used as check points there is a higher possibility that the RMS error is not an accurate representation of model fit. This was not the case here as accuracy was comparable to cases in literature with more check points. It is important to stress that not only do the number of control and check points affect the accuracy but also their location and configuration. An optimal distribution would require the GCP network to fully encompass the area of interest and preferably at multiple elevations. The Full Distribution model was chosen as a 'benchmark' for cloud comparisons due to consistently well-optimised models.

Next, the digital elevation models (DEMs) obtained from the sparse clouds derived using different GCPs configurations were compared. DEMs were obtained from cloud points interpolated to a 0.5 m grid for computational efficiency. Using simple linear regressions, differences between elevations derived using different GCP configurations were investigated. Figure 17 shows comparisons for all models derived from images collected using Samsung PL50. Similar results are obtained for all other cameras and are given in Appendix 4. Points are densest around the regression line, indicating that the

elevations in models fit closely to each other. However, at closer inspection, the best fit is at medium and higher elevations which coincides with topography that is generally closer to GCPs. There are more discrepancies at lower elevations, on the beach due to the distance from the camera and the increasingly oblique views. Elevations from the model obtained using configurations of groyne only GCPs as control (in Figure 17 – ‘AllGroyne’ and ‘GroyneLow’) tend to exhibit the lowest RMSE values with elevations from the model obtained using the “AllDefence” model. RMSE values range from ~0 m for ‘AllGroyne’ versus ‘AllDefence’ to 0.025 m for ‘Full’ versus ‘SeawallLow’.

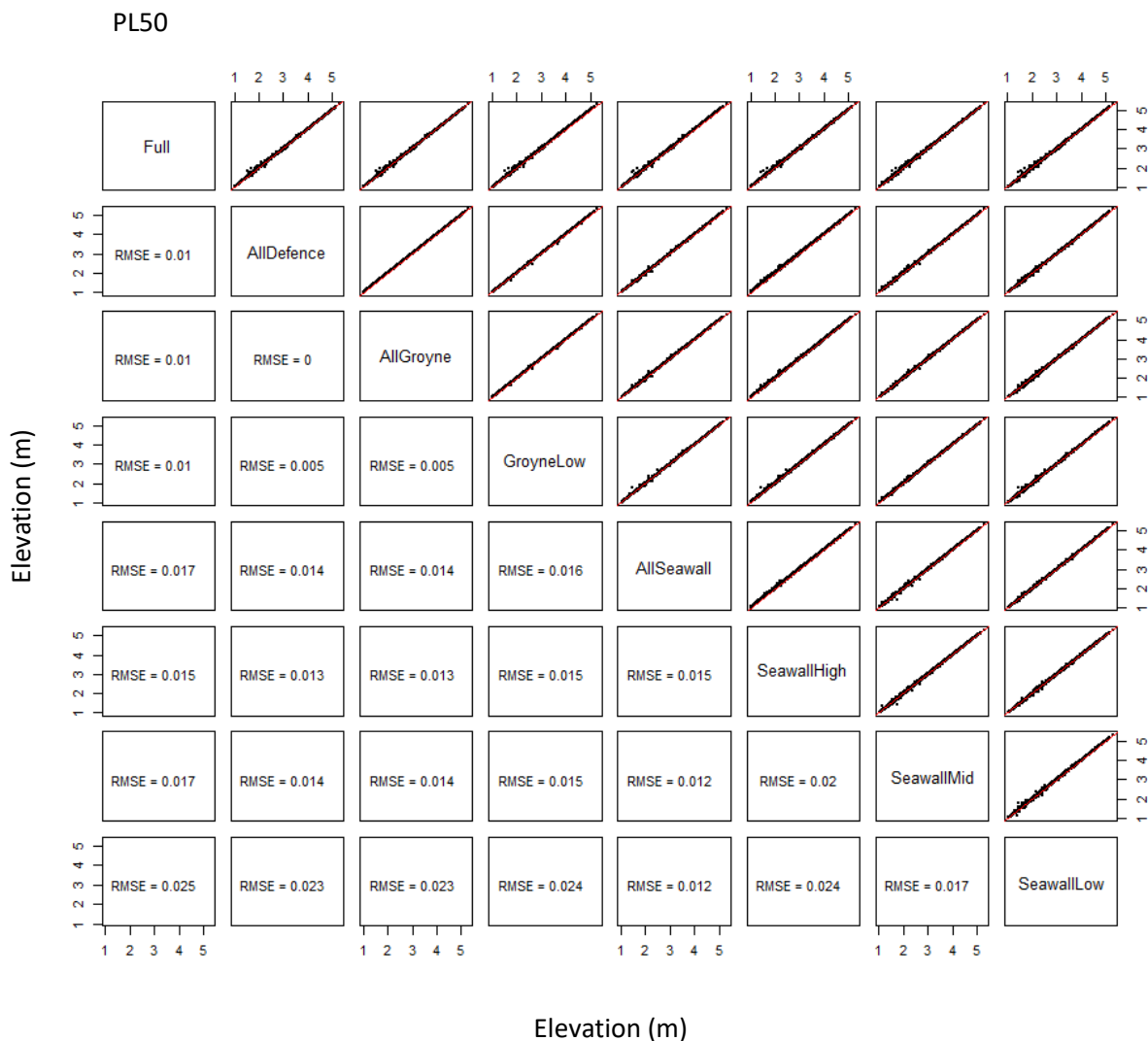


Figure 17 Sparse linear regressions of GCP configurations using the PL50 as an example. RMSE values are displayed for each respective plot. Red lines display a perfect positive 1:1 correlation between the configurations. Minor deviations are evident towards lower elevations.

4.2.3.1. Evaluation of Dense Reconstructions

After sufficient optimisation was performed for each device and its associated GCP configurations, dense reconstructions were carried out as described in 3.2.2. The PL50 and iPhone 6s completed dense reconstruction using aggressive depth filtering, however the iPhone X, Galaxy S5 and EOS 450D required moderate filtering to achieve reconstruction on the Full Distribution models only (Table 16).

Table 16 A table showing details on the dense reconstruction.

| | | |
|-----------|---|---|
| PL50 | Points Quality Depth filtering Depth maps generation time Dense cloud generation time | 18,036,823 Medium Aggressive 2 hours 3 minutes 2 hours 33 minutes |
| iPhone 6s | Points Quality Depth filtering Depth maps generation time Dense cloud generation time | 14,891,480 Medium Aggressive 2 hours 4 minutes 3 hours 41 minutes |
| iPhone X | Points Quality Depth filtering Depth maps generation time Dense cloud generation time | 24,144,329 Medium Moderate 8 hours 16 minutes 4 hours 53 minutes |
| Galaxy S5 | Points Quality Depth filtering Depth maps generation time Dense cloud generation time | 8,098,157 Medium Moderate 1 hours 41 minutes 11 hours 29 minutes |
| EOS 450D | Points Quality Depth filtering Depth maps generation time Dense cloud generation time | 21,806,115 Medium Moderate 6 hours 45 minutes 8 hours 12 minutes |

By producing DoDs between clouds that are optimised to different GCP configurations, a detailed inspection of topographical differences influenced by GCP distribution can be made. DEMs were derived in by the interpolation of dense clouds to a 0.03 m grid using the nearest neighbours method. DEMs and DoDs are produced in CloudCompare. The models optimised by using the Full Distribution GCP configurations were used as benchmark models.

The DoD of the models optimised with 'Full Distribution' and 'Seawall Mid' GCP configuration are shown in Figure 18. Other DoDs can be found in the Appendix 2. Comparisons showed a consistently close fit between the Full Distribution model and the All Defence model as expected due to their GCP count and distribution being similar.

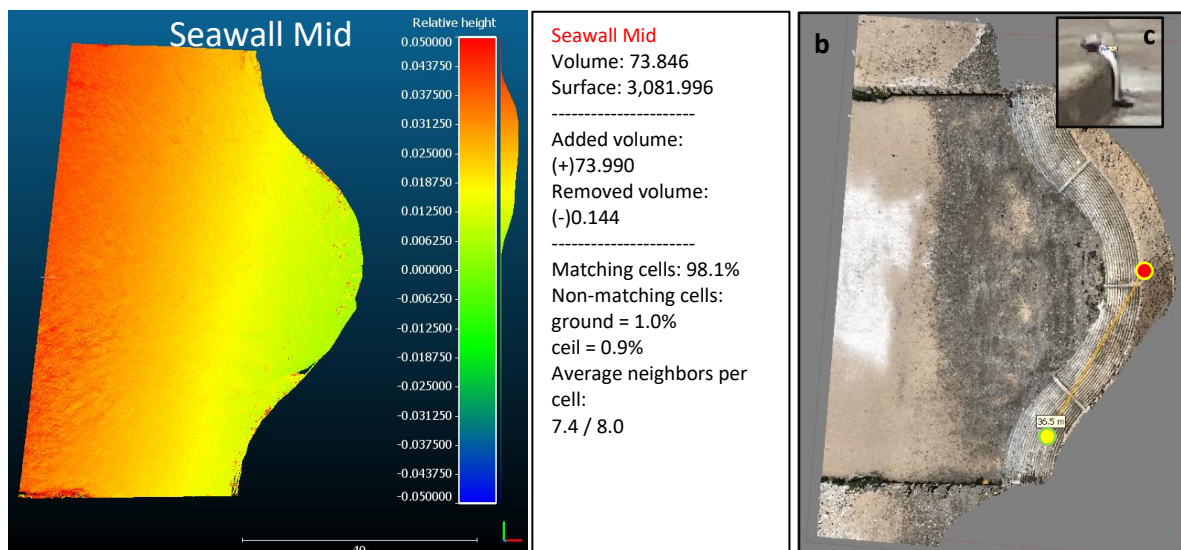


Figure 18 (a) iPhone X DoD between the benchmark Full Distribution Model and the Seawall Mid model. (b) Shows the distance from the camera (red) to the GCP (yellow) (c) Shows an example of the oblique viewing angles for marker placement.

Models optimised using GCPs located on the groynes often displayed close matches to the Full Distribution model. The location and coverage rather than the number of GCPs is likely a greater influencing factor. Models show a consistently high elevation RMS error

when using the seawall in various GCP configurations (Table 18). Displacement in model topography based on Seawall GCPs are often found to show positive vertical error towards the south-western extents and less commonly to the north-western perimeter. Even in the cases of the models optimised using the ‘Seawall’ GCP configurations, a ± 0.05 m vertical deviation is found at ~ 50 m from the seawall where imagery was captured. This results in the largest volumetric change of ~ 74 m³ (Figure 18a) when compared to the ‘Full’ distribution model.

There are likely two possibilities for the large displacements found in the seawall configurations; a) the GCPs do not enclose the area of interest and therefore geometry must be extrapolated outwards from known coordinates resulting in the model being tilted, and b) the targets attached to the seawall were often oblique and distant in imagery and therefore marker placement in PhotoScan was imprecise (Figure 18b and c).

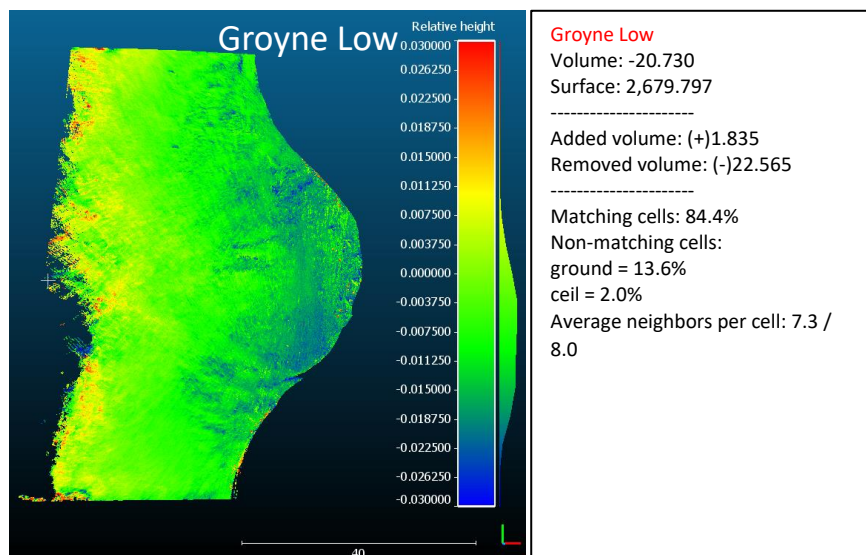


Figure 19 iPhone X DoD between the Full Distribution model and the Groyne Low model.

Figure 19 shows the elevation differences between the models optimised using ‘Full Distribution’ and ‘Groyne Low’ GCP configuration for iPhone X. Here the largest differences

of -0.025m are found further inland. This results in the volume differences of -21 m³ (Figure 19). A few patches displaying consistent differences ran along the seawall in areas containing washed up debris and foam. Due to the more exaggerated geometry of debris compared to the gently sloping beach, it is a potential that changes here are a result of displacement in the horizontal plane being represented as error in elevation.

Table 17 A table displaying the difference in volumes between each GCP configuration.

| Device | GCP Configuration | Volume Added (m3) | Volume Removed (m3) |
|------------------|-------------------|-------------------|---------------------|
| PL50 | All Defence | 9.5 | 0.8 |
| | All Groyne | 6.9 | 1 |
| | Groyne Low | 1.4 | 3 |
| | All Seawall | 40 | 0.2 |
| | Seawall High | 18 | 7.8 |
| | Seawall Mid | 35.7 | 0.2 |
| | Seawall Low | 59 | 0.8 |
| iPhone 6s | All Defence | 2.3 | 4 |
| | All Groyne | 6.1 | 1.4 |
| | Groyne Low | 5.5 | 2.4 |
| | All Seawall | 8.8 | 3.5 |
| | Seawall High | 3.9 | 11 |
| | Seawall Mid | 0.03 | 28.6 |
| | Seawall Low | 22.8 | 2.4 |
| iPhone X | All Defence | 5 | 0.7 |
| | All Groyne | 5.6 | 13.7 |
| | Groyne Low | 1.8 | 22.6 |
| | All Seawall | 14.1 | 0.3 |
| | Seawall High | 45.3 | 0.2 |
| | Seawall Mid | 73.8 | 0.1 |
| | Seawall Low | 14.1 | 0.3 |

The volumes calculated for each GCP configuration comparison is shown in Table 17. Each GCP configuration was compared to the 'Full Distribution' model for each respective device. It shows that the iPhone X had the largest volume difference out of the models that underwent successful dense reconstruction, and when averaged across both negative and positive elevation differences also displayed the largest change.

Elevations from the DEMs derived from dense clouds optimised by using different GCPs configurations were plotted against for linear regression analysis. In this case the clouds were interpolated on a 0.5m grid to make plotting more computationally manageable. Figure 20 (and Appendix 4) shows linear regression analysis for the PL50 between dense clouds and unsurprisingly shows similarities with the plots for the sparse clouds in Figure 18. The dense clouds diverge at lower elevations, as seen also in the sparse linear regressions. There are also some more outliers, and this is not surprising as there are more points in the dense clouds affecting DEM interpolation.

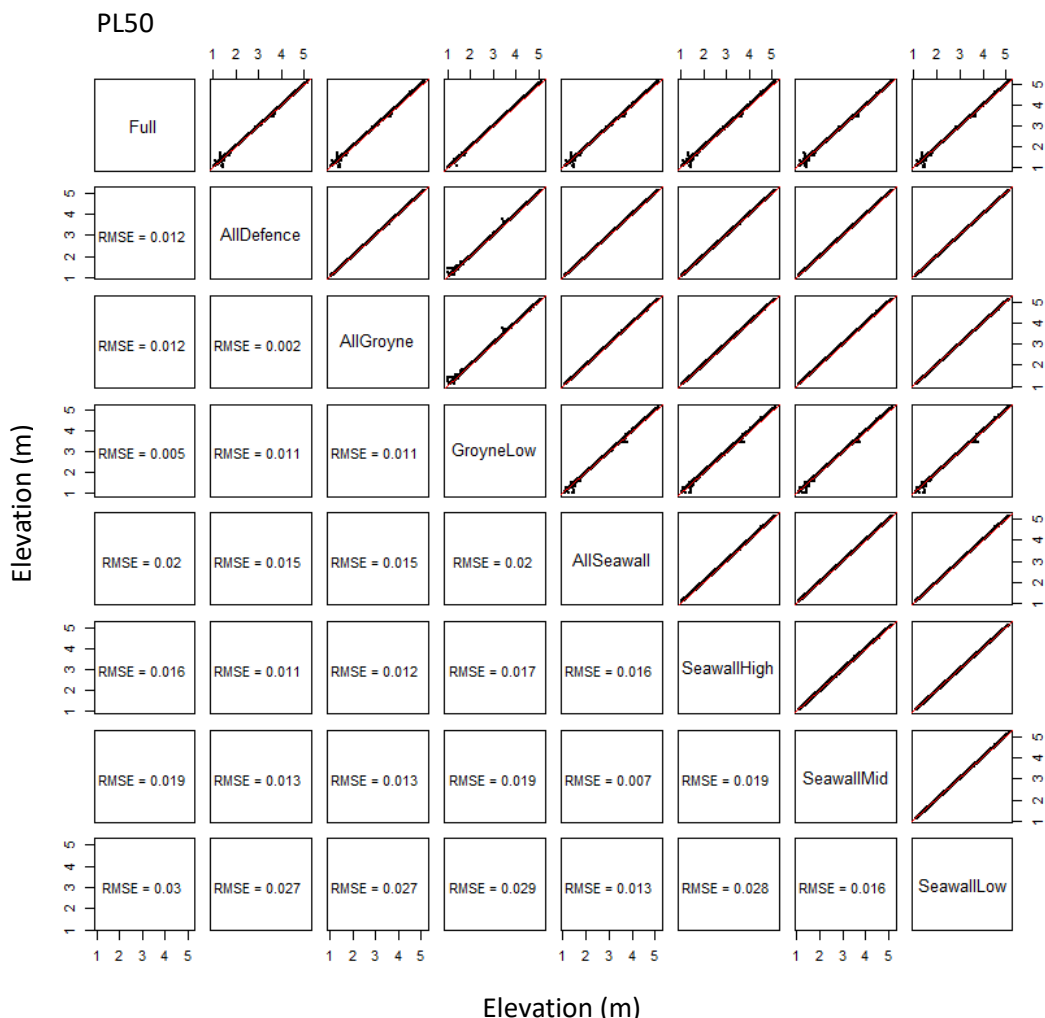


Figure 20 Dense linear regressions of GCP configurations using the PL50 as an example. RMSE values are displayed for each respective plot. Red lines display a perfect positive 1:1 correlation between the configurations. Minor deviations are evident towards lower elevations.

It seems evident that the largest differences usually occur between elevations models that utilise the 'SeawallLow' GCP configuration. Models compared to this typically show a higher RMSE, between 0.013 m and 0.03 m.

A summary table to show the RMSE values derived from the statistical program R based off 0.5 m gridded DEMs shows the magnitude of error in the DoDs. RMSE values could only be generated for all configurations on data from three of the devices. This is because these were the only three which underwent successful dense reconstruction.

Table 18 A summary table of RMSE derived from the dense linear regression analysis. Data here was based on the 0.5m grids for the PL50, iPhone 6s and iPhone X exported from CloudCompare.

| Device | GCP Configuration | RSME (m) |
|-----------|-------------------|----------|
| PL50 | All Defence | 0.012 |
| | All Groyne | 0.012 |
| | Groyne Low | 0.005 |
| | All Seawall | 0.02 |
| | Seawall High | 0.016 |
| | Seawall Mid | 0.019 |
| | Seawall Low | 0.03 |
| iPhone 6s | All Defence | 0.006 |
| | All Groyne | 0.004 |
| | Groyne Low | 0.004 |
| | All Seawall | 0.006 |
| | Seawall High | 0.008 |
| | Seawall Mid | 0.013 |
| | Seawall Low | 0.013 |
| iPhone X | All Defence | 0.002 |
| | All Groyne | 0.008 |
| | Groyne Low | 0.02 |
| | All Seawall | 0.015 |
| | Seawall High | 0.017 |
| | Seawall Mid | 0.026 |
| | Seawall Low | 0.005 |

The table shows the iPhone 6s to show the most consistently low RMSE, indicating that the models are least affected by a change in GCP configuration out of the three models tested.

4.2.4. The Effect of Different Devices on Model Accuracy

Next the models derived from images collected by different cameras were compared. The models optimised using 'Full Distribution' were only compared by looking at errors at check points. These were investigated for sparse and dense clouds.

4.2.4.1. *Evaluating Tie Point Geometry*

Figure 21, 22 and 23 display histograms of errors in x, y and z coordinates respectively at check points for all cameras. When visualising the spread of error in the models, despite a small sample size, results display similarities to a normal distribution. On average errors across x, y and z coordinates seem to concentrate around 0 m for the PL50, suggesting the model is the most accurate. However, care needs to be taken as this is very small sample. The PL50 consistently yielded lower standard deviations than those of the other devices. The errors in coordinates for the Galaxy S5 show the widest spread (Figure 21 - 23). Interestingly, errors in z coordinates are narrowly distributed and centred around 0 m for all except the Galaxy S5 in-built camera.

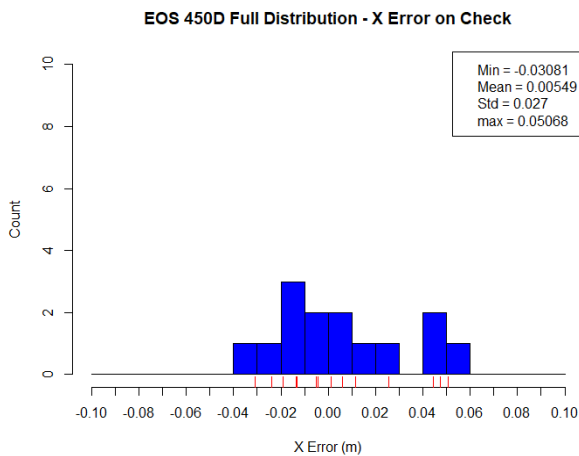
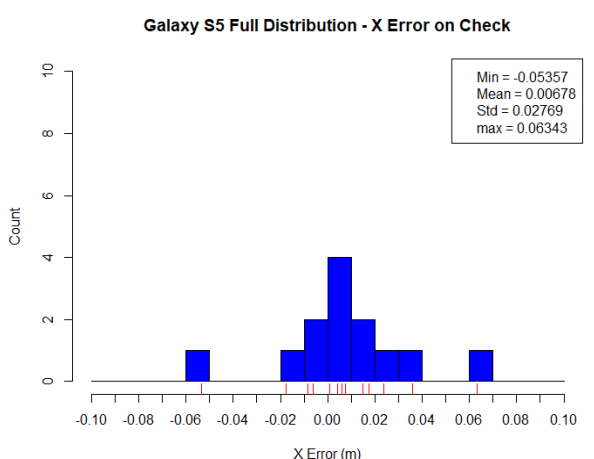
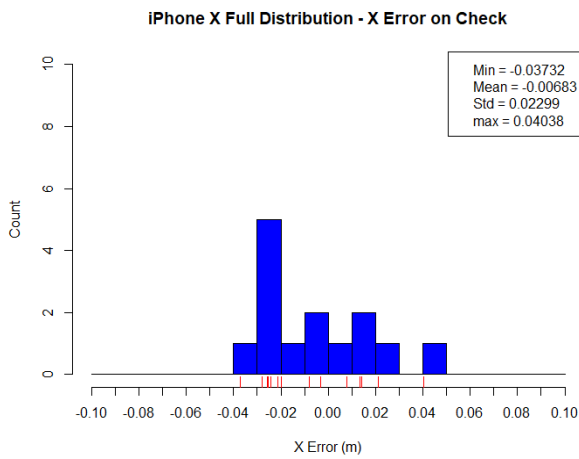
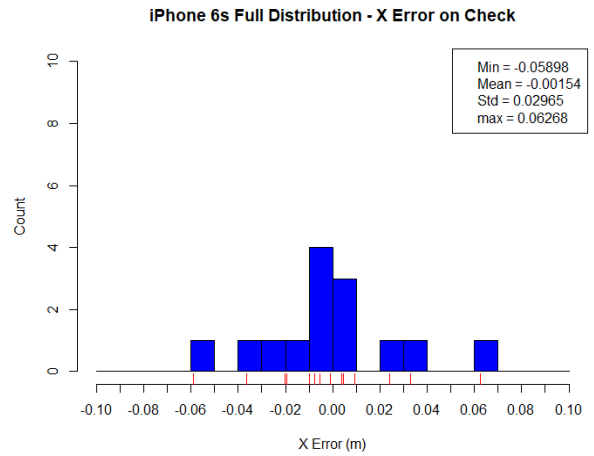
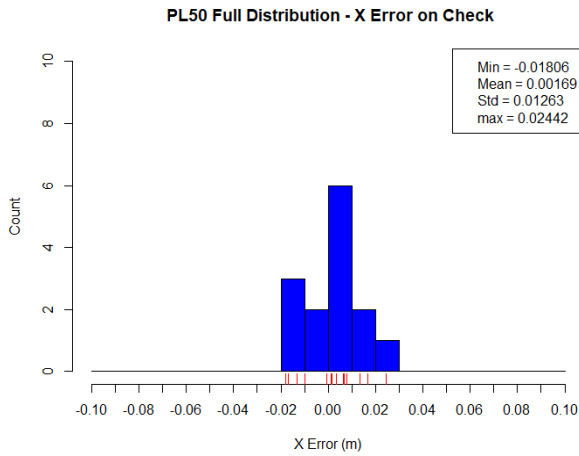


Figure 21 'Full Distribution' histograms displaying the spread of error in the x horizontal dimension for each device. The PL50 shows the highest concentration of error around 0m, whereas the iPhone 6s, iPhone X, Galaxy S5 and EOS 450D all show outliers greater than ± 0.4 m.

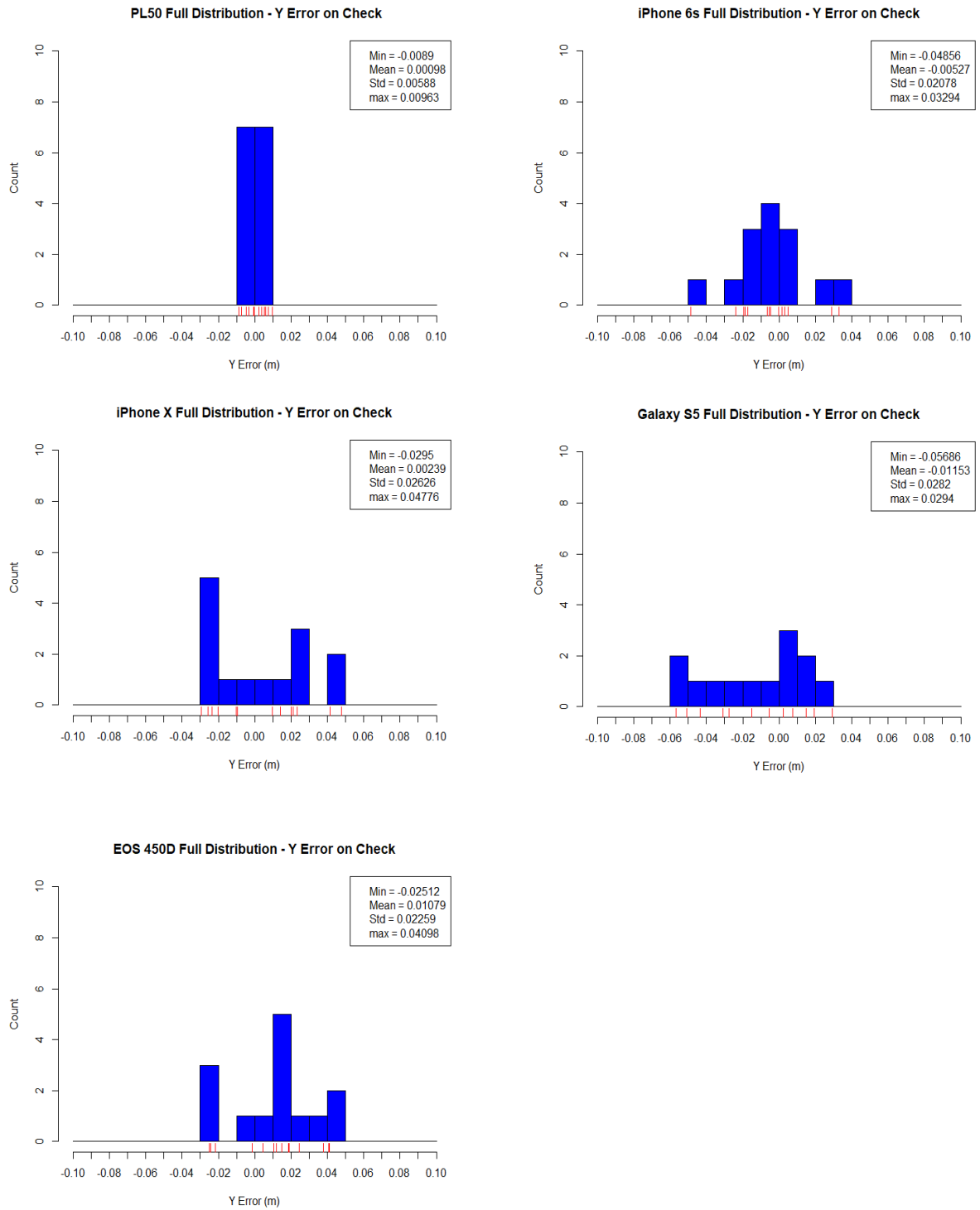


Figure 22 'Full Distribution' histograms displaying the spread of error in the y horizontal dimension for each device. The PL50 shows the highest concentration of error around 0m, whereas the iPhone 6s, iPhone X, Galaxy S5 and EOS 450D all show a wider spread of error. Error in this dimension is lower than that in the x dimension.

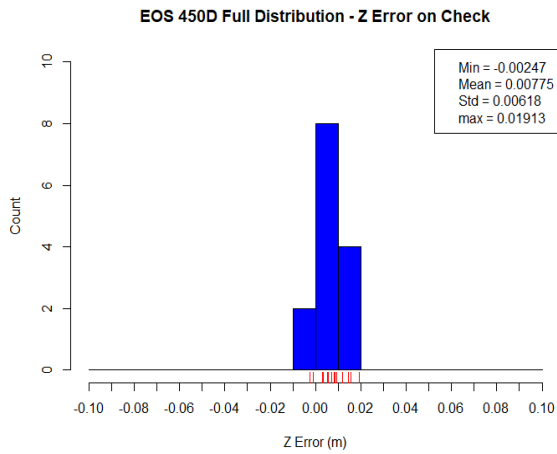
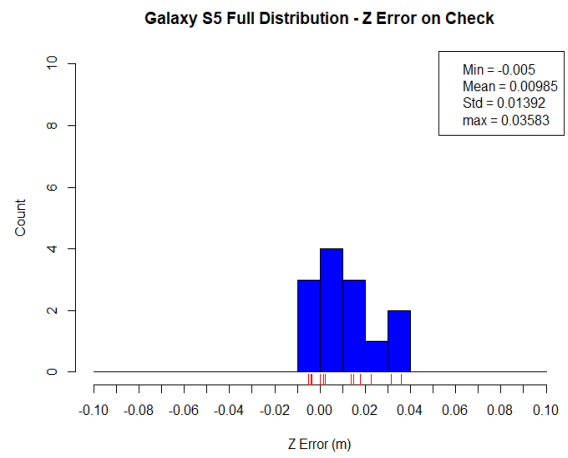
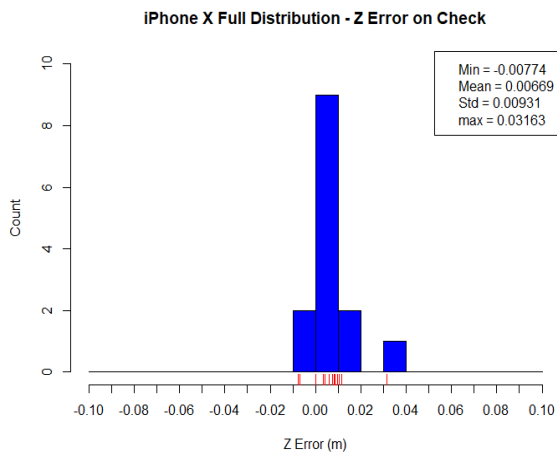
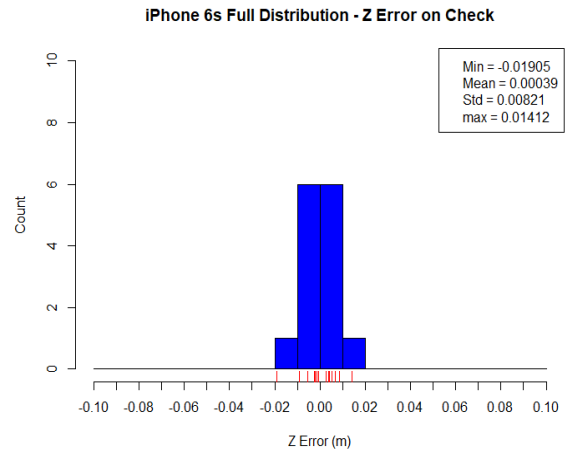
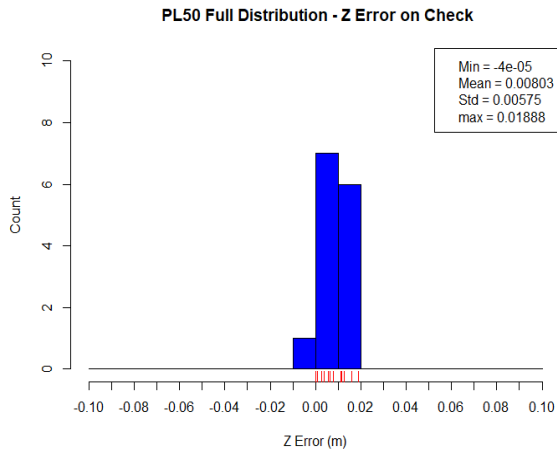


Figure 23 Histograms displaying the spread of error in the z vertical dimension for each device. All devices show a high concentration of error around 0 m with the EOS 450D showing the most spread error.

All mean values of error were highly centred around zero in the x and z coordinates with values of order millimetres. This was not entirely true for y coordinates, as values for the Galaxy S5 and EOS 450D (Figure 22 and Figure 23) extended into the centimetres. This is likely an effect from the oblique viewing angle present in the y direction on the seawall GCPs.

GCP locations are given in Figure 24 to visualise the distribution of vertical errors across the groyne cell. Points with high red or blue saturation suggest larger errors for the vertical component, in the positive and negative direction respectively. A relatively large portion of these vertical error components tend to lie around the seawall, with a few sparsely distributed elsewhere. Viewing angles for targets attached to the seawall presented more of a challenge for choosing marker location within PhotoScan and thus often contain larger pixel errors. This is especially true on the extremities such as GCP 1,9,18, 24 and 25 which were removed from some models due to high inaccuracies.

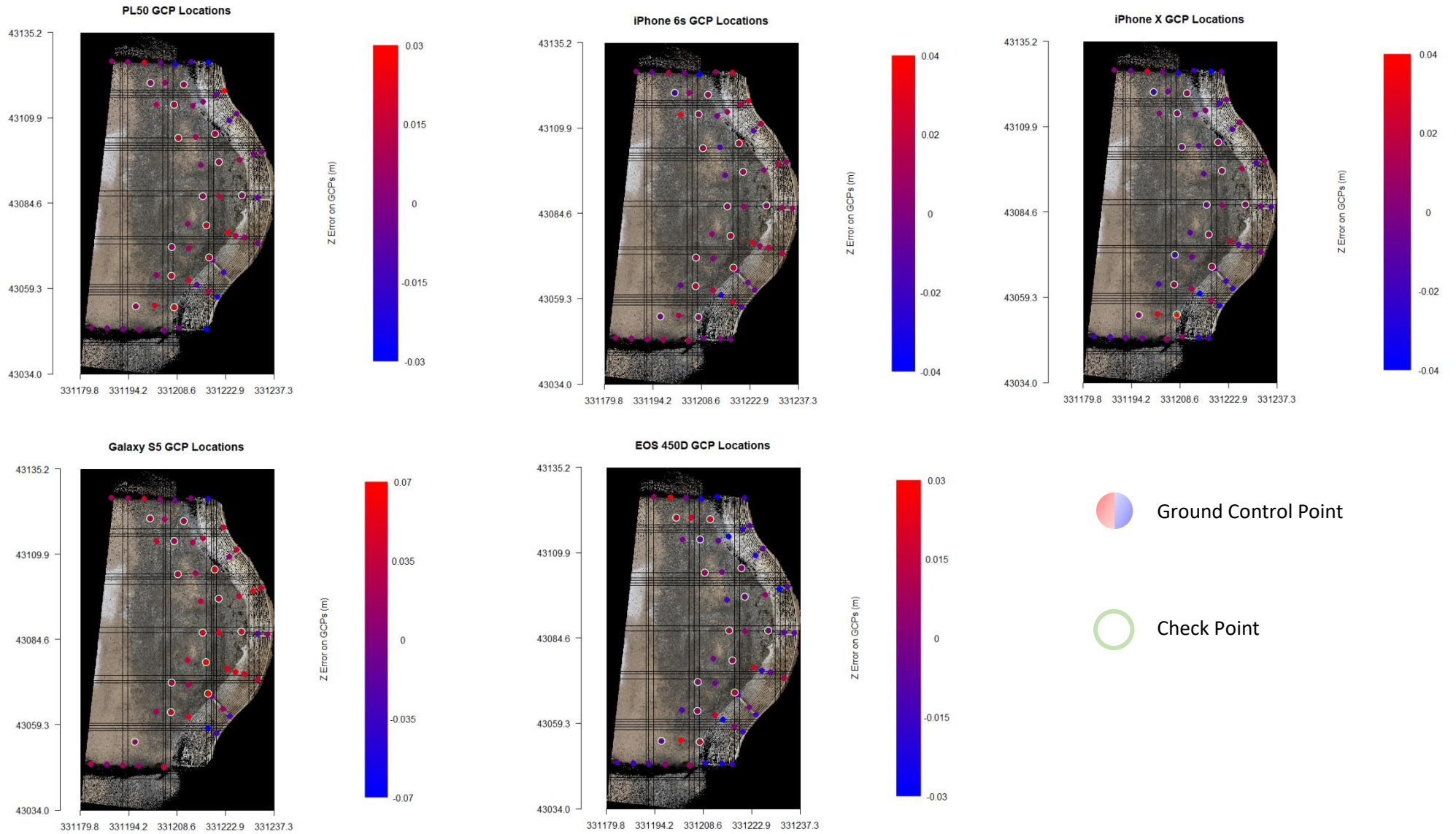


Figure 24 GCP locations with a colour grading representing z error for the 'Full Distribution' for each device with respect to the GCP position.

Elevations from the sparse clouds derived from images obtained using different cameras are plotted against each other in Figure 25. Linear regressions show significantly more deviation at lower elevations (Figure 25). As suggested by previous results showing similar trends. Deviations are largest in comparison between clouds derived from other cameras rather than GCP configuration when comparing the sparse point clouds – differences in elevation here range from 0.032 m for the PL50 versus the iPhone 6s and 0.052 m for the Galaxy S5 versus the EOS 450D.

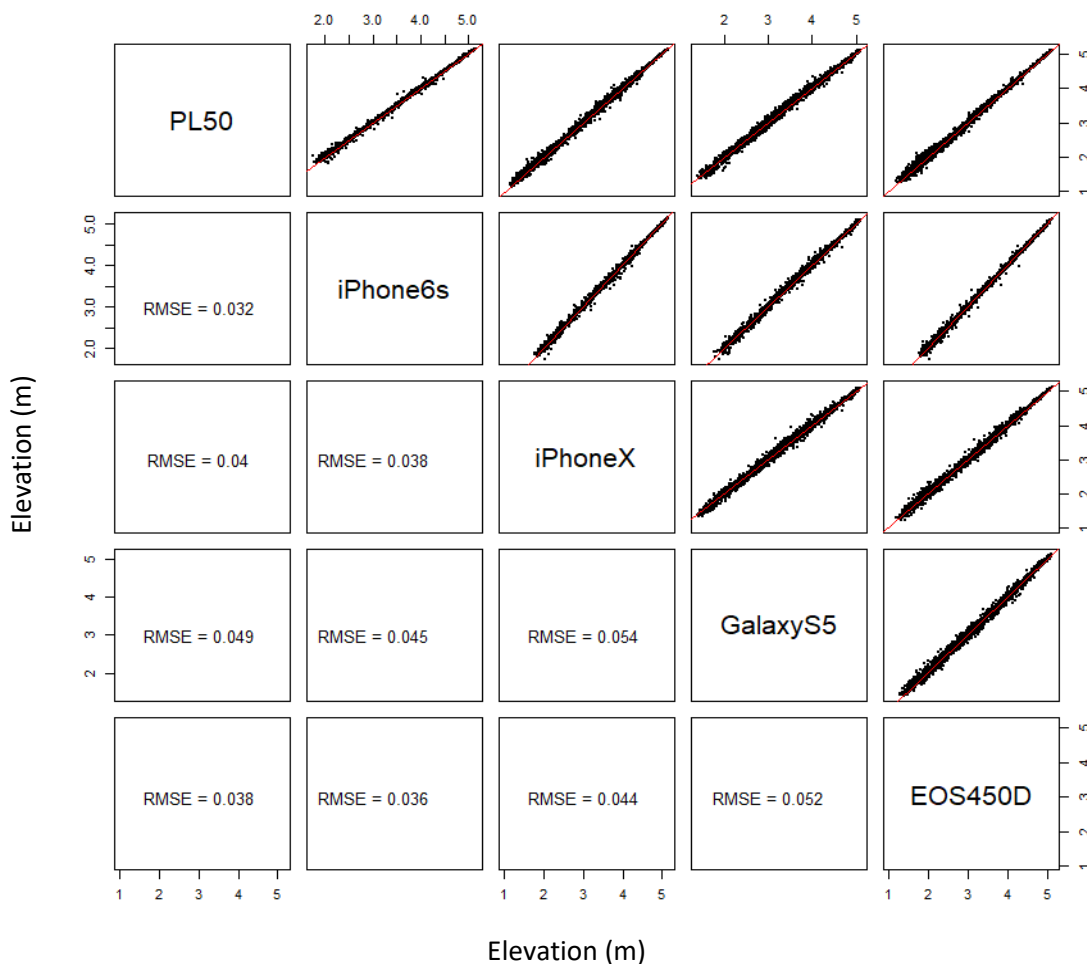


Figure 25 Linear Regressions of elevations between device DEMs generated from sparse clouds. The red lines represent a perfect positive correlation.

As in the previous analysis, larger discrepancies are observed at lower elevations down on the beach. The largest deviations are observed in comparisons involving the Samsung Galaxy S5 and the Canon EOS 450D, but also there is quite a bit of deviation between them suggesting that the cameras, their respective settings and the way the images are taken can influence the accuracy of results.

4.2.4.2. Comparison of Dense Reconstructions

Elevations from models obtained by different cameras were plotted against each other (Figure 26). Interestingly, increased surface deviations are not as noticeable between

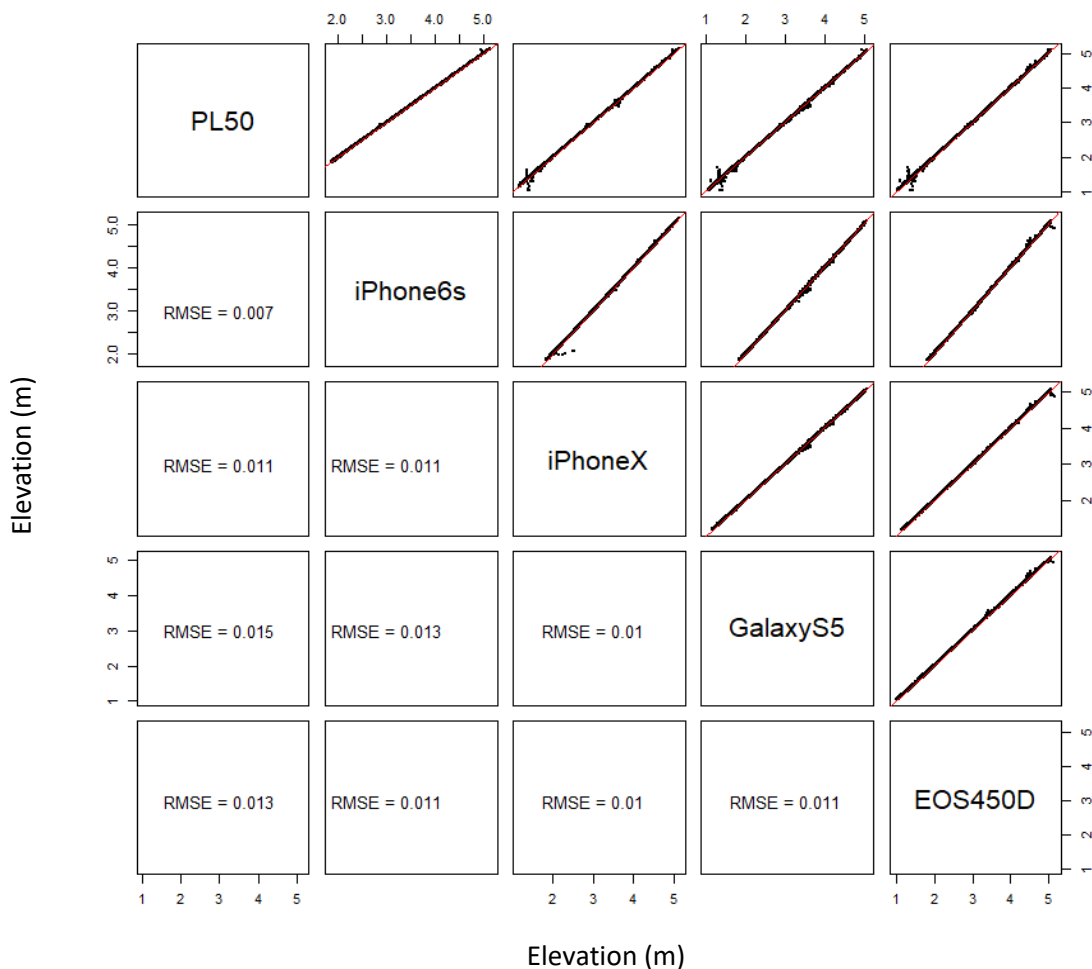


Figure 26 Linear Regressions showing relationships between dense reconstructions generated from each device. Red lines represent a perfect positive correlation.

the dense DEMs—there is not a significant systematic trend of lower elevation deviation. Additionally, RMSE values decrease significantly after the dense reconstruction process (Figure 26). This is coherent with the cloud filtering methods used, which remove obvious outliers – a step that is not performed until dense reconstruction. Prior to filtering, the sparse clouds had much more noise present, especially in the Galaxy S5 and EOS 450D models (Figure 25).

Monitoring changes in beach volume is a key factor in understanding beach dynamics, and thus is the area of interest for this study. Although comparisons are directly measured as elevation change, volumetric change can also be worked out between clouds. Comparisons between DEMs obtained by different cameras show consistent deviations towards the seawall (eastwards) as illustrated in Figure 27, Figure 28 and in Appendix 3. Scales here have been chosen to visualise topographical deviations according to the magnitudes they operate on; the scales for these DoDs are either 0.02 m or 0.03 m as a maximum elevation. It should be noted, that the largest divergence towards the seawall is shown in comparisons involving the Galaxy S5 and EOS 450D. This could be a result of a tilt in model alignment, consequently causing a positive and negative shift at both the east and west extents of the DEM (Figure 27). DoDs derived from model pairs including the EOS 450D also have a systematic defect propagating from central regions northwards. This defect explains the sporadic distribution of point about the regression line in Figure 26. DoDs here present changes that are significantly lower than those inflicted by a change of GCP configuration. The least accurate DEMs also result in the largest volume difference; the largest of which is for the Galaxy S5 and the EOS 450D. Figure 28 shows a DoD between the PL50 and

iPhone 6s where the deviation tends to be much lower than the Galaxy S5 and EOS 450D.

PL50 - EOS 450D

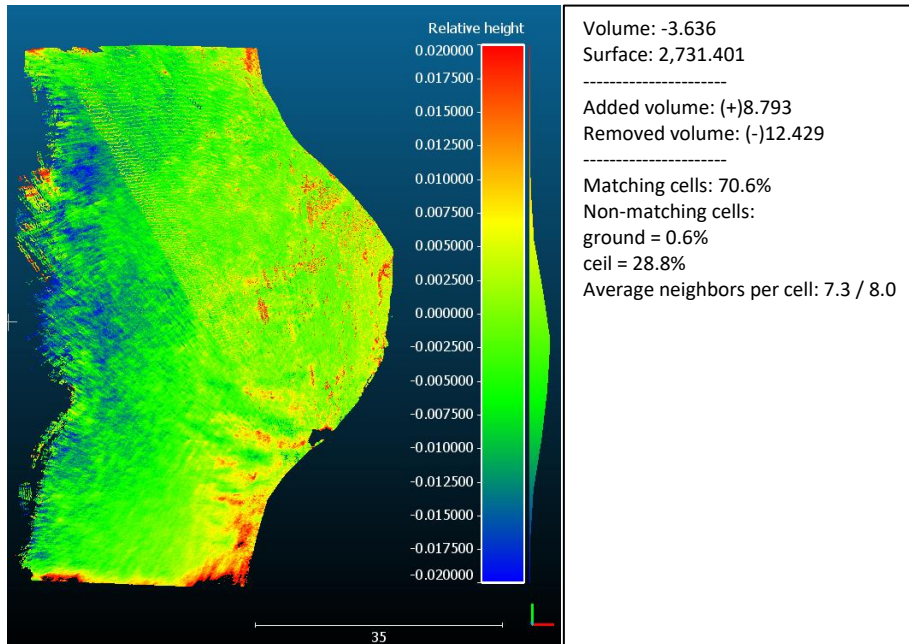


Figure 27 DoD between PL50 and EOS 450D. The DoD displays deviations in elevation of the EOS 450D DEM with reference to the PL50 DEM.

PL50 – iPhone 6s

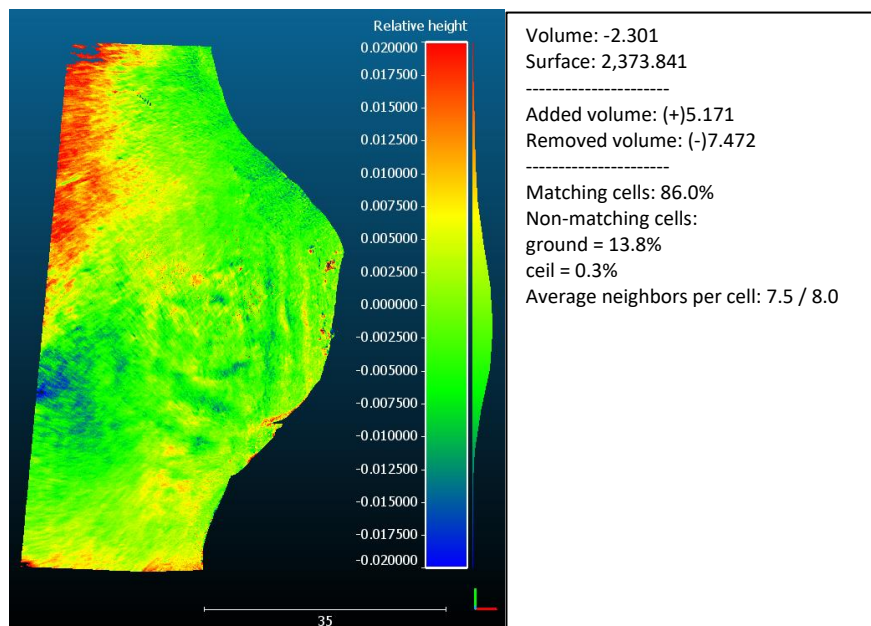


Figure 28 DoD between PL50 and iPhone 6s. The DoD displays deviations in elevation of the iPhone 6s DEM with reference to the PL50 DEM.

4.3. Implementing Citizen-led Coastal Photogrammetry

This section describes the challenges and successes of implementing photogrammetry as a coastal data collection activity for members of the Rossall Beach Residents and Community Group. It reviews the level of engagement from participants during the data collection process and participants' feedback gained for both sessions. The first session served as an initial assessment into the structural framework required for citizen-integrated coastal monitoring and involved an indoor and outdoor activity. This was followed in the next month with a more refined session, being based solely on the beach.

4.3.1. Session 1

Participation numbers for the outdoor activity of session 1 declined from 18 taking part in the indoor session, to 12 continuing outdoors. This was a result of the various responsibilities of the volunteers and a few who were not able to participate due to cold weather conditions. Nevertheless, the 12 volunteers who did participate in the outdoor session, performed the task in the proscribed manner (see Methodology section). The task was performed with high enthusiasm and appeared to follow the correct procedure. Here we look at the feedback gained from the participants.

Questions 1 – 5 in the feedback forms (Appendix 5 and Appendix 8) were centred around the participants' understanding of project aims and objectives and their involvement within the programme. Overall feedback was positive with a high level of understanding shared between individuals. Crucially, there was consensus

among the participants about clarity of the aims and objectives of the project regarding coastal monitoring and how it is important in their lives (Figure 29a).

When asked about the indoor activity, citizens appeared to find the table-top 3D model generation difficult (Figure 29b). General enthusiasm towards the indoor 3D model generation was high, although when asked in person about their understanding of the 3D model generation process, relatively few said they had understood the procedure. The volunteers were split into 5 groups each with a laptop, and usually contained at least one member who had understood the procedure instructions.

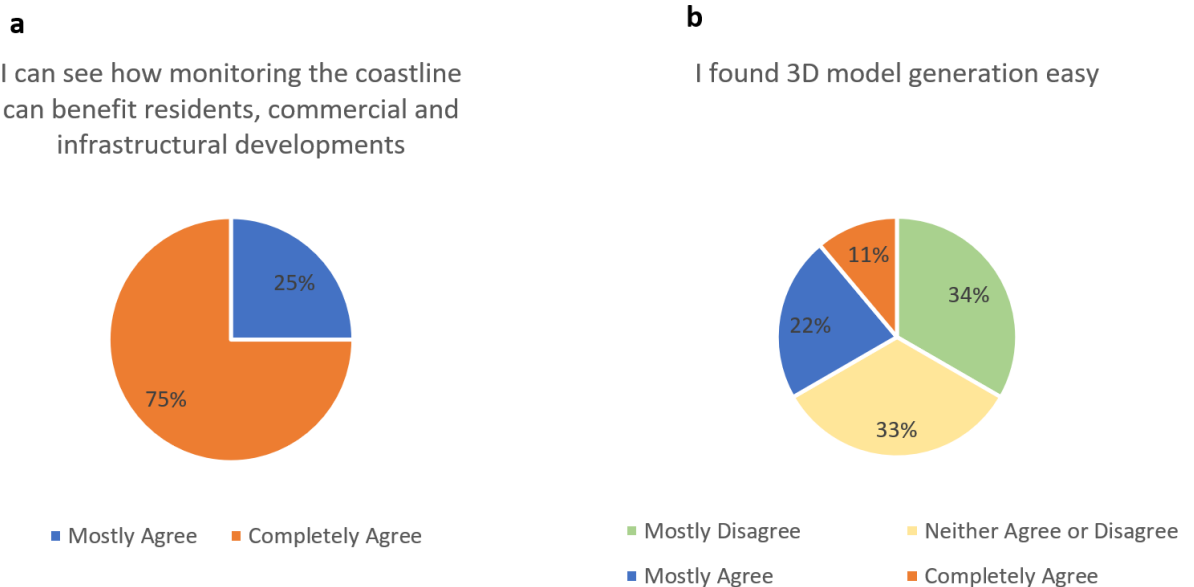


Figure 29 Pie charts displaying views expressed by The Rossall Beach Residents and Community Group. (a) Shows the proportion of participants who understand the benefits coastal monitoring has on developments. (b) The level of difficulty encountered for 3D model generation by participants.

For the outdoor session, volunteers responded positively when asked if they found imaging the coast easy. 57% of participants said they felt confident in the data collection procedure and followed the technique closely to the researcher's demonstration, where 43% were mostly confident performing the task (Figure 30a).

When asked, if they were able to independently upload data through the data transfer site wetransfer.com, 88% of participants responded as either mostly agreeing or completely agreeing (Figure 30b). This is interesting as only 50% of participants successfully transferred their data wirelessly. One volunteer attempted to transfer the data, however, was unsuccessful and had deleted the photos before a second attempt could be made. This shows that, although many volunteers assumed they were able to transfer the data, without performing it, their understanding may have been incorrect. Another potential is the loss of motivation once removed from the study and therefore reduced chances of retrieving data. It is for this reason, that the second session was adapted to account for this.

Having this monitoring session as a part of The Rossall Beach Residents and Community Group regular meeting was something that 86% of volunteers were happy with, however it was not unanimous. If this style of coastal research were to be conducted by members of this community group, then 57% would be happy with a periodicity of once a month, 29% once a week and 14% of once a year. These figures are based on a small sample size of 12 (questionnaires were filled out after the outdoor session) and thus requires a larger sample size to confidently represent the coastal group, however, this acts as an indication of participant perceptions towards coastal data collection.

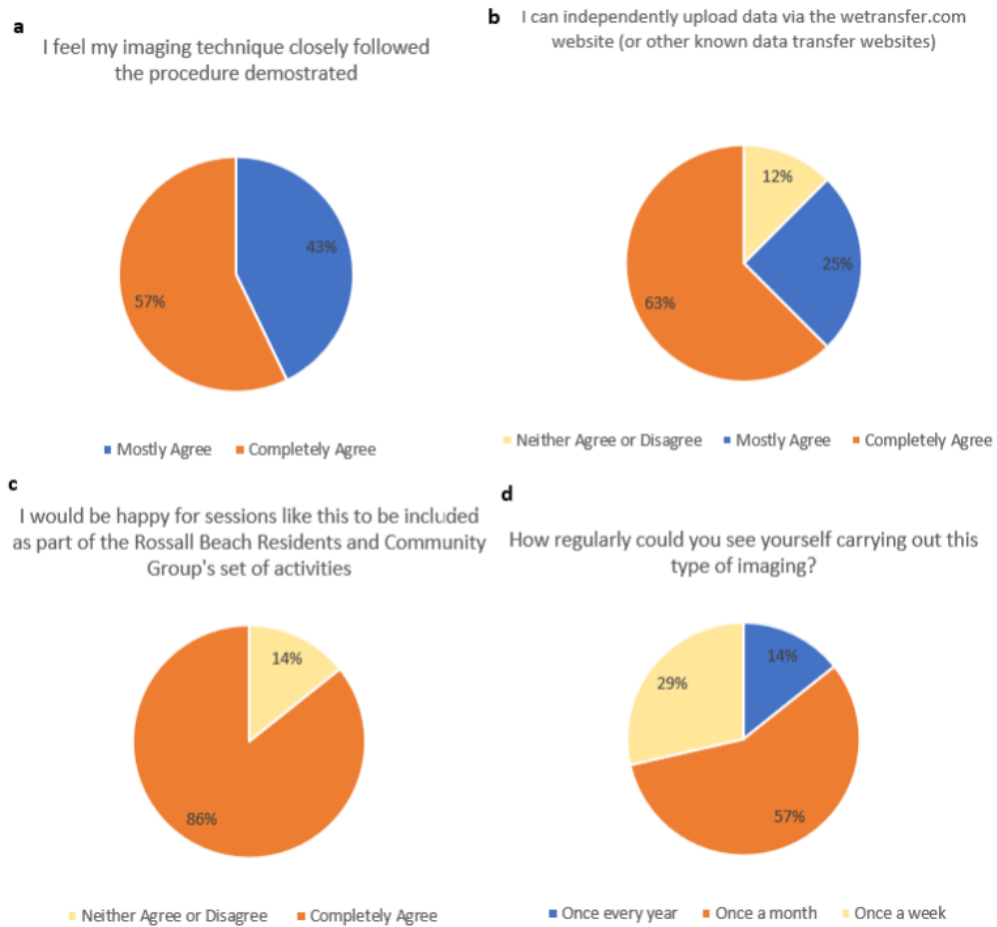


Figure 30 Pie charts displaying views expressed by The Rossall Beach Residents and Community Group. (a) How participants performed the imaging technique. (b) Participants' willingness to have coastal photogrammetry incorporated into their set of activities. (c) Participant views on how often they might conduct this type of data collection in the future.

4.3.2. Session 2

Feedback from the first session indicated that citizens did not absorb the intended information about SfM 3D model generation. For this reason, the indoor session was removed from activities conducted in the second session. Instead emphasis was focused on the technique for image capture rather than the method behind the processing of imagery. Volunteers were handed information packs detailing the requirements for coastal photogrammetry.

The second session hosted fewer participants than before, and thus a more in-depth engagement model was able to be established. Motivation from the volunteers was high, and the procedure was conducted as required despite a relatively strong persistent wind. The day was overcast and thus provided ideal light conditions for photogrammetry. Manual hard-wired data collection was instigated for data upload this session due to the low volume of data retrieved from the last session. Participants met for a post-field meeting, whereby data was collected, and questionnaires were filled out.

One volunteer did not complete the questionnaire and thus results displayed only represent 4 out of 5 volunteers. Of the 4 participants, 75% showed confidence in following the image capture procedure with the remaining 25% not knowing whether they did or not. Interestingly, 50% of the volunteers stated they found the task enjoyable, and the other 50% mostly agreeing. This might be due to the large number of images collected in this session of >200 per person. The importance of the study and the effect that coastal monitoring has in their lives seemed to be unanimously agreed upon. The significance of correct scene and camera conditions was understood; however, the citizens showed less confidence in being able to identify what the correct conditions might be. This is an important factor to understand to reduce the collection of unusable coastal imagery. In future sessions, the participants could be further trained, and examples given that they can relate to and therefore understand more intuitively.

5. Discussion

5.1. Comparison of Session Frameworks

Session 1 provided an initial insight into survey design when incorporating citizens into data collection. Data collected during this session was successful for dense cloud generation, which was facilitated by the reduced image quantities. However, scene coverage was limited by the relatively low number of images taken per person and the 50% success rate of data transfer. This resulted in clouds having to be merged to produce a model spanning the length of the groyne cell. This segmentation of beach topography into several point clouds was not suitable for device comparisons, as the point clouds generated did not contain sufficient overlap for geometry comparisons.

The GCP network in the first session was distributed throughout the scene, however, visibility of GCP targets was compromised due to the camera positions. A large gap in data caused by an obstructing berm, resulted in numerous GCPs being obscured in the photos and thus could not be reconstructed. Imagery was captured in an easterly direction with the western side of the berms being well exposed and thus undergoing successful 3D reconstruction. The area of no-data behind the western face of the berm, would require imagery to be taken from the east looking west. The presence of the stepped revetment to the east, enabled a gain in height to be made if images were to be taken from on top. This prompted the second session to incorporate imagery taken in a westerly direction from the top of the stepped revetment.

Survey design for the second session was refined from observations made during the first session. Despite fewer participants being present for the second session, data

capture per participant was considerably higher. Each photoset covered the whole groyne cell in this session and enabled the coverage of >2000 m² of mixed shingle and sand beach. This allowed for a more robust comparison of data from participants as point clouds contained significant overlap – no less than 60% overlap between any device (James and Robson, 2012; Agisoft, 2016). The ability to use the stepped revetment as a guideline for image-taking aided in data collection efficiency, and combined with groynes as boundaries, led to a robust data capture area.

5.2. The Optimum GCP Configuration

Given the small sample size of this study, it is not possible to conclude with 100% confidence that GCP configurations that include groynes provide the highest accuracy in all scenarios, however, results gained from this study agree with literature – a GCP network that encompasses the scene works best (James and Robson, 2012; Brunier et al., 2016; Agisoft, 2016). Results derived from this project suggest that a combination of groyne and seawall defences offer the highest average accuracy after bundle adjustment – 0.035 m on GCP check points between all devices. However, if limited to only one permanent structure, dense reconstruction analysis suggests that using GCPs located on structures perpendicular to the linear route of data capture – in this case the groynes – provides the best match to the 'Full Distribution' model.

Linear regressions of DEMs also suggest that GCP configurations involving groynes match closely with each other. Lower elevations diverge from the regression line generated from sparse and dense DEMs. Lower elevations occur at increasing distances from the seawall, implying a higher chance of topography being located

outside the confines of GCP distribution and an increased distance from the camera, both of which lead to higher RMSE values (Clapuyt et al., 2015). This reinforces the argument that maintaining expansive GCP coverage where possible is best to ensure model geometry is highly accurate (James et al., 2017a).

The optimum control network that does not include GCPs situated on sediment, is the configuration that involves all defence GCPs. This is to be expected as it spans the largest coverage whilst also containing the highest quantity of GCPs, however, where a coastal structure has only one orientation, then those that are perpendicular to the shore provide the greatest model accuracy.

5.3. Configuration Application Along the Fylde

Successful geometry reconstructions consistently achieved RMSE values of <0.05 m when optimised using bundle adjustments including GCPs of known position. The GCPs were collected with accuracy values of ± 0.02 m (provided by the dGNSS) suggesting a confidence in surface topography of ± 0.07 m on average for all configurations for each device when accounting for a cloud geometry and alignment of $\sim \pm 0.05$ m. There is a strong link between GCP distribution and geometry/ point cloud orientation accuracy when designing surveys. From this, it is evident that survey designers should aim to maximise coverage across the scene of interest and encompass, where possible, the entire scene. Extrapolation beyond the confines set up by GCPs rapidly decreases topographical accuracy and therefore limits the extent of geometric confidence (James and Robson, 2012; Agisoft, 2016; James et al., 2017a). For each DoD shown, deviations in surface topography never exceeded ± 0.05 m across all GCP configurations and

device comparisons. These measures of confidence do not achieve cross-shore accuracies achieved by GNSS beach profile surveys – which are a direct consequence of GNSS equipment accuracy – however they enable full topographical measurements in x, y and z directions.

The Fylde coastline, is predominantly defended by hard defences. 17km of the coastline is comprised of seawalls, 6km of which have additional groynes. As permanent features are required to establish a GCP network suitable for continued citizen-led monitoring, these hard defences are relied on. As a result, the most common form of configuration that is enabled along the Fylde coastline would be the seawall configurations. Where possible, a combination of elevations on the seawall should be utilised, however, structural characteristics might restrict this. Furthermore, many parts of the coastline do not have the same geometry as the groyne cell tested in this study. Linear seawall formations would result in increasingly obliquity on GCP viewing angles. This could add to increased y error in GCP placement within imagery.

In this study the deviation in point cloud accuracy for seawall only configurations exhibited characteristics of model tilt, whereby data increasingly diverges from the reference 'Full Distribution' model. This effect would be difficult to remove entirely along other parts of the 17km hard-defended coast where permanent structures might only run along the back of the beach, so this reduced accuracy would have to be taken into account when interpreting results.

To summarise, this study contributes knowledge towards defining an optimum GCP configuration for a CS data collection programme in a coastal environment. An optimum GCP configuration would include the use of permanent structures that

protrude out perpendicular to the shoreline to encompass the scene of interest along with a permanent structure running parallel to the beach. The structures should be permanent so that the GCP survey only needs to be conducted once and updated a little as possible. When setting the GCP targets on the permanent structures they should be clearly visible, and where possible, should be positioned so that they are parallel with the plane of the image collected by the camera. Distances should not be too large between the camera and GCP as to avoid the misidentification of the GCP centroid.

In a scenario where there are no perpendicular permanent structures on the coast, then a raised seawall or similar sea structure positioned at the back of the beach, can be used for GCP positioning. In this scenario, results gained from this investigation suggest that the model will be more prone to tilting, and therefore differences in elevation are likely to increase the further from the structure the topography is. Results from this study imply that differences could be up to ± 0.05 m if GCPs are positioned only to one side of the model.

5.4. Device Performance

Perhaps surprisingly, the standalone DSLR camera provided the largest systematic error, with noise propagating from the southeast region of the model to the northwest. This proved difficult to remove using the point removal tool within CloudCompare (Girardeau-Montaut, 2003). The excessive points were present above the active layer in this model and positioned close to the ground, making point removal problematic. This excessive noise displays false visual surface features that can

influence quantitative interpretation and would therefore not be a suitable visual tool for coastal decision making. It should be understood however, that this is an issue related to the dense reconstruction procedure, which was present in all clouds but was difficult to remove for this particular point cloud. Overall, model geometries displayed minimal signs of deviation between devices. The much larger influence on geometry results from the control network. Smartphones in general performed well, however, some models required excessive manual intervention to remove noisy data – although this could be reduced if depth filtering was set to ‘aggressive’ (Agisoft, 2016).

The sample size was small and thus further work would be required, however, the results gained from this study supports findings from literature where built-in smartphone cameras exhibit similar, and in some cases better, topographical accuracy than standalone cameras (Prosdocimi et al., 2015; Micheletti et al., 2015a).

Additionally, this project brings to light the high-resolution 3D models generated by smartphones. Models produced using these cameras provided dense point clouds displaying resolutions that are high enough to identify small-scale coastal processes such as toe scour (Sutherland et al., 2006). On average the models had a point density of 0.3 points/cm² and contained millions of points – between ~8 million for the Galaxy S5 and 24 million for the iPhone X. This high resolution enables the possibility to study the topography of processes that are undetectable to many other monitoring methods such as airborne LiDAR.

5.5. Citizen Motivations

The study carried out has demonstrated that CS projects can be utilised in the collection of coastal data, which importantly, is scientifically useful and can be used to successfully generate 3D topographic models. More trials would be needed to determine whether engagement was truly successful, however, feedback from each session yielded positive participant stances towards coastal photogrammetry. Literature suggests that if a study has contextual meaning in a person's life, then they are more likely to absorb information provided to them (Hails and Kinderlerer, 2003; Sturgis and Allum, 2004). It suggests that their level of engagement is based upon their interest in the topic. From this study, the volunteers expressed an understanding of how coastal processes can affect them either directly, from coastal flooding during storm events, or indirectly, through negative impacts inflicted on infrastructure and commercial developments. The residents seemed to possess lay expertise regarding the Fylde Coast which in coastal topography facilitates the efficient identification of developing erosional features such as toe scour or the more widely affecting, beach lowering. Local qualitative knowledge of sediment levels along large sections of coast seemed be present among the volunteers, which could help in the discovery of erosional features such as toe scour along the coast. This provides a means for efficient detection-and-monitoring if combined with the community group's ability to perform photogrammetric coastal surveys.

Overall perceptions towards the photogrammetric approach were positive, however, adverse weather conditions are likely to affect data collection abilities. This was observed during the first session, as participation decreased when transitioning

from the indoor to the outdoor activity due to a cold, consistent wind from the Irish Sea. Furthermore, feedback gained from the questionnaire during the first session regarding data transfer appeared to show 86% percent were comfortable transferring data wirelessly via data transfer websites (Figure 30c), yet only 50% of data was retrieved. This could be related to declining motivations once separated from community activities.

Overall, observations made on the community group suggest a highly motivated coastal group collectively. However, the data transfer procedure seemed to be the biggest challenge when conducting field studies with this group, and momentum in proactive engagement is required if data collection is to happen in their own time.

5.6. A Comparison to Other Topographical Methods

In this study, photogrammetric surveys using smartphones operated by citizens have been shown to provide suitable accuracies that are consistently lower than <0.05 m when compared to check points. As it currently stands, airborne LiDAR surveys cover larger swaths of coastline, with freely available data that yield accuracies of between 0.25 m and 2.0 m ground sampling distance (x and y) and between 0.12 m and 0.35 m in the vertical (z) dimension (Miles, 2014), however, the frequency is much lower than the potential offered by photogrammetric surveys conducted by citizens.

This study has demonstrated the capability of citizen-derived imagery as a source of data for SfM; exhibiting maximum inaccuracies of up to ~ 0.07 m at distances of 50 m offshore – an area of especially high erosion during storm events therefore often

requiring diligent monitoring (Wyre Borough Council, 2004). If this type of CS project became an integral part of community activities, then monitoring frequency could increase significantly at high spatial resolutions. Volunteers stated they would be willing to integrate data collection for SfM photogrammetry into The Rossall Beach Residents and Community Group's set of activities (Appendix 9B).

5.7. The Potential Framework for a Citizen Science Coastal Data Collection Programme

Due to the intensity and length of the sessions run for this study, it would be feasible to run similar sessions at 6-month intervals, and more frequently as expertise develops within the group. The sessions are planned to be run by the partner SME, Jane Littlewood from The Rabbit Patch Ltd. who has built knowledge and understanding of the SfM process. Running of the sessions would involve demonstrations out on the beach by leaders of the project to participants followed by the data collection activity.

Areas of topographic interest should be investigated to determine whether the surroundings are fit for a GCP network to be established following the guidelines set out in section 5.3. If the guidelines can be followed, then a GCP network can be established and repeated surveys can take place, though if only localised measurements are required then something with a known distance should be included in the models – however model accuracy can only be made with respect to other models. If a GCP network is established, then model accuracy can be tested against points of known coordinates and measurements can be related to other disconnected models. When conducting the survey models should be produced in

batches of two or more to increase the likelihood of generating successful models. This also provides the added benefit of cross-referencing models with each other for further topographic assessment (Prosdocimi et al., 2015). This helps to identify erroneous data by showing topographical differences through visual DEMs of difference and the data can be extracted for use within other statistical tests such as providing RMSE values shown in section 4.2.

The idea of community group data collection extends beyond organised sessions by establishing a deep knowledge of the SfM process into participants with the potential for data collection in their own time. By having participants who are capable and encouraged by project leaders to carry out the SfM imaging procedure, the ability to monitor the coastline at short notice becomes achievable. This opens the possibility for rapid post-storm beach surveys to take place when researchers might not be able to gather equipment, human resources or be in the vicinity to carry out the research themselves.

6. Conclusions

This study had 2 primary objectives regarding data outputs from a coastal SfM-orientated CS project: (1) To assess the accuracy of point cloud products of a coastal environment derived from imagery collected by citizens, and (2) analyse the response from participating public members towards the SfM imaging procedure. This conclusion revisits the objectives set out at the start of this project and reviews the successes and problems encountered throughout.

6.1. Assessing the Accuracy of Citizen-derived Coastal Point Cloud Products

Images acquired during this study proved to be a viable source of data for scientifically useful 3D models. The act of capturing imagery was undertaken successfully in both sessions, however, lesser practiced tasks such as data transfer were identified to be a limiting factor on the volume of gathered data. Despite this, images that were transferred from participant to researcher generated successful high-density topographic models which can be manipulated to suit the objective of study – whether large-scale beach morphological changes are to be monitored therefore requiring low density point cloud/DEM products or small-scale processes such as toe-scour utilising the high-density nature of the point cloud.

6.1.1. Suitability of Citizen-Derived Imagery

Citizen-derived imagery has displayed the potential for use within a scientific domain. At this point it still requires a brief set of instructions and training into the technique

for data collection. For this reason, it is a suitable tool for coastal community groups as they provide a dedicated group of willing volunteers, however, further analysis would need to be conducted into minimising the quantity of photos needed for successful point cloud reconstruction if the method were to be applied to the wider public.

Overall, this thesis suggests that citizen-derived imagery is a viable data source for coastal monitoring, however it highlights the difficulties involved with acquiring data from volunteers and processing it efficiently. If the computing power is sufficient, then depth filtering can increase to provide cleaner models and thus reduce manual post-processing tasks.

6.1.2. Point Clouds Prior to Georeferencing

Sparse point cloud generation was successful for each device throughout both sessions which demonstrates the fact that the correct imaging procedure had been performed. In total out of both sessions only one device did not manage to produce the full dense point cloud reconstruction- the CUBOT X15. This shows that there is a high success rate in the geometry reconstructions from a citizen-derived dataset. Sparse geometry could be reconstructed with ease, however, where dense reconstructions are necessary processing times are significantly increased. Dense point clouds were successfully produced across the full range of GCP configurations for the PL50, iPhone 6s and iPhone X, however, were limited to only the 'Full Distribution' GCP configuration for the Galaxy S5 and EOS 450D due to processing time constraints (Table 16). The processing and post-processing times required to produce dense point clouds require

hours. It seems that for the coastal setting, noise is introduced relatively easily and needs to be accounted for. This means more aggressive depth filtering settings are recommended if computing power allows (Agisoft, 2016), however increased processing times result from this as shown in the Methodology. Occasionally, processing times results in the SfM procedure to be halted and resumed on a less aggressive filter setting. To ensure the maximum leverage from the collected data is achieved, multiple participants photographed the same scene.

This study proves that from a single CS session, multiple 3D models can be produced thus providing the ability for model to model assessment. This allows for deviations in topography to be analysed between model without the need for georeferencing. However, to gain further insight into model accuracy the use of real-world coordinates needs to be used to relate point cloud reconstructions to points of known coordinates.

6.1.3. Georeferenced Clouds

Reconstructed dense clouds were georeferenced with a variety of GCP configurations. Each configuration manipulates model geometry and therefore has a direct effect on the accuracy of the 3D models. This study has tested 8 different varieties of GCP configuration to attempt to understand the different model topographies that might be generated in various locations along the coast. Where a typical research investigation would establish the most ideal GCP network to achieve minimal RMSE - such as investigations carried out by James et al. (2017a) - this study investigates non-ideal GCP setups due to constraints that are intrinsic to the nature of a CS project of

this kind. This CS project requires GCPs to be permanent to remove the need for repeated GNSS surveys – often resulting in GCP placement to be on coastal structures. This study has revealed that coastal structures that run perpendicular to the shoreline provide, on average, the best model accuracies. Between the PL50, iPhone 6s and iPhone X when ‘All Groyne’ GCP configurations were compared to their respective ‘Full Distribution’ reference models, RMSE was ≤ 0.012 m suggesting the models were highly similar. This is coherent with literature which suggests a GCP network encompassing the area of study provides the least error in linear and non-linear geometries (James and Robson, 2012; James et al., 2017a). When each GCP configuration is averaged for each device, model accuracies are slightly lower than other photogrammetry studies (James and Robson, 2012; Prosdocimi et al., 2015), however, RMSE still falls far below those from Airborne LiDAR or satellite acquired optical imagery (Miles, 2014).

When comparisons were made between devices for each of their respective ‘Full Distribution’ models, initially sparse point cloud products would suggest larger deviations in topography. However, once the number of outliers were removed during the dense reconstruction procedure RMSE values were brought down to similar magnitudes to the GCP configurations. RMSE ranged from 0.007 m (for the PL50) to 0.015 m (for the Galaxy S5) between all devices after filtering. This shows that there is minimal impact inflicted on model topography using the cameras included in this study. When compared to other SfM studies in the geosciences that often use DSLR cameras, this model produced in this study provide slightly lower accuracies but they act as a guide for what is achievable by citizen-operated smartphone SfM.

6.2. The Response from Participants

This thesis reviewed other citizen science projects to understand the engagement type suitable for a coastal monitoring method. In-field observations and feedback questionnaires helped shape an understanding of the group's knowledge of their coastal environment as well as their comprehension of the SfM data collection process. Throughout the study it has been evident that motivations towards coastal maintenance and arising issues has been high, with a generally positive and proactive attitude. The group were willing to undertake tasks requiring hundreds of photos to be taken in windy, cold conditions. This was significant if data collection is to occur during months with increased wave activity and sediment transport processes, as these will likely be in periods of less favourable weather conditions.

However, it was also evident that participation numbers dropped considerably when transitioning between the indoor activity in the first session, to the outdoor activity. The same is true for the transition from the first session in September, to the second session in later October 2018. Although conclusions cannot be drawn from two occasions alone, it seems logical that fewer participation numbers occur in less favourable conditions. Despite this, the data gathered covered the entire area of study and thus a topographical insight could be gained. This study aids scientific understanding about a SfM CS project conducted on a beach, both from a social and technical standpoint.

6.3. Contributions to Research and Coastal Management

Citizen science projects have huge implications on research and coastal management. By integrating science into the public domain vast improvements can be made to the issues often faced within the scientific community: (1) The lack of available human resources often limits professional scientific activity, (2) considering the huge expanse of coastline, the diversity of topographies and their constant changing morphologies, a comprehensive understanding of this environment requires intensive research over space and time (Garcia-Soto and van der Meeren, 2017). This CS study enhances our understanding of what a CS project might look like when trying to generate coastal topography from public-acquired data.

By utilising smartphones that have penetrated and proliferated throughout most of the developed world we can record measurements of the coastal environment on scales that were previously unachievable. This study proves that the SfM photogrammetry technique can be carried out successfully to produce highly accurate topographic models. In a collaborative effort between scientists and community group members, it is possible to generate dense point clouds which provide vital information on the large- and small-scale processes that shape the coast – The Rossall Beach Residents and Community Group is an example of such a success. The data from this study is of a higher resolution than the current periodical airborne LiDAR surveys conducted by the EA (Miles, 2014) and has the potential to be far more frequent and adaptive. Additionally, this project was conducted through the enthusiasm of the

participants, requiring no cost – a factor that is limiting to both scientific research and coastal management.

6.4. Contributions to Public Engagement within Coastal Science

This CS project contributes towards deepening the public understanding of the coastal environment, the impacts climate change has and the role that humans are playing in the driving of such change (Garcia-Soto and van der Meeren, 2017). It has demonstrated that members of the Rossall Beach Residents and Community Group are willing to incorporate SfM sessions into their scheduled activities which suggests that there is an interest in the outcomes achieved by such a programme. By participating in these sessions, citizens are encouraged to record data on areas that are highly dynamic or host erosional features such as toe scour.

This immersion within a coastal setting and the data capture of coastal processes has shown to increase public awareness into what processes affect the shape of the coastline. After the sessions were conducted, participants understood how coastal erosion such as toe scour can be detrimental to sea defences. Incremental improvements to coastal literacy like those achieved during this study help to build a scientific way of thinking and importantly build confidence in scientific research.

6.5. Future Work

Currently there is still work that can be done to develop citizen-led coastal photogrammetry as a viable source of scientific data. On the small scale, operated by

community groups, the methods for coastal photogrammetry do not require too much complexity. The study showed that with only a few volunteers, a full groyne cell can be surveyed in x, y and z dimensions and produce accuracies capable of detecting morphological change in coastal environments. More research would be needed to identify how social interactions fluctuate throughout the year due to weather and what effect this has on monitoring key coastal erosion such as toe scour - whose scale this study is focused on. However, it has been evident that coastal community groups are likely to be willing to perform surveys as part of the activities conducted as it holds interest and relevance in their lives.

If project scales are to increase and measurements are to be undertaken by the public, then informal training will become difficult. Instead some form of infrastructure might have to be developed; for example, information boards detailing instructions on the SfM procedure. Additionally, further research would have to be conducted into the minimal number of images required for different coastal environments to adhere to a method more suited to the general public.

7. References

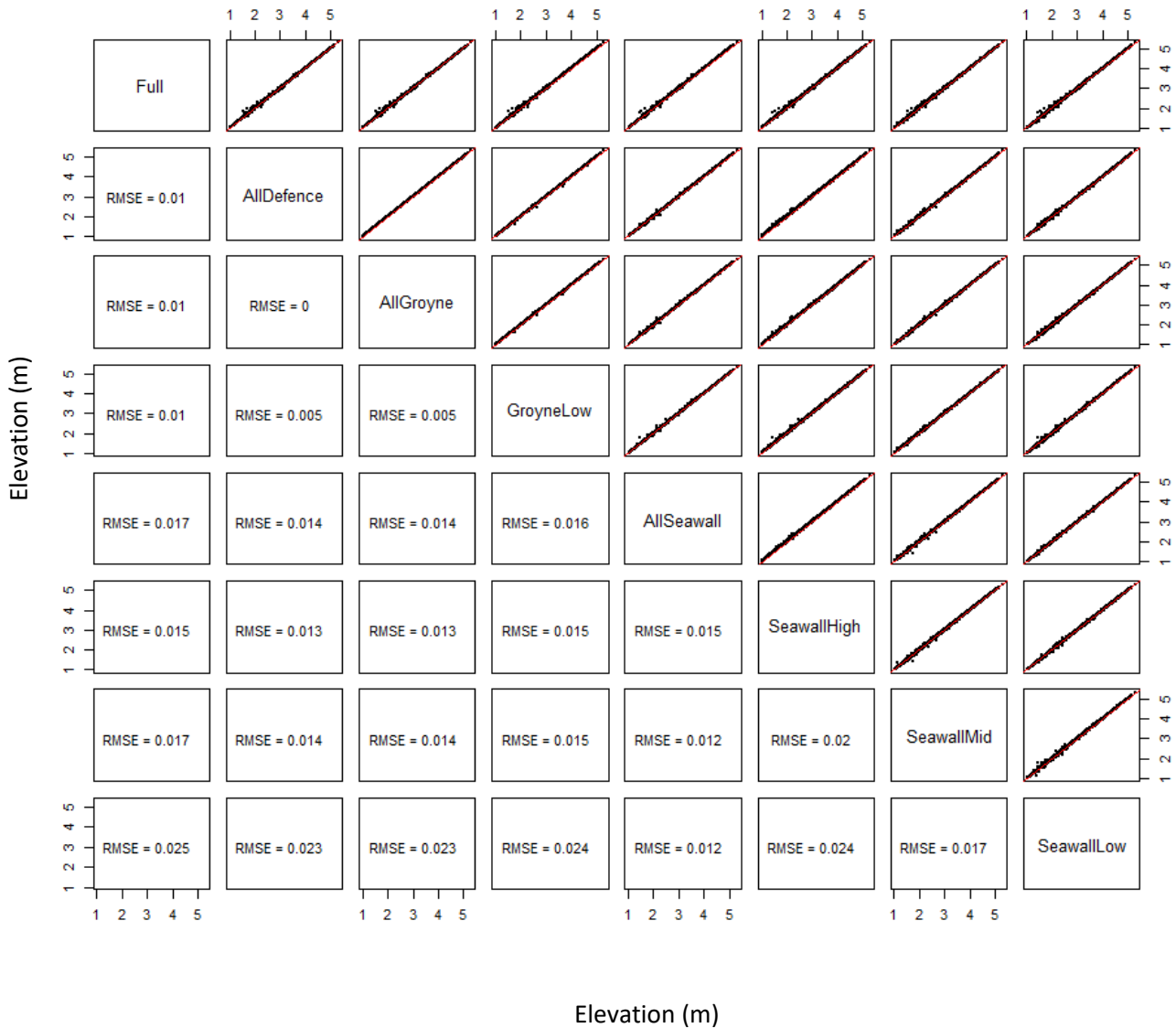
- Agisoft 2016. Agisoft Photoscan User Manual: Professional Edition, Version 1.2. *In*: AGISOFT (ed.).
- Agisoft 2018. Agisoft PhotoScan Professional. 1.4.5 ed.
- Airbus Defence and Space 2015. Coastline Changes and Satellite Images - Storms over La Salie Beach, French Atlantic Coast.
- Bradbury, A., Rogers, J. & Thomas, D. 2012. Delivering benefits through evidence. Environment Agency, Bristol: Environment Agency.
- Brunier, G., Fleury, J., Anthony, E. J., Pothin, V., Vella, C., Dussouillez, P., Gardel, A. & Michaud, E. 2016. Structure-from-Motion photogrammetry for high-resolution coastal and fluvial geomorphic surveys. *Geomorphologie-Relief Processus Environnement*, 22, 147-161.
- Clapuyt, F., Vanacker, V. & Van Oost, K. 2015. Reproducibility of UAV-based earth topography reconstructions based on Structure-from-Motion algorithms. *Geomorphology*, 260, 4-15.
- Cracknell, A. P. 1999. Remote sensing techniques in estuaries and coastal zones. *International Journal of Remote Sensing*, 19, 11.
- De Alegria Arzaburu, A. R., Ilic, S. & Gunawardena, Y. 2007. A study of intertidal bar dynamics using the Argus video system. *Coastal Sediments' 07*.
- Earlie, C., Masselink, G., Russell, P. & Shail, R. 2015. Application of airborne LiDAR to investigate rates of recession in rocky coast environments. *Coastal Conservation*, 19, 14.
- Environment Agency. 2018. *data.gov* [Online]. Available: <https://data.gov.uk/dataset/6a117171-5c59-4c7d-8e8b-8e7aefe8ee2e/lidar-composite-dtm-1m> [Accessed].
- Esa 2013. Sentinel-2. *In*: AGENCY, E. S. (ed.).
- Garcia-Soto, C. & Van Der Meeren, G. 2017. Advancing Citizen Science for Coastal and Ocean Research. *In*: MCDONOUGH, N. (ed.). European Marine Board.
- Girardeau-Montaut, D. 2003. CloudCompare.
- Hails, R. & Kinderlerer, J. 2003. The GM public debate: context and communication strategies. *Nature Reviews Genetics*, 4, 819-825.
- Harley, M. D., Turner, I. L., Short, A. D. & Ranasinghe, R. 2011. Assessment and integration of conventional, RTK-GPS and image-derived beach survey methods for daily to decadal coastal monitoring. *Coastal Engineering*, 58, 194-205.
- Hassaballah, M., Abdelmgeid, A. A. & Alshazly, H. A. 2016. Image Features Detection, Description and Matching. *Studies in Computational Intelligence*, 34.
- James, M. R. & Robson, S. 2012. Straightforward reconstruction of 3D surfaces and topography with a camera: Accuracy and geoscience application. *Journal of Geophysical Research-Earth Surface*, 117.
- James, M. R., Robson, S., D'oleire-Oltmanns, S. & Niethammer, U. 2017a. Optimising UAV topographic surveys processed with structure-from-motion: Ground control quality, quantity and bundle adjustment. *Geomorphology*, 280, 51-66.
- James, M. R., Robson, S. & Smith, M. W. 2017b. 3-D uncertainty-based topographic change detection with structure-from-motion photogrammetry: precision

- maps for ground control and directly georeferenced surveys. *EARTH SURFACE PROCESSES AND LANDFORMS*, 43, 19.
- Jones, H. W. 2018. The Recent Large Reduction in Space Launch Cost. *International Conference on Environmental Systems*. Albuquerque, New Mexico.
- Lipakis, M., Chrysoulakis, N. & Kamarianakis, Y. 2018. *Shoreline extraction using satellite imagery*.
- Liu, Y., Li, M., Zhou, M., Yang, K. & Mao, L. 2013. Quantitative Analysis of the Waterline Method for Topographical Mapping of Tidal Flats: A Case Study in the Dongsha Sandbank, China. *Remote Sensing*, 5, 20.
- Micheletti, N., Chandler, J. & Lane, S. 2015a. Investigating the geomorphological potential of freely available and accessible Structure-from-Motion photogrammetry using a smartphone. *Earth Surface Processes and Landforms*, 40, 13.
- Micheletti, N., Chandler, J. & Lane, S. 2015b. Structure from motion (SfM) photogrammetry. *British Society for Geomorphology, Geomorphological Techniques*.
- Miles, A. 2014. *Towards an understanding of intertidal forms and processes on the Fylde Coast through integrating field observations, remotely sensed data and morphodynamic models.*, Lancaster University.
- Miles, A., Ilic, S., James, M. & Whyatt, D. 2013. Morphological evolution around a groyne structure at Cleveleys beach, Northwest England, during a range of wave conditions.
- Mlambo, R., Woodhouse, I., Gerard, F. & Anderson, K. 2017. Structure from motion (SfM) photogrammetry with drone data: A low cost method for monitoring greenhouse gas emissions from forests in developing countries. *Forests*, 8, 68.
- Nazia, P. 2018. Engineers accused of botching £27m Blackpool sea wall. *The Guardian*, 06.08.18.
- Pikelj, K., Rusžić, I., Ilic, S., James, M. J. & Kordić, B. 2018. Implementing an efficient beach erosion monitoring system for coastal management in Croatia. *Ocean and Coastal Management*, 156, 16.
- Prosdoci, M., Calligaro, S., Sofia, G., Dalla Fontana, G. & Tarolli, P. 2015. Bank erosion in agricultural drainage networks: new challenges from structure-from-motion photogrammetry for post-event analysis. *Earth Surface Processes and Landforms*, 40, 1891-1906.
- Rstudio 2015. RStudio: Integrated Development for R. RStudio, Inc., .
- Satellite Imaging Corporation 2007. GEOEYE-1 Fact Sheet. *In: CORPORATION, S. I.* (ed.).
- Sibson, R. 1981. A brief description of natural neighbour interpolation. *Interpreting Multivariate Data*, 15.
- Sturgis, P. & Allum, N. 2004. Science in society: re-evaluating the deficit model of public attitudes. *Public Understanding of Science*, 13, 55-74.
- Sutherland, J., Brampton, A. & Whitehouse, R. 2006. Toe scour at seawalls: monitoring, prediction and mitigation. *41st Defra Flood and Coastal Management Conference*.
- United Nations. Fact Sheet: People and Oceans. The Ocean Conference, 2017 New York.
- Usgs 2018. LANDSAT (L8) DATA USERS HANDBOOK.

- Visit Fylde Coast. 2018. *Anchorsholme Coast Protection Scheme* [Online]. The Rabbit Patch Ltd. Available: <https://visitfleetwood.info/about/seafront/rossall-coastal-defence-scheme/> [Accessed].
- Westoby, M. J., Dunning, S. A., Woodward, J., Hein, A. S., Marrero, S. M., Winter, K. & Sugden, D. E. 2015. Sedimentological characterization of Antarctic moraines using UAVs and Structure-from-Motion photogrammetry. *Journal of Glaciology*, 61, 1088-1102.
- Wigmore, O. & Mark, B. 2018. High altitude kite mapping: evaluation of kite aerial photography (KAP) and structure from motion digital elevation models in the Peruvian Andes. *International journal of remote sensing*, 39, 4995-5015.
- Williams, J. 2013. Sea-Level Rise Implications for Coastal Regions. *Journal of Coastal Research*, 12.
- Wulder, M., Masek, J., Cohen, W., Loveland, T. & Woodcock, C. 2012. Opening the archive: How free data has enabled the science and promise of Landsat. *Remote Sensing of Environment*, 122, 8.
- Wyre Borough Council 2004. Wyre Flood and Coastal Defence Strategy Plan.
- Yao, S., Aliakbarpour, H., Seetharaman, G. & Palaniappan, K. 3D patch-based multi-view stereo for high-resolution imagery. Geospatial Informatics, Motion Imagery, and Network Analytics VIII, 2018. International Society for Optics and Photonics, 106450K.

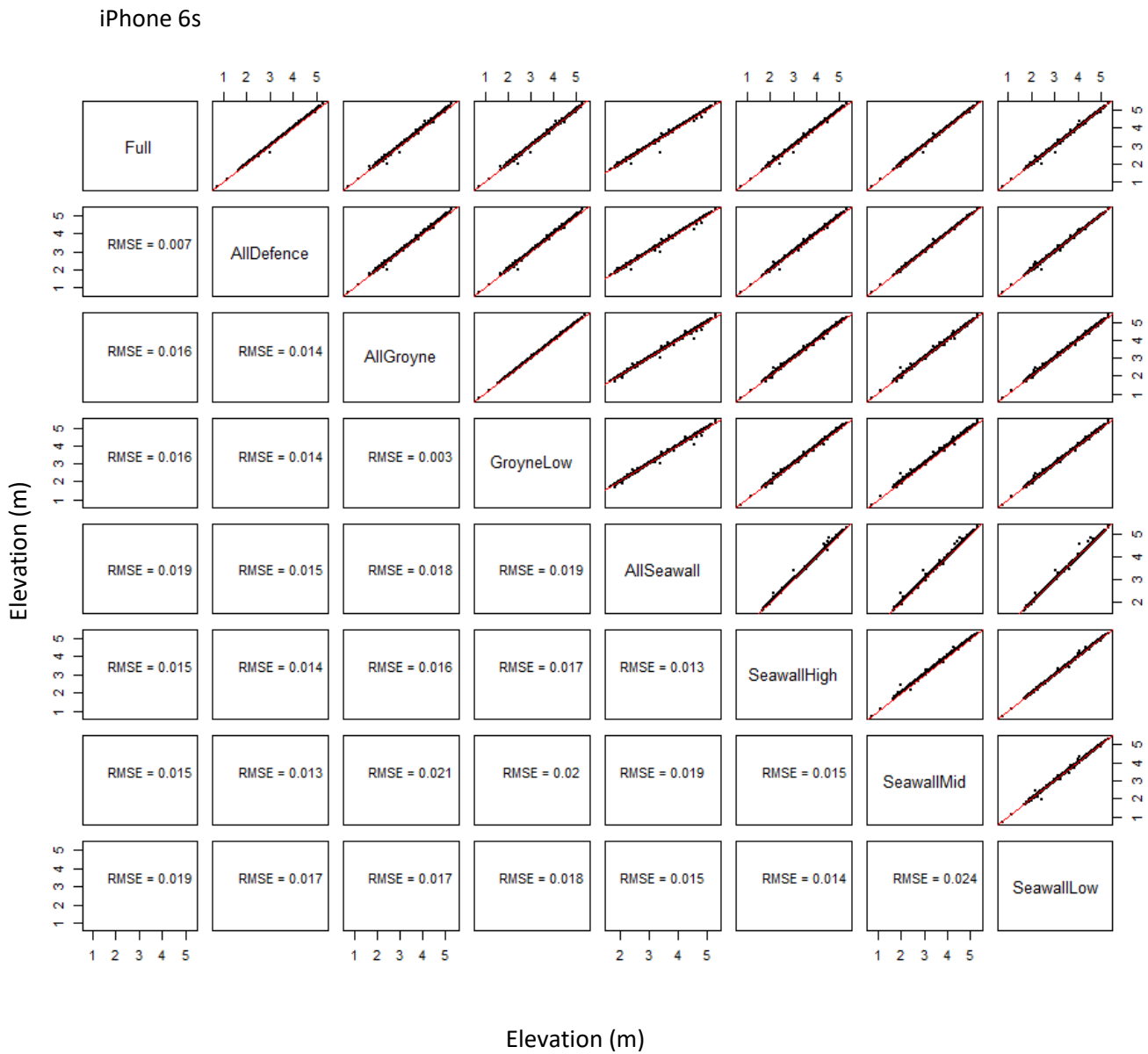
Appendix 1A – GCP Configuration Linear Regressions (Sparse) – PL50

PL50



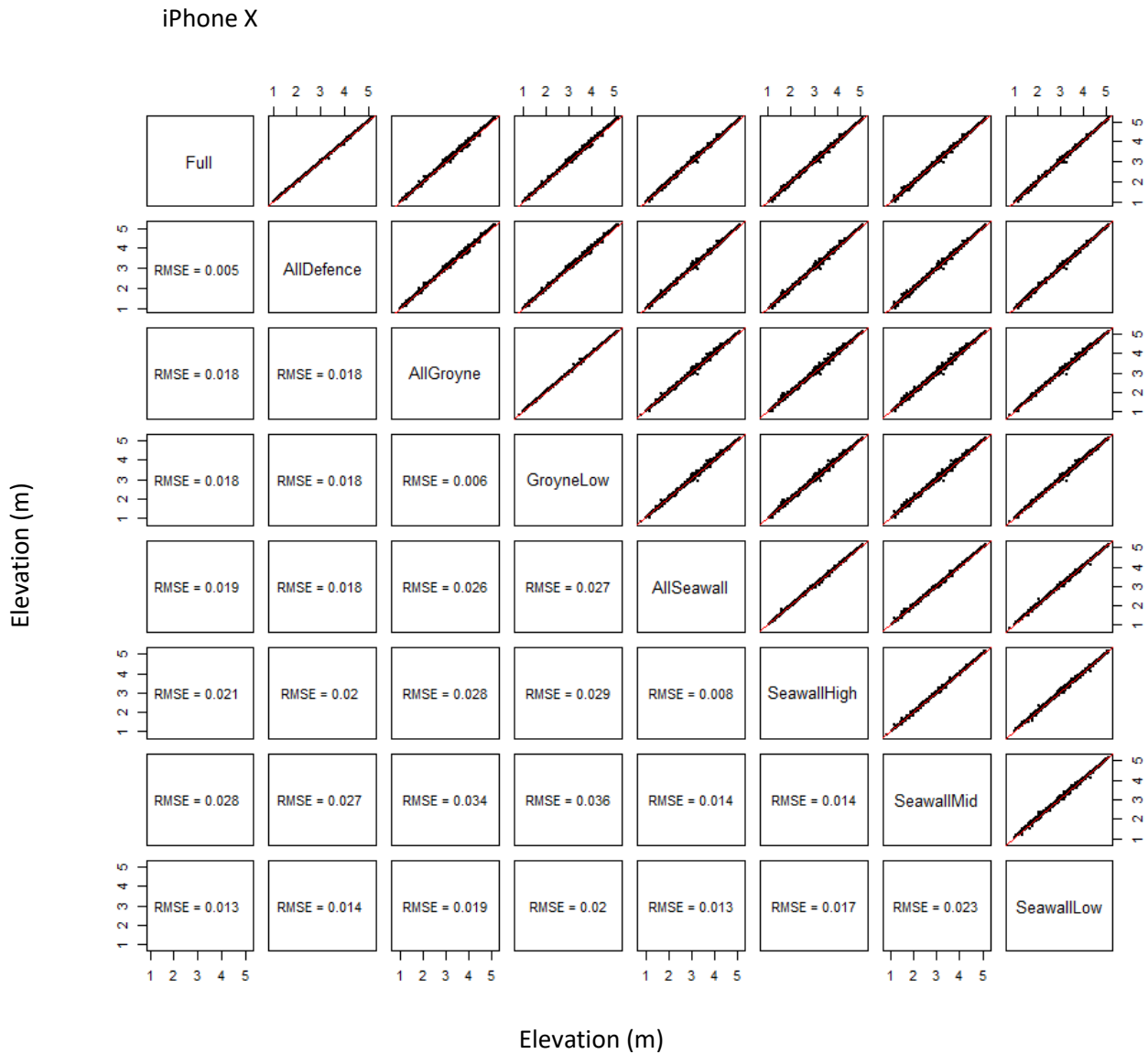
Linear regressions of Samsung PL50 GCP configurations. The red lines indicate a perfect 1:1 positive correlation

Appendix 1B – GCP Configuration Linear Regressions (Sparse) – iPhone 6s



Linear regressions of iPhone 6s GCP configurations. The red lines indicate a perfect 1:1 positive correlation

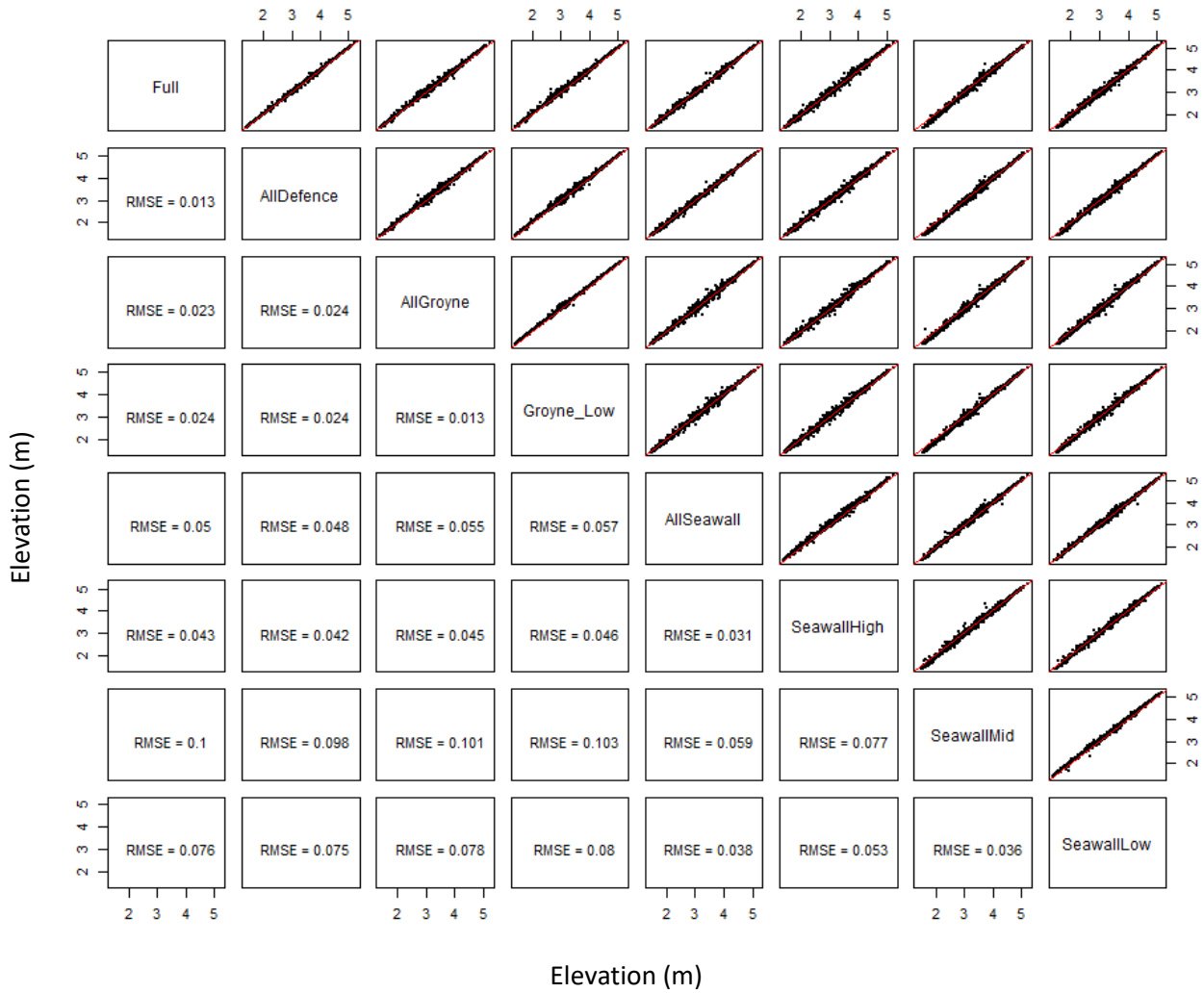
Appendix 1C – GCP Configuration Linear Regressions (Sparse) – iPhone X



Linear regressions of iPhone X GCP configurations. The red lines indicate a perfect 1:1 positive correlation

Appendix 1D – GCP Configuration Linear Regressions (Sparse) – Galaxy S5

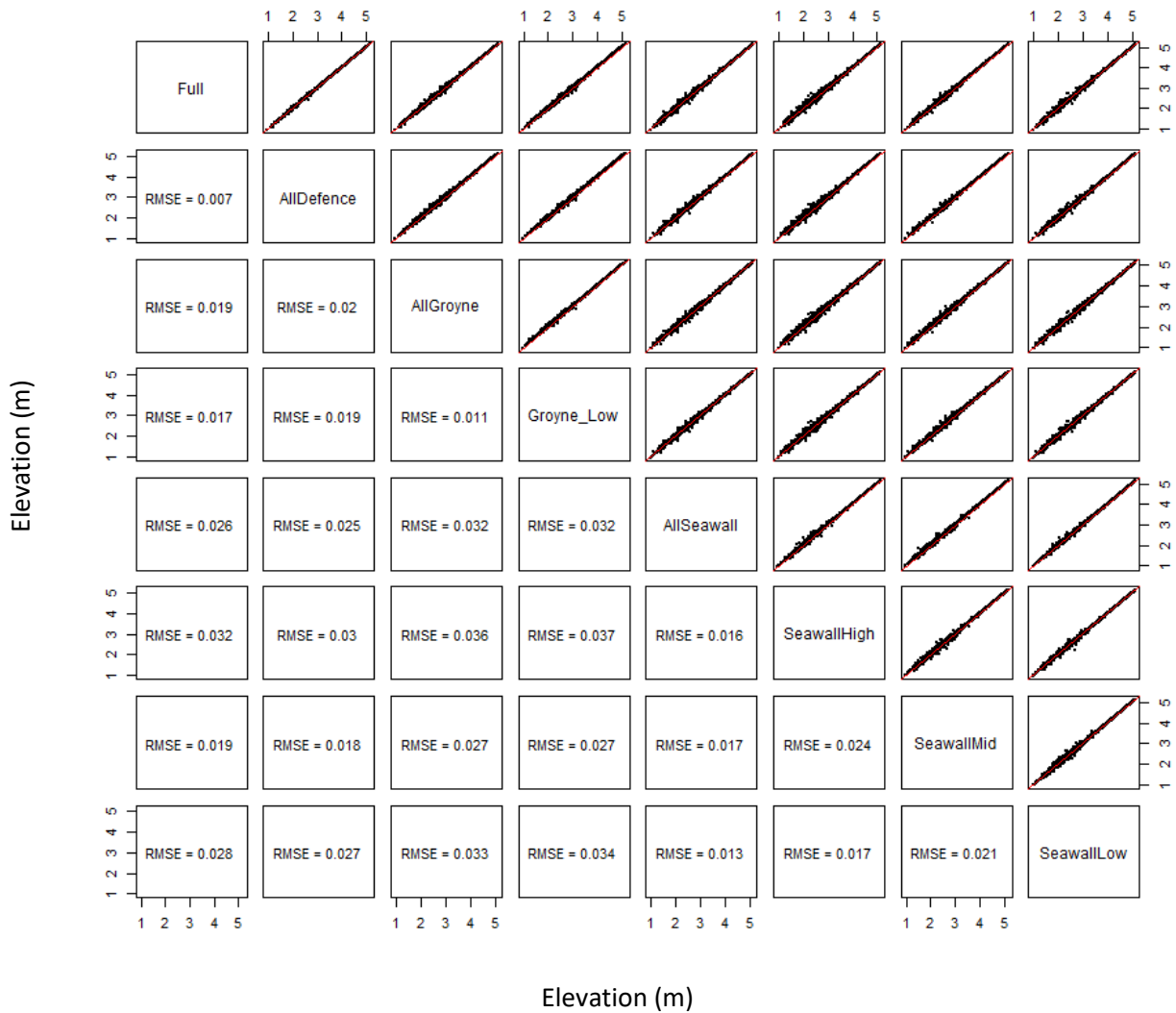
Galaxy S5



Linear regressions of Galaxy S5 GCP configurations. The red lines indicate a perfect 1:1 positive correlation

Appendix 1E – GCP Configuration Linear Regressions (Sparse) – EOS 450D

EOS 450D



Linear regressions of Galaxy S5 GCP configurations. The red lines indicate a perfect 1:1 positive correlation.

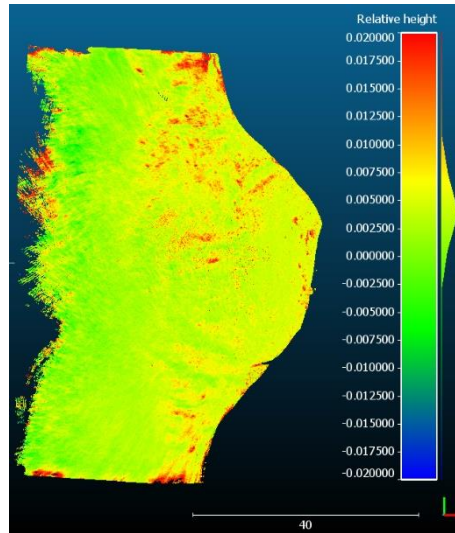
Appendix 2A – DoDs for PL50

All Defence

Volume: 8.720
Surface: 2,712.729

Added volume: (+)9.549
Removed volume: (-)0.829

Matching cells: 85.8%
Non-matching cells:
ground = 0.1%
ceil = 14.1%
Average neighbors per cell: 7.3 /
8.0

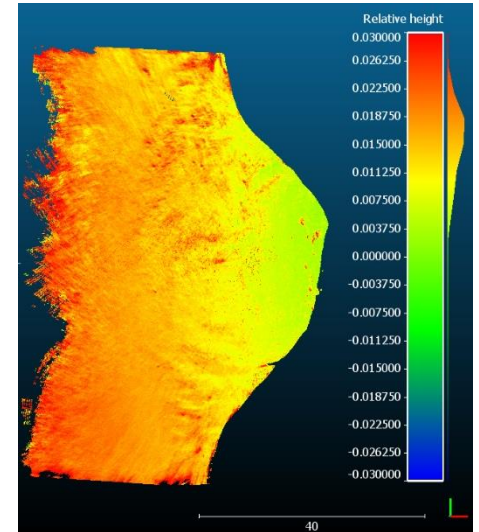


All Seawall

Volume: 39.368
Surface: 2,712.543

Added volume: (+)39.559
Removed volume: (-)0.192

Matching cells: 85.8%
Non-matching cells:
ground = 0.1%
ceil = 14.1%
Average neighbors per cell: 7.3 /
8.0

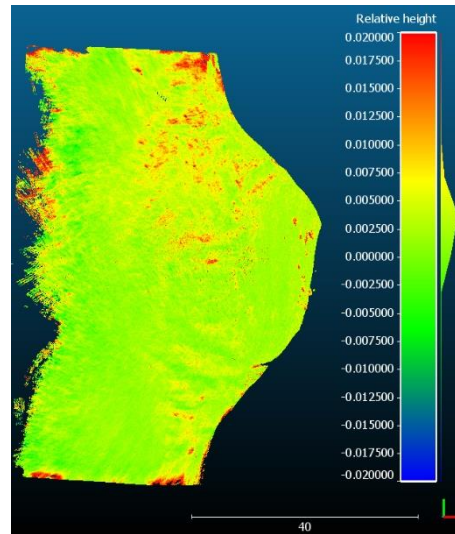


All Groyne

Volume: 5.959
Surface: 2,712.520

Added volume: (+)6.930
Removed volume: (-)0.970

Matching cells: 85.8%
Non-matching cells:
ground = 0.1%
ceil = 14.1%
Average neighbors per cell: 7.3 /
8.0

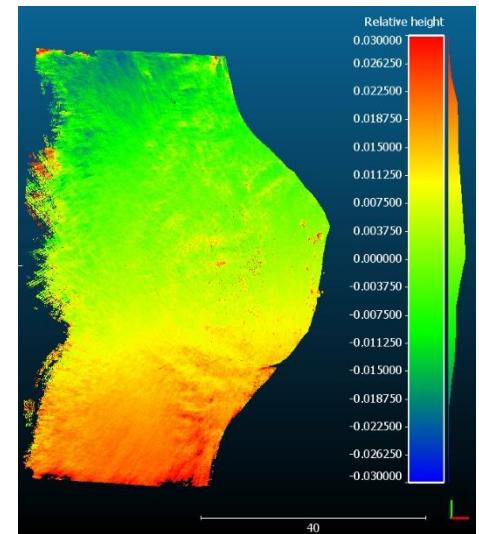


Seawall High

Volume: 10.204
Surface: 2,712.541

Added volume: (+)18.045
Removed volume: (-)7.841

Matching cells: 85.8%
Non-matching cells:
ground = 0.1%
ceil = 14.1%
Average neighbors per cell: 7.3 /
8.0

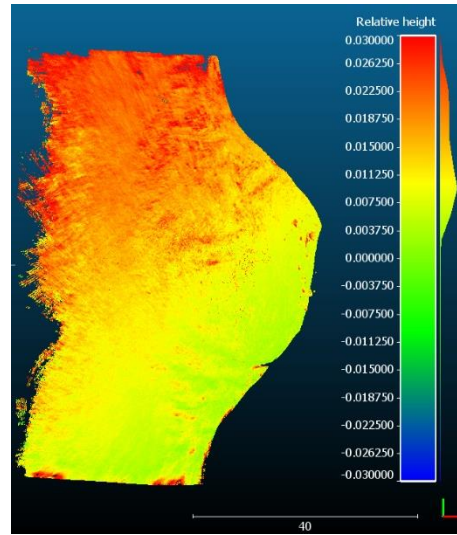


Seawall Mid

Volume: 35.523
Surface: 2,712.412

Added volume: (+)35.727
Removed volume: (-)0.205

Matching cells: 85.8%
Non-matching cells:
ground = 0.1%
ceil = 14.1%
Average neighbors per cell: 7.3 /
8.0

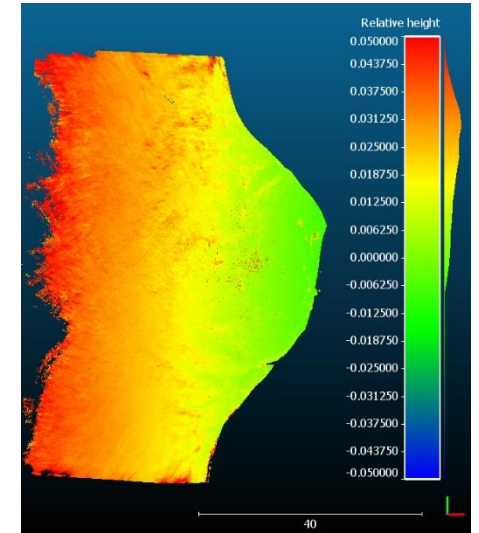


Seawall Low

Volume: 58.181
Surface: 2,711.975

Added volume: (+)59.015
Removed volume: (-)0.833

Matching cells: 85.7%
Non-matching cells:
ground = 0.1%
ceil = 14.2%
Average neighbors per cell: 7.3 /
8.0

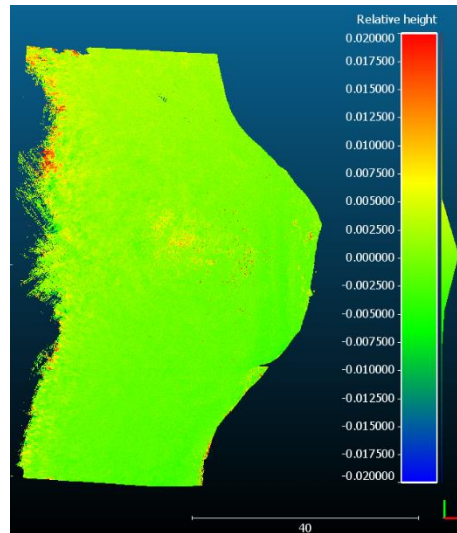


Groyne Low

Volume: -1.532
Surface: 2,655.750

Added volume: (+)1.484
Removed volume: (-)3.015

Matching cells: 95.4%
Non-matching cells:
ground = 2.1%
ceil = 2.4%
Average neighbors per cell: 7.3 /
8.0



DoDs between the Full distribution GCP configuration model and other variants of GCP configurations for the PL50

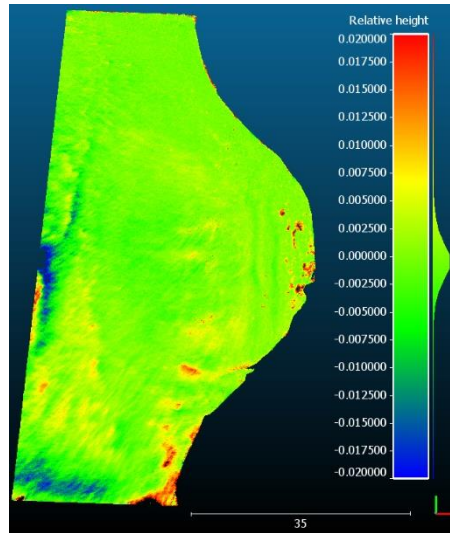
Appendix 2B – DoDs for iPhone 6s

All Defence

Volume: -1.631
Surface: 2,396.020

Added volume: (+)2.323
Removed volume: (-)3.954

Matching cells: 99.3%
Non-matching cells:
ground = 0.3%
ceil = 0.4%
Average neighbors per cell: 7.4 /
8.0

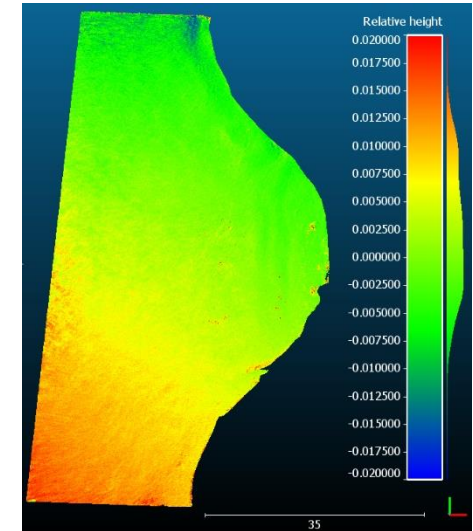


All Seawall

Volume: 5.306
Surface: 2,391.529

Added volume: (+)8.842
Removed volume: (-)3.536

Matching cells: 98.9%
Non-matching cells:
ground = 0.5%
ceil = 0.6%
Average neighbors per cell: 7.4 /
8.0

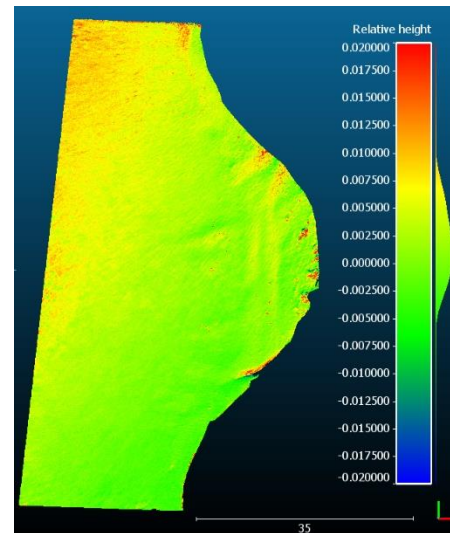


All Groyne

Volume: 4.661
Surface: 2,389.388

Added volume: (+)6.099
Removed volume: (-)1.439

Matching cells: 98.9%
Non-matching cells:
ground = 0.6%
ceil = 0.5%
Average neighbors per cell: 7.4 /
8.0

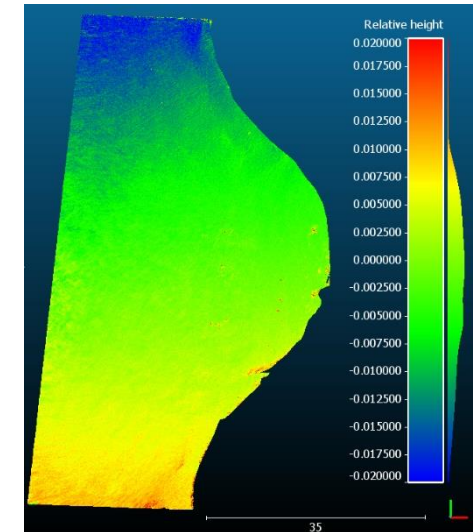


Seawall High

Volume: -6.976
Surface: 2,391.339

Added volume: (+)3.862
Removed volume: (-)10.838

Matching cells: 62.8%
Non-matching cells:
ground = 37.2%
ceil = 0.0%
Average neighbors per cell: 7.4 /
8.0

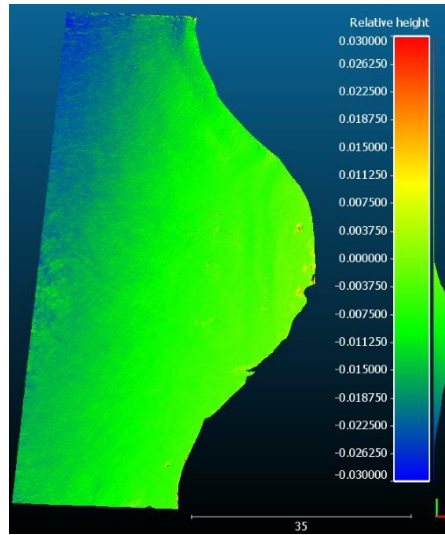


Seawall Mid

Volume: -28.552
Surface: 2,391.271

Added volume: (+)0.030
Removed volume: (-)28.583

Matching cells: 98.9%
Non-matching cells:
ground = 0.5%
ceil = 0.6%
Average neighbors per cell: 7.4 /
8.0

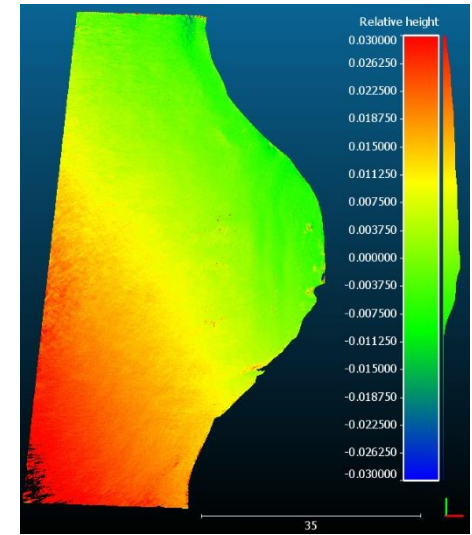


Seawall Low

Volume: 20.427
Surface: 2,391.232

Added volume: (+)22.818
Removed volume: (-)2.391

Matching cells: 98.9%
Non-matching cells:
ground = 0.5%
ceil = 0.6%
Average neighbors per cell: 7.4 /
8.0

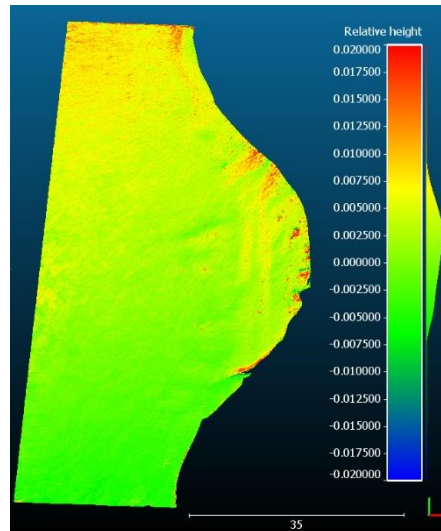


Groyne Low

Volume: 3.113
Surface: 2,389.187

Added volume: (+)5.505
Removed volume: (-)2.392

Matching cells: 98.9%
Non-matching cells:
ground = 0.6%
ceil = 0.5%
Average neighbors per cell: 7.4 /
8.0



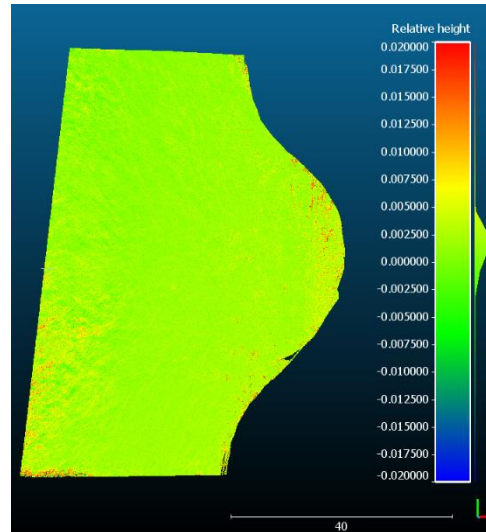
Appendix 2C – DoDs for iPhone X

All Defence

Volume: 4.336
Surface: 3,086.962

Added volume: (+)4.998
Removed volume: (-)0.662

Matching cells: 98.3%
Non-matching cells:
ground = 0.8%
ceil = 0.8%
Average neighbors per cell: 7.4 /
8.0

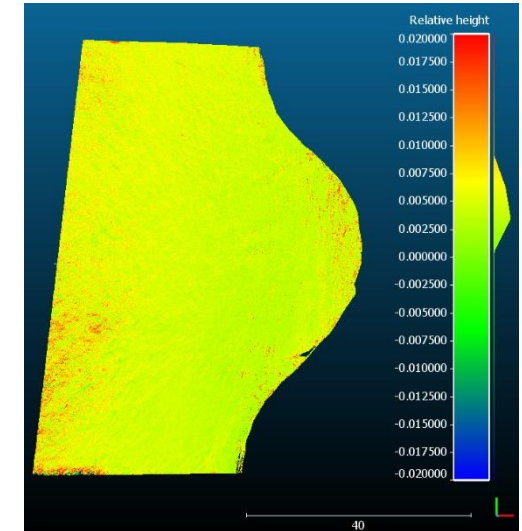


All Seawall

Volume: 13.807
Surface: 3,084.709

Added volume: (+)14.113
Removed volume: (-)0.306

Matching cells: 98.2%
Non-matching cells:
ground = 0.9%
ceil = 0.9%
Average neighbors per cell: 7.4 /
8.0

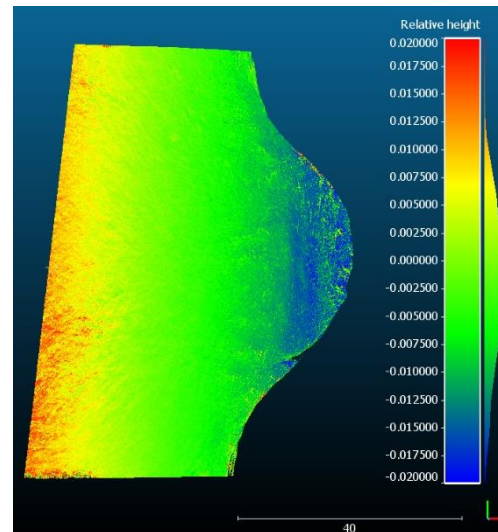


All Groyne

Volume: -8.033
Surface: 3,084.871

Added volume: (+)5.609
Removed volume: (-)13.643

Matching cells: 98.2%
Non-matching cells:
ground = 0.9%
ceil = 0.9%
Average neighbors per cell: 7.4 /
8.0

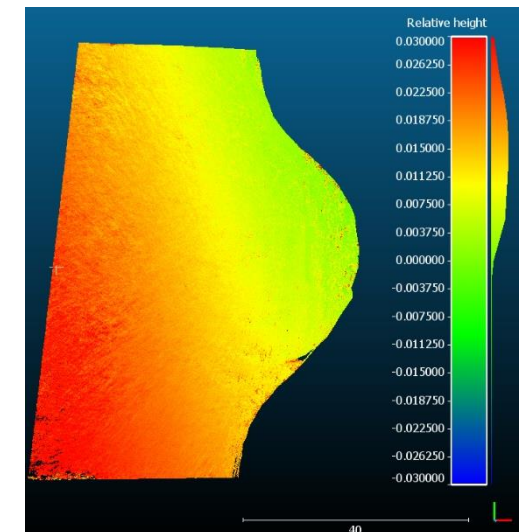


Seawall High

Volume: 45.025
Surface: 3,083.632

Added volume: (+)45.245
Removed volume: (-)0.220

Matching cells: 98.2%
Non-matching cells:
ground = 0.9%
ceil = 0.9%
Average neighbors per cell: 7.4 /
8.0

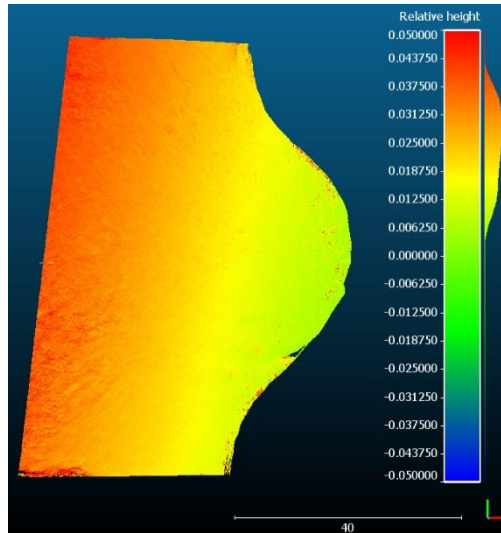


Seawall Mid

Volume: 73.846
Surface: 3,081.996

Added volume: (+)73.990
Removed volume: (-)0.144

Matching cells: 98.1%
Non-matching cells:
ground = 1.0%
ceil = 0.9%
Average neighbors per cell: 7.4 /
8.0

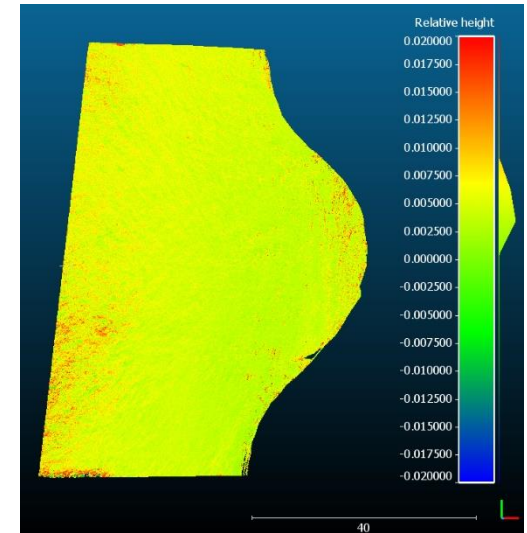


Seawall Low

Volume: 13.807
Surface: 3,084.709

Added volume: (+)14.113
Removed volume: (-)0.306

Matching cells: 98.2%
Non-matching cells:
ground = 0.9%
ceil = 0.9%
Average neighbors per cell: 7.4 /
8.0

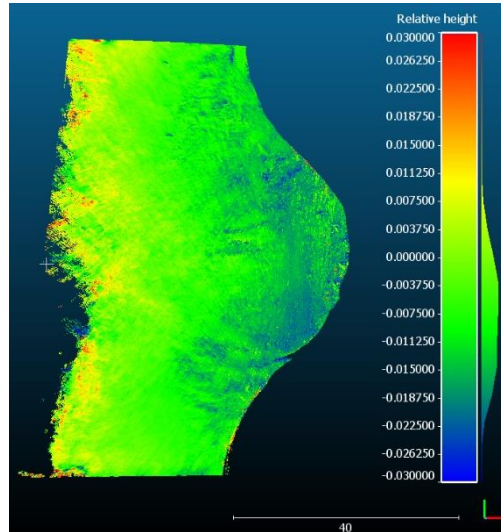


Groyne Low

Volume: -20.730
Surface: 2,679.797

Added volume: (+)1.835
Removed volume: (-)22.565

Matching cells: 84.4%
Non-matching cells:
ground = 13.6%
ceil = 2.0%
Average neighbors per cell: 7.3 /
8.0



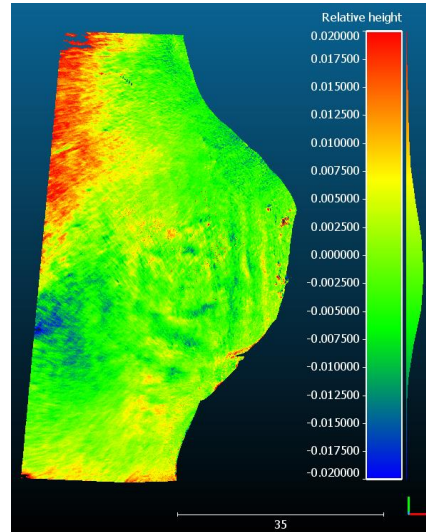
Appendix 3 – DoDs Between Devices

PL50 – iPhone6s

Volume: -2.121
Surface: 2,330.311

Added volume: (+)5.037
Removed volume: (-)7.158

Matching cells: 83.5%
Non-matching cells:
ground = 13.8%
ceil = 2.7%
Average neighbors per cell: 7.5 /
8.0

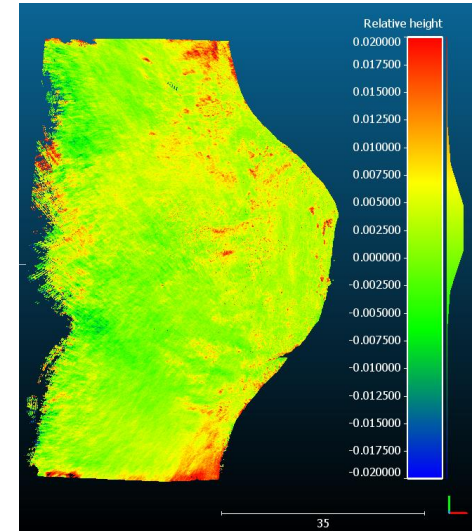


PL50 - iPhoneX

Volume: 6.042
Surface: 2,695.289

Added volume: (+)7.616
Removed volume: (-)1.574

Matching cells: 86.0%
Non-matching cells:
ground = 0.6%
ceil = 13.3%
Average neighbors per cell: 7.3 /
8.0

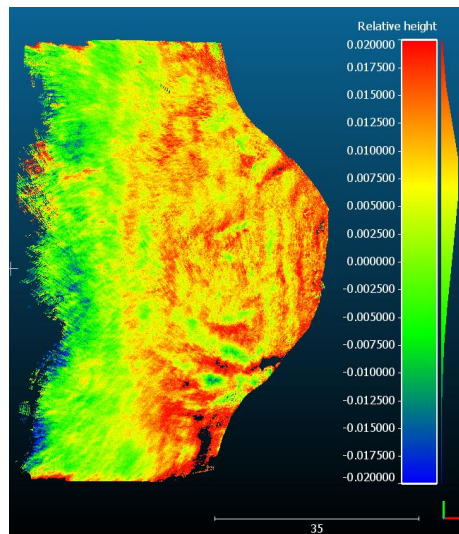


PL50 - GalaxyS5

Volume: 10.699
Surface: 2,281.599

Added volume: (+)14.206
Removed volume: (-)3.507

Matching cells: 74.2%
Non-matching cells:
ground = 14.1%
ceil = 11.7%
Average neighbors per cell: 6.3 /
8.0

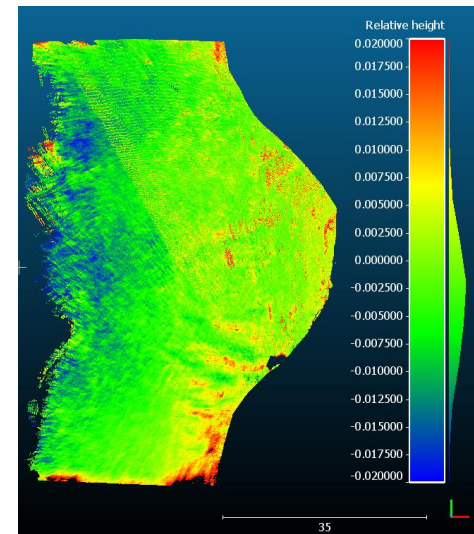


PL50 – EOS450D

Volume: -10.860
Surface: 2,649.712

Added volume: (+)2.802
Removed volume: (-)13.662

Matching cells: 82.4%
Non-matching cells:
ground = 2.0%
ceil = 15.6%
Average neighbors per cell: 7.3 /
8.0

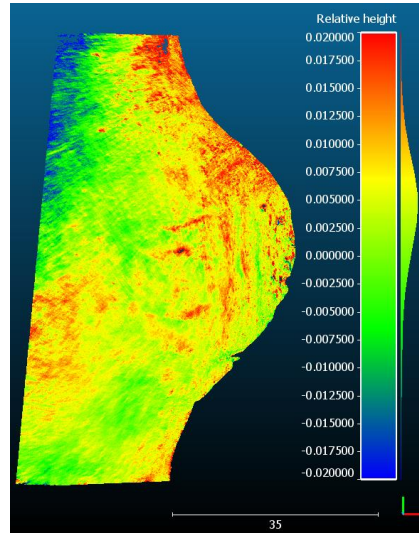


iPhone6s - iPhoneX

Volume: 7.995
Surface: 2,362.720

Added volume: (+)11.279
Removed volume: (-)3.284

Matching cells: 74.9%
Non-matching cells:
ground = 1.3%
ceil = 23.8%
Average neighbors per cell: 7.5 /
8.0

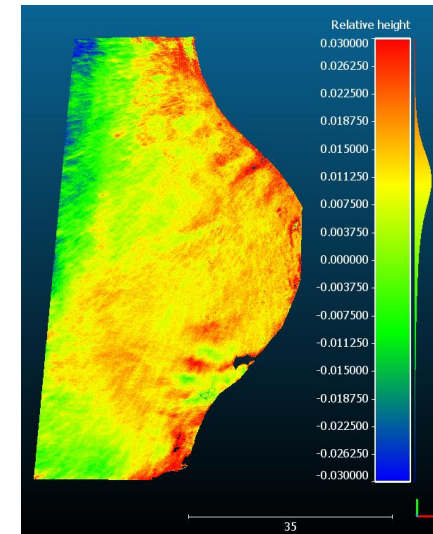


iPhone6s – GalaxyS5

Volume: 14.157
Surface: 2,003.796

Added volume: (+)17.553
Removed volume: (-)3.395

Matching cells: 65.9%
Non-matching cells:
ground = 13.2%
ceil = 20.9%
Average neighbors per cell: 6.4 /
8.0

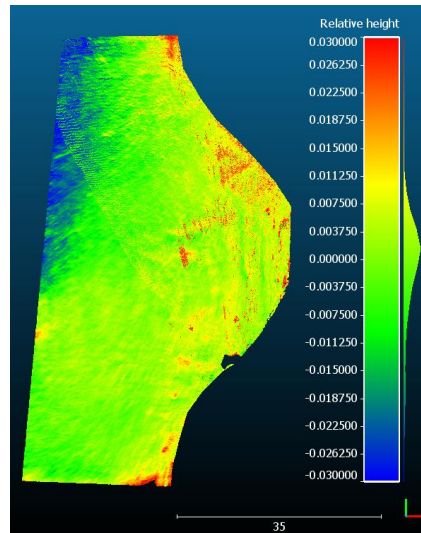


iPhone6s – EOS450D

Volume: -5.146
Surface: 2,297.773

Added volume: (+)4.944
Removed volume: (-)10.089

Matching cells: 70.6%
Non-matching cells:
ground = 3.3%
ceil = 26.2%
Average neighbors per cell: 7.5 /
8.0

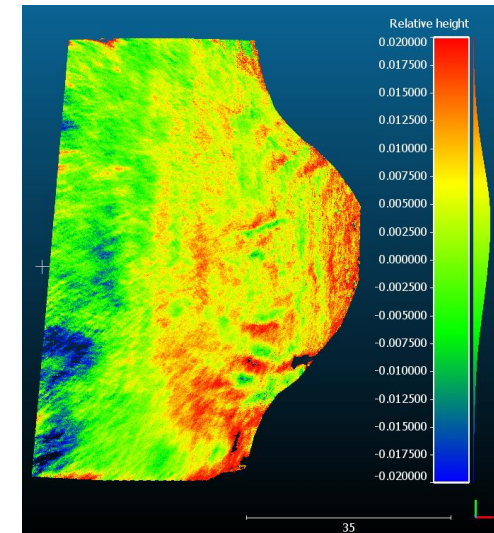


iPhoneX – GalaxyS5

Volume: 3.483
Surface: 2,534.719

Added volume: (+)10.038
Removed volume: (-)6.555

Matching cells: 78.7%
Non-matching cells:
ground = 18.0%
ceil = 3.3%
Average neighbors per cell: 6.3 /
8.0



iPhoneX – EOS450D

Volume: -20.674

Surface: 2,981.992

 Added volume: (+)1.022

Removed volume: (-)21.695

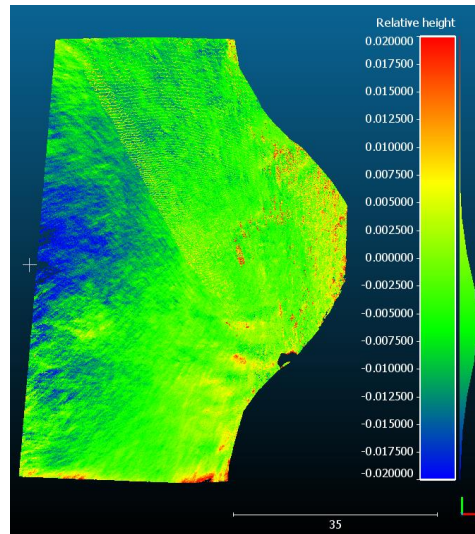
 Matching cells: 90.9%

Non-matching cells:

ground = 4.0%

ceil = 5.1%

Average neighbors per cell: 7.4 /
 8.0



GalaxyS5 – EOS450D

Volume: -20.959

Surface: 2,574.233

 Added volume: (+)1.908

Removed volume: (-)22.867

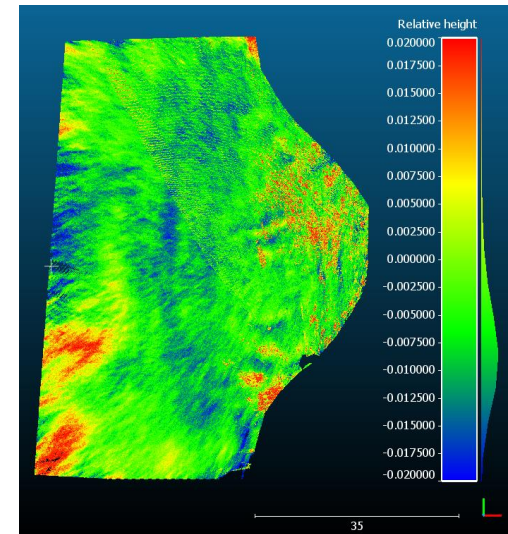
 Matching cells: 80.0%

Non-matching cells:

ground = 2.1%

ceil = 17.9%

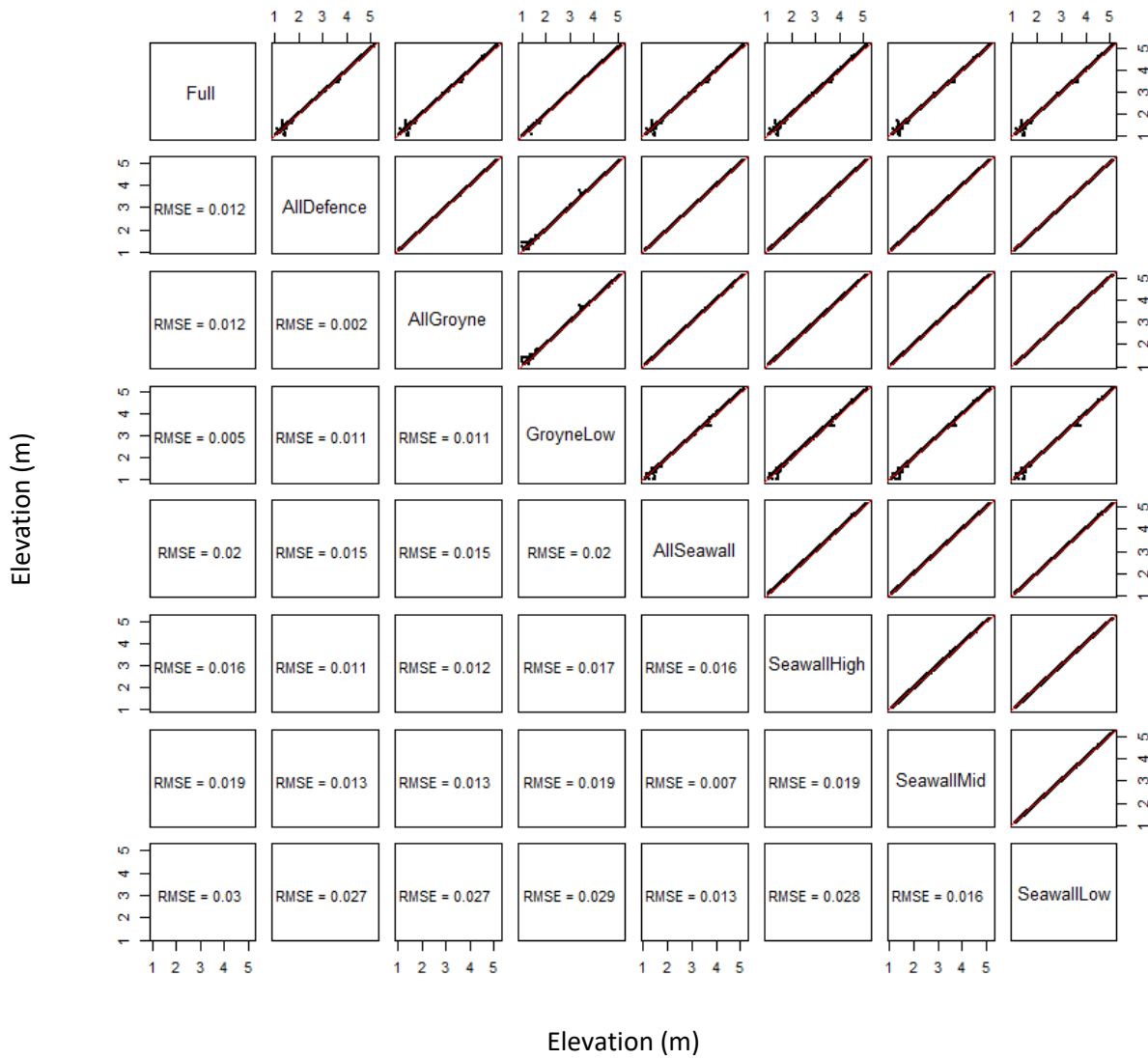
Average neighbors per cell: 6.2 /
 8.0



DoDs of Full Distribution models for each device pair. Note: negative and positive values are purely relative.

Appendix 4A – GCP Configuration - Linear Regressions (Dense) – PL50

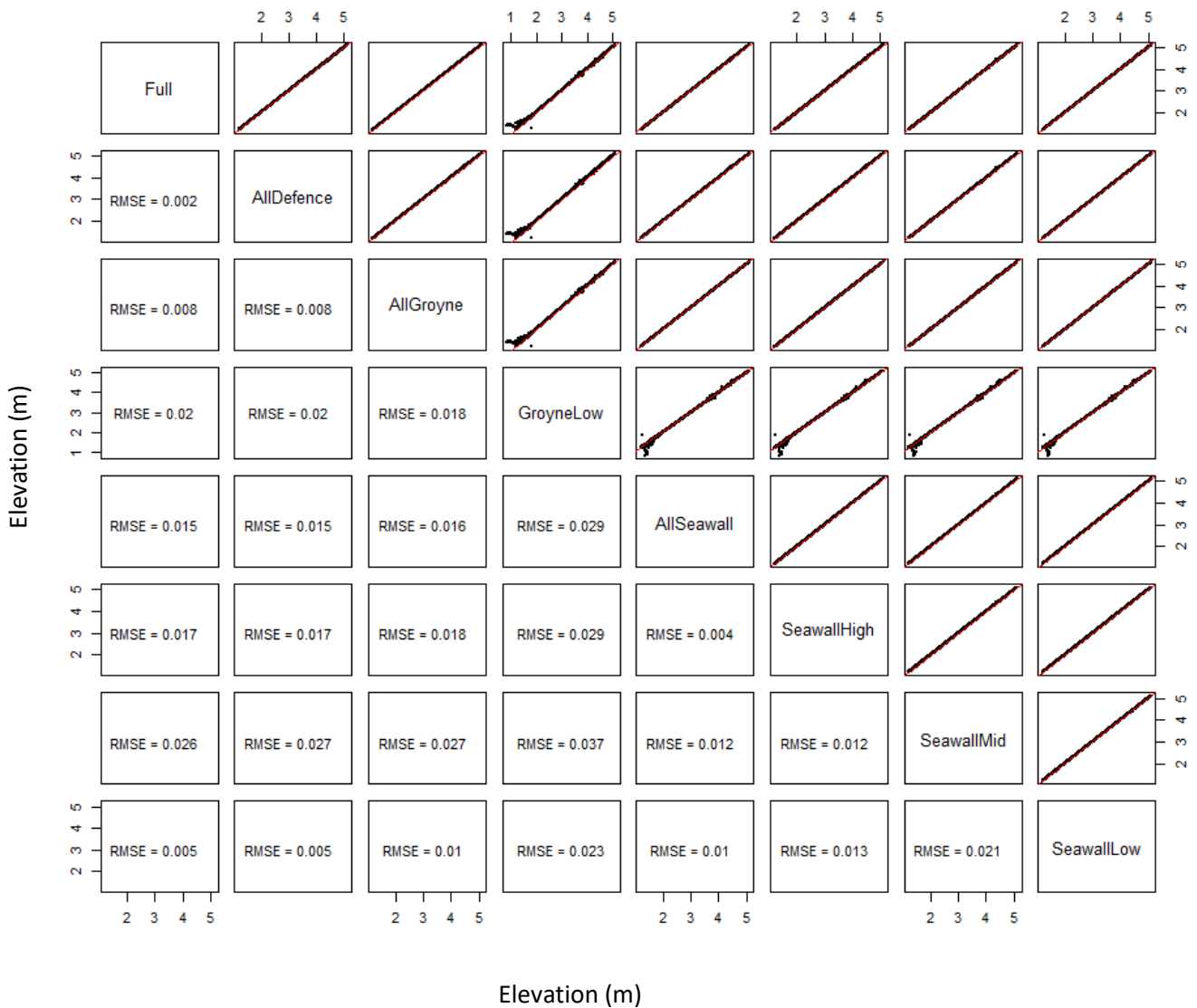
PL50



Linear regression for GCP configurations for the PL50. Red lines indicate a perfect 1:1 positive correlation.

Appendix 4C – GCP Configurations Linear Regressions (Dense) – iPhone X

iPhone X



Linear regression for GCP configurations for the iPhone X. Red lines indicate a perfect 1:1 positive correlation.

Appendix 5 – Feedback Questionnaire 1

FEEDBACK QUESTIONNAIRE

Thanks for taking part in today's activity, your data will really go a long way! I hope you've enjoyed it and you can go home happy knowing you've helped your coastline - and a very happy university student.

If you do have time, it would be huge help if you could spare a couple of minutes to fill out this questionnaire. This questionnaire is anonymous.

The following questions require a mark in the most appropriate box. Below, indicates what each number means:

1 = I completely disagree

2 = I somewhat disagree

3 = I neither agree nor disagree

4 = I somewhat agree

5 = I completely agree

ON THE BEACH

I have a clear understanding of what this project aims to achieve

| 1 | 2 | 3 | 4 | 5 |
|---|---|---|---|---|
| | | | | |

I have a clear understanding of how my involvement helps this project

| 1 | 2 | 3 | 4 | 5 |
|---|---|---|---|---|
| | | | | |

I can see how monitoring the coastline can benefit residents, commerce and infrastructural developments

| 1 | 2 | 3 | 4 | 5 |
|---|---|---|---|---|
| | | | | |

I clearly understand what toe scour is and how it can be detrimental to coastal structures

| 1 | 2 | 3 | 4 | 5 |
|---|---|---|---|---|
| | | | | |

I found the table-top practical session a very useful prior step before heading outside

| 1 | 2 | 3 | 4 | 5 |
|---|---|---|---|---|
| | | | | |

I clearly understand what scene conditions are most ideal for this project

| 1 | 2 | 3 | 4 | 5 |
|---|---|---|---|---|
| | | | | |

I clearly understand why the scene conditions are important and how each condition can affect processing

| 1 | 2 | 3 | 4 | 5 |
|---|---|---|---|---|
| | | | | |

I clearly understand how and why the camera settings are important

| 1 | 2 | 3 | 4 | 5 |
|---|---|---|---|---|
| | | | | |

I clearly understand how the correct technique for capturing imagery plays an important role for this project

| | | | | |
|---|---|---|---|---|
| 1 | 2 | 3 | 4 | 5 |
| | | | | |

I can independently download data onto my desktop/laptop

| | | | | |
|---|---|---|---|---|
| 1 | 2 | 3 | 4 | 5 |
| | | | | |

I can independently upload data via the wetransfer.com website (or other known data transfer websites)

| | | | | |
|---|---|---|---|---|
| 1 | 2 | 3 | 4 | 5 |
| | | | | |

I found 3D model generation easy

| | | | | |
|---|---|---|---|---|
| 1 | 2 | 3 | 4 | 5 |
| | | | | |

I can identify and upload the correct files vis the wetransfer.com website (or other known data transfer websites)

| | | | | |
|---|---|---|---|---|
| 1 | 2 | 3 | 4 | 5 |
| | | | | |

If you have any comments about how the indoor session went, how it could have gone differently, is there anything I missed that I should have included? or anything else whatsoever – write it here!

OUTDOOR SESSION

I collected my images on the coastline easily

| | | | | |
|---|---|---|---|---|
| 1 | 2 | 3 | 4 | 5 |
| | | | | |

I feel my imaging technique closely followed the procedure demonstrated

| | | | | |
|---|---|---|---|---|
| 1 | 2 | 3 | 4 | 5 |
| | | | | |

I can see myself doing this on a regular basis

| | | | | |
|---|---|---|---|---|
| 1 | 2 | 3 | 4 | 5 |
| | | | | |

I would be happy for sessions like this to be included as part of the Rossall Beach Residents and Community Group’s set of activities

| | | | | |
|---|---|---|---|---|
| 1 | 2 | 3 | 4 | 5 |
| | | | | |

If you have any comments about how the outdoor session went, how it could have gone differently, is there anything I missed that I should have included? or anything else whatsoever – write it here!

Appendix 6 – Feedback Questionnaire 2

FEEDBACK QUESTIONNAIRE 2

Thanks for taking part in today's activity, your data will really go a long way! I hope you've enjoyed it and you can go home happy knowing you've helped your coastline - and a very happy university student.

If you do have time, it would be huge help if you could spare a couple of minutes to fill out this questionnaire. This questionnaire is anonymous.

The following questions require a mark in the most appropriate box. Below, indicates what each number means:

1 = I completely disagree

2 = I somewhat disagree

3 = I neither agree nor disagree

4 = I somewhat agree

5 = I completely agree

Before you begin please tick this box if you are a returning volunteer

ON THE BEACH

1. I have a clear understanding of what this project aims to achieve.

| 1 | 2 | 3 | 4 | 5 |
|---|---|---|---|---|
| | | | | |

2. Taking the images on the coastline was easy.

| 1 | 2 | 3 | 4 | 5 |
|---|---|---|---|---|
| | | | | |

3. My imaging technique closely followed the procedure demonstrated.

| 1 | 2 | 3 | 4 | 5 |
|---|---|---|---|---|
| | | | | |

4. Taking images on the beach was enjoyable.

| 1 | 2 | 3 | 4 | 5 |
|---|---|---|---|---|
| | | | | |

5. I have a clear understanding of how my images will be used.

| 1 | 2 | 3 | 4 | 5 |
|---|---|---|---|---|
| | | | | |

6. I can see how monitoring the coastline can benefit residents, commerce and infrastructural developments.

| 1 | 2 | 3 | 4 | 5 |
|---|---|---|---|---|
| | | | | |

7. I clearly understand what scene conditions are ideal for this project.

| 1 | 2 | 3 | 4 | 5 |
|---|---|---|---|---|
| | | | | |

8. I understand why these scene conditions are important.

| 1 | 2 | 3 | 4 | 5 |
|---|---|---|---|---|
| | | | | |

9. I clearly understand how and why the camera settings are important.

| 1 | 2 | 3 | 4 | 5 |
|---|---|---|---|---|
| | | | | |

10. I clearly understand how the correct technique for capturing imagery plays an important role for this project.

| | | | | |
|---|---|---|---|---|
| 1 | 2 | 3 | 4 | 5 |
| | | | | |

11. I can see myself doing this on a regular basis.

| | | | | |
|---|---|---|---|---|
| 1 | 2 | 3 | 4 | 5 |
| | | | | |

12. I would be happy for group session like this to be included as a part of Rossall Beach Residents and Community Group's set of activities.

| | | | | |
|---|---|---|---|---|
| 1 | 2 | 3 | 4 | 5 |
| | | | | |

If you have any comments about how the outdoor session went, how it could have gone differently, is there anything I missed that I should have included? or anything else whatsoever – write it here!

Appendix 7 – SfM Instructions

A



THE GUIDE TO 3D MODEL GENERATION

Using VisualSfM

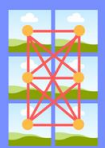
OPEN VISUALSfM + IMPORT PHOTOS

- Open the VisualSfM software from your desktop screen
- Once VisualSfM has loaded, go to 'File' > 'Open+ Multi Images' and navigate to the folder with your photos.
- Highlight the photos you want to import by clicking the first image once, then scrolling to the last and press shift+click.
- Select 'Open'
- Wait a few seconds and your images will load into the software



IMAGE MATCHING

- Begin by selecting 'SfM' > 'Pairwise Matching' > 'Compute Missing Matches'
- The software at this point is identifying which photos share features.
- Be patient - This can take a few minutes!
- Once the Log Window displays "Pairwise Matching, finished" you know the processing has been completed.



BUILD A SPARSE POINT CLOUD

- At this point you want to select 'Reconstruct Sparse'
- You should see in real-time a cloud of points forming with their associated camera positions (the rectangles you see)
- Once the Log Window displays "3D construction, finished" you know the processing has been completed.
- You can move the points around by: Rick-click mouse drag = Rotation: Left-click mouse drag = Translation



BUILD A DENSE POINT CLOUD

- Go to 'SfM' > 'Reconstruct Dense'
- A window should pop up. Save your file in a location you can remember, and use a memorable name.
- In this step, the software is building a much denser point cloud
- Be patient - This is usually the longest step!
- Once the Log Window displays "dense reconstruction, finished" you know the processing has been completed.
- To view the model select 'View' > 'Dense 3D Points' - and you should see your model!
- You can move the points around by: Right-click mouse drag = Rotation: Left-click mouse drag = Translation



UPLOAD YOUR MODEL

- Refer to the 'UPLOAD DATA' section on the 'IMAGE COLLECTION IN A COASTAL ENVIRONMENT' infographic.
- Where it says "locate and upload your coastal images", instead locate and upload the "filename.nvm" and "filename.0.ply" files. They should be in the same folder!
- Continue with the instructions from the 'UPLOAD DATA' section and you're done!

B



IMAGE COLLECTION IN A COASTAL ENVIRONMENT

Collecting images suitable for coastal management



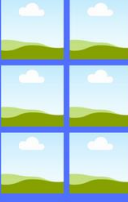
1 - THE SCENE CRITERIA

- The scene should be static
- Objects with high reflectivity should be minimised
- Vegetation should be minimised - The moving stems/leaves can affect results!
- The scene should preferably have lots of texture and features
- Diffuse lighting conditions are ideal - Bright, cloudy days are best!



2 - CAMERA SETTINGS

- Avoid using the flash on your camera
- If possible, use fixed focal lengths on your camera
- Fish eye lens' are best avoided (e.g. GoPro)
- Avoid using the zoom function on your camera



3 - TAKING YOUR PHOTOS

- Take as many images as you can/want from as many locations as possible. The more the merrier!
- Images should have approximately 60% overlap between neighbouring images
- Keep distances relatively short between your image locations
- Try to capture as many angles of the scene as possible. This will help build the 3D model!
- Aim for 10s - 100s of photographs of the scene



4 - DATA UPLOAD

- Before you start. This step will require a little bit of ingenuity!
- Visit www.wetransfer.com
- Click the 'Add your files' button then locate and upload your coastal images.
- In the 'Email to' box, type the email you wish to send the images to - Emails are found at the bottom of this page!
- In the 'Your email' box, type the email you are sending it from - This is your email!
- Click 'Transfer', wait for the files to be uploaded and you're done!



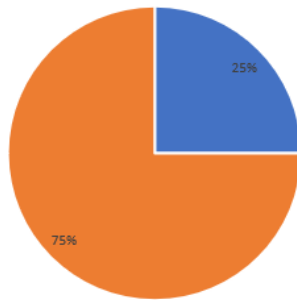
CONTACT INFORMATION

- Michael Lusty - m.lusty@lancaster.ac.uk
- Jane Littlewood - jane@therabbitpatch.co.uk

Information sheets provided for the community group members

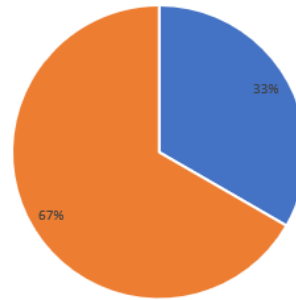
Appendix 8 – Session 1 Feedback

1) I have a clear understanding of what this project aims to achieve



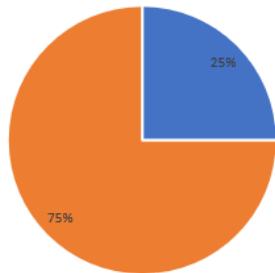
■ Mostly Agree ■ Completely Agree

2) I have a clear understanding of how my involvement helps this project



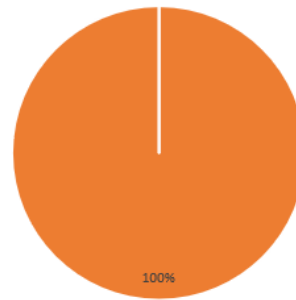
■ Mostly Agree ■ Completely Agree

3) I can see how monitoring the coastline can benefit residents, commercial and infrastructural developments



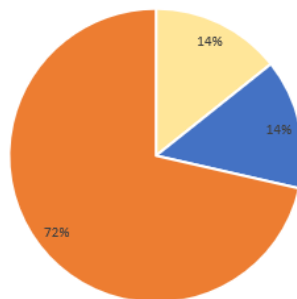
■ Mostly Agree ■ Completely Agree

4) I clearly understand what toe scour is and how it can be detrimental to coastal structures



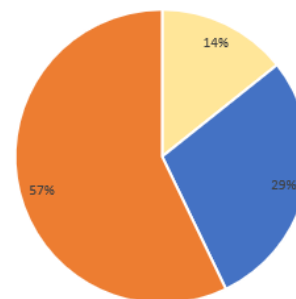
■ Completely Agree

5) I found the table-top practical session a very useful prior step before heading outside



■ Neither Agree or Disagree ■ Mostly Agree ■ Completely Agree

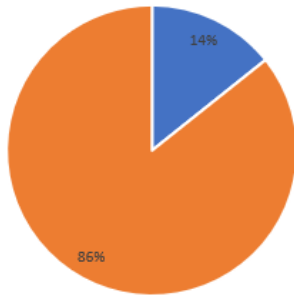
6) I clearly understood what scene conditions are most ideal for this project



■ Neither Agree or Disagree ■ Mostly Agree ■ Completely Agree

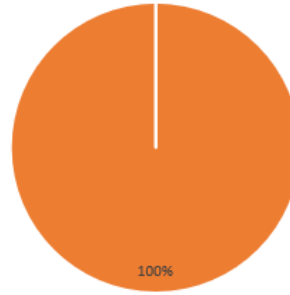
Pie charts displaying results from the feedback questionnaire from session 1.

7) I clearly understand why the scene conditions are important and how each condition can affect processing



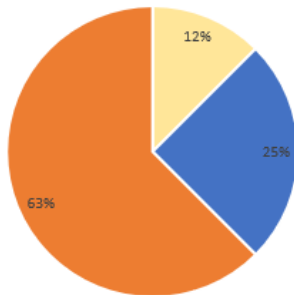
■ Mostly Agree ■ Completely Agree

8) I clearly understand how the correct technique for capturing imagery plays an important role for this project



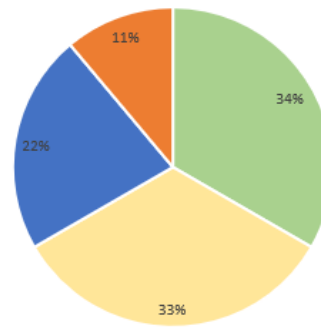
■ Completely Agree

9) I can independently upload data via the wetransfer.com website (or other known data transfer websites)



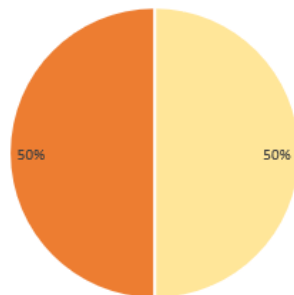
■ Neither Agree or Disagree ■ Mostly Agree ■ Completely Agree

10) I found 3D model generation easy



■ Mostly Disagree ■ Neither Agree or Disagree
■ Mostly Agree ■ Completely Agree

11) I can identify and upload the correct files via the wetransfer.com website (or any other known data transfer websites)



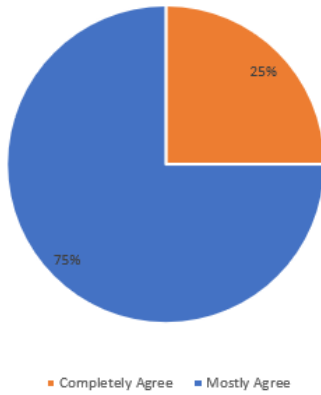
■ Neither Agree or Disagree ■ Completely Agree

can

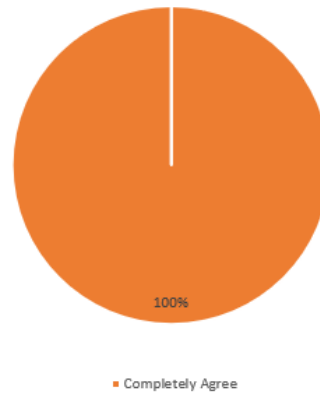


Pie charts displaying results from the feedback questionnaire from session 1

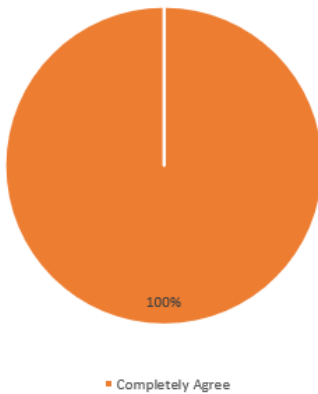
7) I clearly understand what scene conditions are ideal for this project.



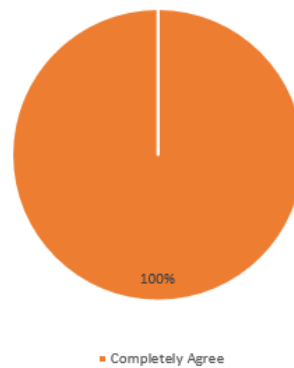
8) I understand why these scene conditions are important.



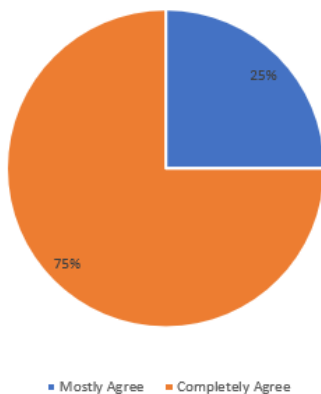
9) I clearly understand how and why the camera settings are important.



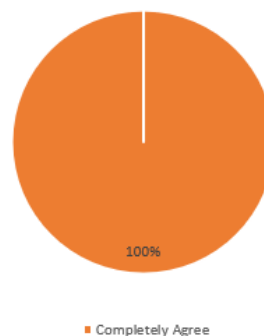
10) I clearly understand how the correct technique for capturing imagery plays an important role for this project.



11) I can see myself doing this on a regular basis.



12. I would be happy for group session like this to be included as a part of Rossall Beach Residents and Community Group's set of activities.



Pie charts displaying results from the feedback questionnaire from session 2